University of Cincinnati

Date: 8/21/2014

I, SAGIL   JAMES , hereby submit this original work as part of the requirements for the degree of Doctor of Philosophy in Mechanical Engineering.

It is entitled:

Study of Vibration Assisted Nano Impact-Machining by Loose Abrasives (VANILA)

Student's name: **SAGIL   JAMES**

This work and its defense approved by:

Committee chair: Sundaram Murali Meenakshi, Ph.D.

Committee member: Sundararaman Anand, Ph.D.

Committee member: Anil Mital, Ph.D. P.E.

Committee member: David Thompson, Ph.D.

15125

Study of Vibration Assisted Nano Impact-Machining by Loose Abrasives (VANILA)

Sagil James

Dissertation submitted to the faculty of the University of Cincinnati in partial fulfillment of the requirements for the degree of

Doctor of Philosophy

In

Mechanical Engineering

Dr. Murali Sundaram
Dr. Sam Anand
Dr. David Thompson
Dr. Anil Mital

March 2015

Abstract

Nanomachining of hard and brittle materials such as glass and ceramics is a challenge. Mechanical based techniques such as nanoindentation or nano scratching are feasible but direct contact of tool with the workpiece in such processes causes large scale tool wear. In this research, the target specific machining capability of single point tool based processes is combined with the hard and brittle material machining abilities of abrasives, to achieve *Vibration Assisted Nano Impact-machining by Loose Abrasives (VANILA process)* - a novel hybrid nanomachining process that uses a single-point AFM probe with loose abrasives and vibration assistance to perform target specific impact-based machining of nanoscale features on hard and brittle materials.

The feasibility of the VANILA process is verified both theoretically using analytical modeling and experimentally on silicon and borosilicate glass substrates. Patterns of nano-cavities are successfully machined to verify the controllability and repeatability aspect of the process. A predictive model for Material Removal Rate (MRR) during the VANILA process is developed and validated through experimentation. Molecular Dynamics Simulations (MDS) have been performed to gain fundamental understanding of material removal mechanisms involved in the VANILA process. A material removal mechanism map is constructed to capture the effects of critical process parameters on the material removal mechanism. Further tool wear during this process is theoretically modeled and the tool wear mechanism is investigated using MDS. It is found that the tool tip radius and the abrasive grain size significantly affect the tool wear mechanism.

Acknowledgements

Table of Contents

List of Figures

VII

List of Tables

List of Symbols

Tool variables

f_t	Frequency of vibration of tool (KHz)
A_t	Amplitude of vibration of tool (nm)
V_t	Velocity of tool tip (m/s)
E_t	Elastic modulus of tool material (GPa)
v_t	Poisson's ratio of tool
a_t	Maximum acceleration at tool tip (m/s^2)
k_t	Spring constant of tool (N/m)
Q_t	Quality factor of tool
R_t	Radius of tool tip (nm)

Process Parameters/ Operating Variables

t	Time (s)
T	Bulk Temperature (K)
F_{impact}	Tool impactg force (pN)
F_{drag}	Viscous drag force (pN)
F_{grav}	Gravitational force (pN)
I	Ultrasonic energy flux (J·m^{-2}·s^{-1})
V_{Th}	Thermophoretic velocity (m/s)
$\dot{\gamma}$	Shear rate (s^{-1})
∇T	Temperature gradient (K/m)
k_{El}	Equivalent elasticity constant
$damp$	Damping factor (fs)

Abrasive grain variables

E_a	Elastic modulus of abrasives (GPa)
R_a	Radius of abrasive grain (nm)
ρ_a	Density of abrasive grain (kg/m^3)
v_a	Poisson's ratio of abrasive grain
V_a	Velocity of abrasive grain (m/s)
Ω_a	Ang. velocity of abrasive grain (rad/s)
k_a	Thermal conductivity of grain (W/mK)
ϕ	Volume fraction of abrasive grains
m_a	Mass of abrasive grain (g)

Fluid variables

μ_{fl}	Dynamic viscosity of fluid (kg/(m.s)
v_{fl}	Kinematic viscosity of fluid (m^2/s)
ρ_{fl}	Density of fluid (kg/m^3)
K_n	Knudsen number
V_{fl}	Velocity of fluid (m/s)
k_{fl}	Thermal conductivity of fluid (W/mK)
P_c	Cavitation shockwave pressure (MPa)

Constants

g	Acceleration due to gravity (m/s^2)
k_B	Boltzmann constant (J/K)
c	Speed of sound (m/s)

Chapter 1: Introduction

Nanotechnology has gained tremendous attention over the past decade and is expected to increase even more in the coming years. Nanostructured materials have already found application in almost every field of science and engineering including medicine, space research, and automotive industry and so on. Development of ultraprecision process to handle materials at nanoscale forms the basis for further advancements in nano-based research. Success of nano science has already been achieved in Silicon based chip industry and it is evident from the miniaturized electronic products which are released in market today. Yet, the incapability of machining a broader range of materials including metals ceramics and polymers have limited the widespread impact of nanotechnology. Even though there have been considerable efforts to manipulate metals and polymers at nanoscale, ceramics nanomachining is still in its infancy.

Advanced engineering ceramics and composites in general are tougher and stronger with improved mechanical, chemical and wear resistant properties and have unique ferromagnetic, magnetoresistive, ionic, dielectric, ferroelectric, piezoelectric, pyroelectric, electronic, superconducting, and electro-optical properties. However, owing to their hard and brittle nature, these ceramic materials pose a challenge for most of the conventional nanomachining process such nanoscratching and nanoindentation. Also, being non- electrically conductive, nano electro-physical and chemical processes fails to machine ceramic materials. Abrasive machining have demonstrated its effectiveness in machining ceramics at a macro scale; while scaling the parameters down could open opportunities to conduct ceramic machining even at nano scales.

With the assistance of ultrasonic vibration and using a tool with nano dimensions, the abrasive nanomachining of ceramics could be conducted more effectively.

This research explores the possibility of combining the target specific machining capability of single point tool based processes along with the hard and brittle material machining abilities of abrasives, to develop *Vibration Assisted Nano Impact-machining by Loose Abrasives (VANILA process)* - a novel hybrid nanomachining process that uses a single-point AFM probe with loose abrasives and vibration assistance to perform target specific impact-based machining of nanoscale features on hard and brittle materials.

1.1 Organization of Chapters

Chapter 2 reviews relevant literature. This review covers several topics including different machining processes relevant to this research, simulation of nanomachining processes, theoretical modeling relevant to this research and tool wear study. Chapter 3 describes the theoretical and experimental studies conducted to find the feasibility of the VANILA process. Chapter 4 includes the mathematical modeling of the VANILA process in which the material removal rate of the process is modeled and evaluated experimentally. Chapter 5 explains the material removal mechanism studies conducted to understand the mode of material removal in the VANILA process. This is followed by Chapter 6 in which the tool wear mechanism and modeling studies are presented. This is following by conclusion in chapter 7.

Chapter 2: Literature Review

The study of the VANILA process is performed using three different research approaches – Theoretical study, Experimentation and Simulation. This chapter focusses on relevant literature related to the different approaches used in this research.

2.1 Machining processes relevant to this research

The VANILA process is a mechanical nanomachining process and is developed by combining the principles of abrasive machining, vibration-assisted machining and single point tip-based nanomachining. The following section provides a brief review of abrasive machining, vibration-assisted machining and mechanical nanomachining processes.

2.1.1 Abrasive Machining

Abrasive machining is a proven material removal process capable of machining a wide range of materials, especially hard and brittle materials [1, 2]. Abrasive materials have several advantages such as high hardness, strength, chemical inertness, and high wear resistance which are essential for machining advanced engineering materials. At nanoscales, abrasive-based machining processes have been already applied successfully in traditional finishing operations such as grinding, honing, lapping, and also in advanced finishing processes such as abrasive flow machining (AFM)[3], magnetorheological finishing (MRF)[4], magnetic float polishing (MFP)[5], magnetorheological abrasive flow finishing (MRAFF)[6], elastic emission machining (EEM)[7], and chemo mechanical polishing (CMP) [8]. These processes can be broadly classified as Loose Abrasive and Fixed Abrasive processes. Loose abrasive machining (LAM)

processes such as lapping [9] uses abrasives such as diamond, SiC, boron nitride, and aluminum oxide for nanomachining wherein the abrasive materials is usually mixed with a liquid medium to form slurry which is introduced between a hard horizontally rotating wheel and the workpiece. Fixed abrasive processes such as nanogrinding [10] and high-speed lapping [11] involves a two body abrasion between the workpiece surface and an abrasive embedded rotating tool.

2.1.2 Vibration-Assisted Machining

Adding of high-frequency vibration is found to be very effective in performance enhancement of abrasive-based machining processes [12]. Ultrasonic machining (USM) [13] is a typical example of vibration-assisted abrasive machining processes that uses high frequency mechanical motion of shaped tools and abrasive slurry to erode materials from hard and brittle workpieces [14]. Micro ultrasonic machining (MUSM) has been gaining popularity as an efficient process in micron-scale machining of non-conductive, brittle and hard-to-machine materials to fine precision and smooth surface finish [15]. However, ultrasonic machining at nanoscale is a yet largely unexplored research area. Moreover, the abrasive finishing processes discussed above are not suitable for target-specific machining of features such as holes, slots, and three-dimensional shapes with nanoscale dimensions. Other advanced techniques such as femtosecond laser machining and focused ion beam machining are technically capable but prohibitively expensive alternates for nanomachining [16]. Hence, there is a need for alternative solutions such as tip based nanomanufacturing processes for nanomachining of difficult-to-machine ceramic and brittle materials.

2.1.3 Mechanical Nanomachining Processes

Nanoscale machining can be primarily classified into – Mechanical machining, Electro-Machining and High energy beam machining processes. Mechanical nanomachining involves nanoscale material removal by mechanical means such as scratching, shearing, abrasion and fracturing. Electro-machining uses electric discharge and/or ionic dissolution in order to remove the material. On the other hand, High energy beam machining uses an intense beam to remove material from substrate surface by heating. Examples of this include Photolithography, Focused Ion Beam (FIB) machining, Laser machining and so on. In comparison to Electro-machining and High energy beam machining, removing materials mechanically has proven to provide higher precision and defect-free/stress-free machining at nano scales. While high energy beam methods tend to damage the surface causing large scale machining (proximity effect), electro-machining method are unable to remove material from non-conductive workpiece materials. Mechanical nanomachining, on the other hand offers the advantage that it does not depend on the electrical or chemical properties of the substrate [17]. Also, mechanical nanomachining processes prevents chemical or residual contamination of the substrate materials [18]. Consequently, researchers have shown a great amount of interest in furthering the scope and increasing the efficiencies of mechanical nanomachining processes. Numerous challenges still remain which need to be addressed before commercializing these nano scale machining operations.

Mechanical nanomachining processes can be broadly classified into three categories – Nanomachining using single point tool, Nanomachining using loose abrasives and Nanomachining using fixed abrasives.

2.1.3.1 Nanomachining using single point tool

Single point tool based nanomachining involves direct contact between the tool and workpiece. Nanoindentation and Nanoscratching are two popular single point tool based nanomachining processes [19, 20]. Nanoindentation process uses a sharp indenting probe in order to penetrate the substrate surface to depths ranging in nanoscales [21]. Primarily, this technique is used to study the surface deformation of a material where the indenter is lowered to the workpiece surface while controlling the force and the resistance in motion is measured. The tip is raised from the substrate and the process is repeated at different locations after moving either the tip or the substrate. The concept of nanoindentation technique can be extended for machining nanoscale substrates by applying high indentation load on the probe tip and thus fabricate nanometer deep holes [22]. Nanoscratching process is an extension of the Nanoindentation technique where the AFM tip is dragged over the substrate surface while ensuring the tip is still in contact with the surface forming nanochannels [19]. The single point tool based nanomachining process involves high forces developed at the tool tip which leads to its frequent breakage. The resultant machined area will have built-up edges and also develop surface stress because of higher machining forces involved. In addition, the contact based nanomachining process can be only used to machine soft and ductile materials as machining of hard and brittle workpiece materials would result in tool tip breakage.

2.1.3.2 Nanomachining using loose abrasives

Lapping is prominent nanomachining process involving loose abrasive grains as a means in fine finishing brittle work materials [23, 24]. The process involves three body abrasion in which the hard abrasive grains roll in between the substrate surface and the lapping disk. Lapping can be

considered to be a nano polishing process mainly for glasses and semiconductor wafers [9]. The tolerances and surface finish of the substrate can be controlled by varying the size and hardness of abrasives. Even though lapping can be used for nanopolishing brittle work pieces, the process is not capable of conducting target specific machining. Target specific means the process is capable of performing machining at any desired location on the substrate.

2.1.3.3 Nanomachining using fixed abrasives

Fixed abrasive processes involve nanomachining using tool or a pellet with abrasive grains bonded firmly on it. One such process is High speed lapping which is a derivative of the lapping process wherein the abrasive grains are fixed on a pellet [11]. The process requires a special high speed lapping machine, in which solid pellets with bonded abrasive grains are used. Nanogrinding is another fixed abrasive ultra-machining process similar to lapping process which uses nano-abrasive-bonded tool for nano polishing surfaces of hard materials such as advanced ceramics [10]. However, unlike lapping, nanogrinding uses a revolving routing plate, known as grinding tool, which has the abrasive grains completely embedded on it [25]. Using solid abrasives instead of loose abrasive grains helps avoid abrasive splashing problem, prevent abrasives mixing with chips and keeps abrasive grains intact as they do not cut each other [26]. However, the redressing process becomes very difficult when using solid pellets which limit the wide usage of this technique. Table 2.1 shows a comparison of various mechanical nanomachining processes discussed above.

7

Table 2.1: Comparison of Selected Mechanical Nanomachining Processes

Process	Nanoindentation	Nanoscratching	Nanogrinding	Lapping Process	
				Loose Abrasives	Fixed Abrasives
Tool	Diamond Tipped Probe	Diamond Tipped Probe	Grinding Wheel	Lapping Disk	Lapping Disk
Abrasive Used	--	--	Multi-grains (Bonded)	Multi-grains (Loose)	Multi-grains (Bonded)
Machining Force	High	High	High	High	High
Process Type	Single point machining	Single point machining	Multi-point Nano Polishing	Multi-point Nano Polishing	Multi-point Nano Polishing
Target Specific	Yes	Yes	No	No	No
Materials	Metals [27], Polymers [28], Glasses [29]	Metals [30], Polymers [31], Ceramics [32]	Ceramics [25, 33]	Ceramics [9], Glasses [23]	Ceramics [34]
Roughness	--	1 nm to 2 nm [30]	0.04 nm – 1.4 µm [25]	1 nm [35] to 3.5 µm [9]	0.88 nm [26] – 0.6 µm [34]
Width of Cut	20 nm to 120 nm width [22]	25 nm to 50 nm [36]	N/A	N/A	N/A
Depth of Cut	2 nm [22] to 80 nm [27]	20 nm to 400 nm [37]	N/A	N/A	N/A

Material removal during the VANILA process has close resemblance to that of other mechanical nanoscale polishing processes involving impacts of abrasive nanoparticles. These include but not limited to fluid jet polishing (FJP) process [38], contact or non-contact chemical mechanical polishing [39, 40] and nanoparticle colloid jet machining [41]. At this scale of wear, the applied loads are very low ranging from μN and down to nN and the impact response is very different from macro- and micro-levels and the substrate surface is likely to remain intact for extended period due low wear rate [42].

2.2 Simulation of Nanomachining Processes

Molecular Dynamics (MD) is a powerful tool for the prediction and analysis of nanomachining processes and for the understanding of the material removal mechanism of the abrasive process at the nanometer scale [43]. MD is a computer simulation technique used to study the motion of atomic particles. This technique calculates the time evolution of interacting atoms by integrating their equations of motion based on statistical mechanics. MD simulation has been used to study the effects of cutting force and specific energy involved in nanocutting process. Crystal orientation and ploughing direction have been found to have a significant influence on the forces including cutting force, thrust force, and width-direction force [44, 45]. The significance of depth of cut in nanomachining has also been investigated using MDS. The chip formation was observed from a depth of cut of 30.0 Å [46].

MD simulations were also used to study the atomic scale friction forces at the interface between the tool and the substrate. MD simulations of nanoscratching revealed that the friction forces increase as the scratch lengths increase while the friction coefficient fluctuates about a constant value and is independent of the scratching speed [47]. MD simulation based studies have been

reported on high-speed nanoindentation by rigid tips in which a relationship between the indentation force and the indent depth was established [48]. Several reports on MD simulation of nanoscale machining to study the mechanism of the chip formation, chip removal, flow of chips during machining and the volume of chips produced are available in the literature. MD simulation study of the effect of crystal orientation in chip formation during nanoscratching of silicon carbide showed that there is significantly more pile-up and chip formation in the [1 1 0] direction [49]. MD simulations were also performed to evaluate the effect of the tool geometry (tool rake angel, tool edge radius, size, shape) on surface formation of the nanomachined substrates. An MD simulation study of AFM-based lithography identified that the tool angle is a significant factor impacting the ploughing forces and noticed that a tool with a larger tip radius required a larger ploughing force, since the tool contacted more work-material molecules and resulted in more compression on the work-material molecules around the tool [45]. Another study revealed that an increase in the negative rake angle resulted in the increase in specific energy along with a rise in the cutting and thrust forces [50].

MD simulations to understand the crack propagation in brittle materials were reported in some studies [51, 52]. Several other aspects of nanomachining, which were studied using MD simulations, include bulk temperature of machining [53], plastic flow [54, 55], and subsurface deformation [50, 54]. However, very few studies are reported on MD simulation of vibration assisted nanoscale processes. These include vibration-assisted nanoscratching processes [54, 56, 57] and nanopolishing using abrasives [55]. Extensive experimental and molecular dynamics simulation studies of Impact Lithography, a nanoscale material removal process that involves hypervelocity impact of nanoparticles on target surface to induce deep penetration and crater

10

formation process, have been reported [58-60]. MD based studies have also been reported on Chemical Mechanical Polishing (CMP) technique in which the mechanical deformation of the workpiece subject to its interaction with abrasive particles were investigated [61]. It is found that the ratio of radii of a particle and an asperity strongly affect the amount of material removed [61]. In general, these MD based studies primarily focused on understanding the effects of process parameters such as impact velocity, cluster size of impacting particle, specific impact energy, and machining time on the crater volume and penetration depth. Tersoff potential function is used for the MD modeling of these hypervelocity impact processes which use silicon-based target materials [59, 62]. It is seen that the majority of MD simulations for nanomachining processes have used Morse, Embedded Atom Model (EAM), and Tersoff as the potential functions. To be more specific, simulations involving metal-metal interactions have used either EAM or Morse potentials processes [44, 45, 53, 63-69], while nanomachining of covalently bonded substrates such as silicon and SiC are done using Tersoff potential function [49, 52, 55]. Table 2.2 shows the application of MD simulations for various nanomachining process, the investigated causes and effects along with the potential used for analysis.
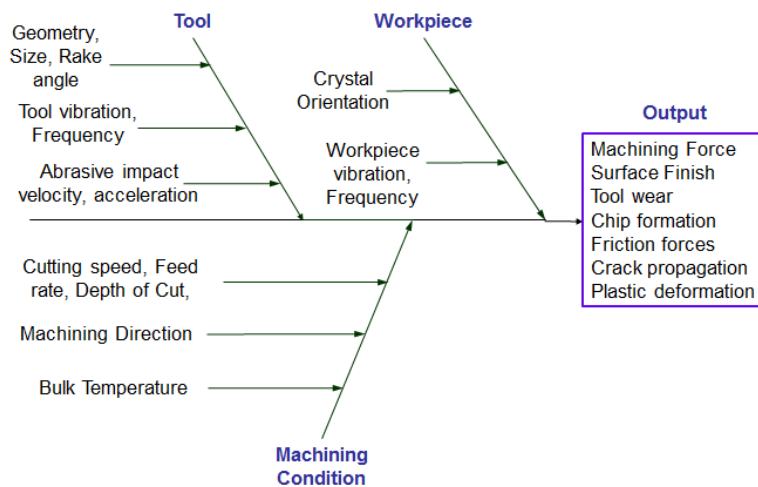
Fig 2.1: Cause-Effect Diagram of MD Simulations for Nanomachining

Table 2.2: MD simulations for various nanomachining processes

	Machining Process	Citation	Cause-Effect	Potential Used
1	Nanoscratching, Nanoploughing, Nanogrooving, Nanomilling, Nanocutting, Nanolithography, Nanopatterning, AFM-based Nanolithography, Single-point turning	Jiaxuan Chen 2008[63]	Chip formation, Burr formation	Morse, EAM
		Vahid Hosseini, Vahdati et al. 2011 [64]	Tool edge radius, Tool geometry - Friction forces, Chip formation, Cutting force	Morse, EAM
		Khan and Sung-Gaun 2010 [53]	Temperature at which process is conducted - Dislocation	EAM
		Cui 2011 [65]	Dislocation, Machining Force	Morse
		Kim et al. 2005 [44]	Tool shape, Forming depth, Crystal orientation, Ploughing direction - Plastic deformation, Surface roughness, Machining Force	Morse
		Komanduri 2001 [50]	Tool Rake angle, Width-to-depth of cut ratio - Subsurface deformation Chip flow, Specific energy, Cutting force	Tersoff
		El-Mounayri et al. 2010 [66]	Tool Rake angle, Depth of cut - Cutting force, Chip formation	EAM
		Oluwajobi 2010 [67]	Depth of cut - Cutting force	Morse
		Shi et al. 2011 [68]	Tool Rake angle, Machining speed, Depth of cut, Feed rate – Machining stress, Temperature, Tool force, Cutting force	Morse
		Hu et al. 2010 [69]	Tool geometry, Depth of cut, Cutting velocity, Bulk temperature- Friction coefficient, Chip volume, Cutting force	EAM
		Noreyan and Amar 2008 [70]	Indenter Size, Scratching depth, Scratching velocity,	Tersoff
2	Vibration assisted Nanomachining	Shimizu 2004 [57]	Tool vibration, Vibration frequency - Cutting force, Plastic deformation, Plastic Flow	Morse
3	Indentation, Hertz Indentation	Shishikura et al. 2010 [52]	Crack initiation	Tersoff
		Plimpton et al. 1998 [51]	Crack propagation	EAM
		El-Mounayri et al. 2010 [47]	Machining speed- Indentation force, Friction forces	Morse, EAM
4	Nanopolishing, PCVL, Abrasive machining	Guo at al. 2006 [55]	Velocity, Acceleration of Abrasives - Machinability	Tersoff

A number of MDS studies have reported on nanoscale cluster impingement, implantation, and surface deposition, repulsion and emission on various substrates [58, 71]. However, most of the impact simulations were not purely mechanical based and involved chemical and mechanical

based material removal. Moreover, they were performed using clusters such as gas atoms, metal atoms or silicon atoms, and so on [72]. There are only very few studies involving impact of hard nanoparticles on solid surface at various angles and velocities [72].

The MDS study of amorphous silica nanoparticle impacting on silicon surface found that amorphous phase transformation and plastic flow inside the impact zone are the main deformations on the substrate [73]. In that study the amorphous silica nanoparticles collides and recoils from the silicon surface causing amorphous phase transformation and plastic flow in the impact zone along with occasional pile-up at the edges of the depressed region. The study also reported that an impact angle between $0°$ and $75°$ caused wider and shallower arc-shaped region along with hill-shaped pile-up formation, while near normal $(90°)$ impacts caused deeper depressed regions.

2.3 Theoretical modeling relevant to this research

2.3.1 Material Removal during Impact Machining Process

The material removal in the VANILA process is achieved by the impacts of accelerated abrasive grains on the surface of brittle workpiece. The mechanism has close resemblance to that of erosion process of brittle materials due to solid particle impact [74-77] and machining processes including abrasive jet machining process [78], non-contact ultrasonic abrasive machining (NUAM) [79] and impact lithography process [58]. Material removal by impact of solid particles is often classified as wear or erosion and it is a complex phenomenon consisting of several simultaneous and interacting processes, typically involving mechanical, chemical and material parameters as well as complex mechanisms [77].

In general, material removal in brittle materials such as glass and ceramics is considered to happen by fracture, crack propagation and chipping [77]. However, under high pressure conditions, brittle-to-ductile transition (BDT) may occur and plastic deformation can happen [80]. A plastic zone is formed beneath the zone of impact and a crack may propagate downwards from the base of the zone of impact normal to the surface [76]. The fracture framework system used to model the impact of solid particles on hard and brittle materials is displayed in figure 2.2. A plastic zone is formed beneath the point of impact and a radial or median crack may propagate downwards from the base of the. After the impact, a lateral crack propagates parallel to the surface from the base of the plastic zone.
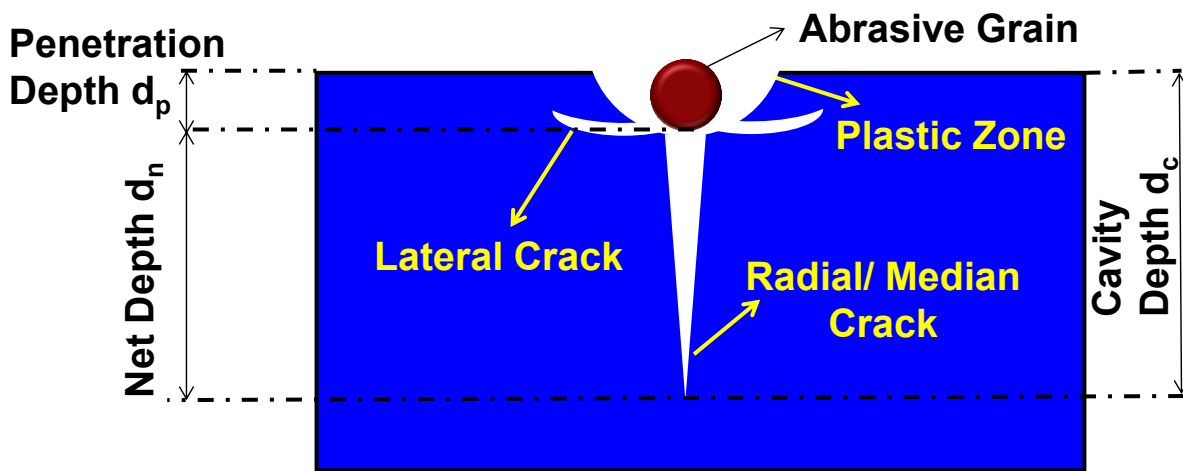
Fig 2.2: Fracture framework used for modeling solid particle impact [81] (after [8, 10, 20])

2.3.1.1 Material Removal in Brittle Mode

Depending on the shape of the indenting grain – blunt or sharp, the fracture patterns are different [82]. Impact of a sharp grain results in the formation of radial/median cracks followed by a lateral crack which propagates outwards nearly parallel to the surface from the base of the plastic

14

zone [78, 83]. However, a blunt or spherical grain impact as in this study has an elastic initial contact, followed by a plastic zone and further forms conical cracks (Hertzian cone cracks).

2.3.1.2 Material Removal in Ductile Mode

Material removal in ductile mode erosion was initially attributed to cutting wear by a mechanical process known as micro-cutting [84]. A material removal model developed based on micro-cutting process predicted that no erosion would occur at normal angle of impact which was contrary to the experimental evidence [85]. Subsequent investigations revealed that an additional mechanism was operative during erosion at normal or large angle impacts which was termed as deformation wear due to repeated hammering action [86]. Studies also revealed that several complex phenomena would occur due to the repeated hammering [77] which include heating/melting of the target and work-hardening [87] and crack development [88]. Other phenomena which could affect the material removal mechanism in ductile mode are thermal softening, lip formation due to extrusion, flake formation, effect of abrasive grain fragmentation, fatigue due to plastic strain reversals and annealing effects. The cause and effects of possible material removal mechanisms in ductile mode machining are shown in Figure 2.3.
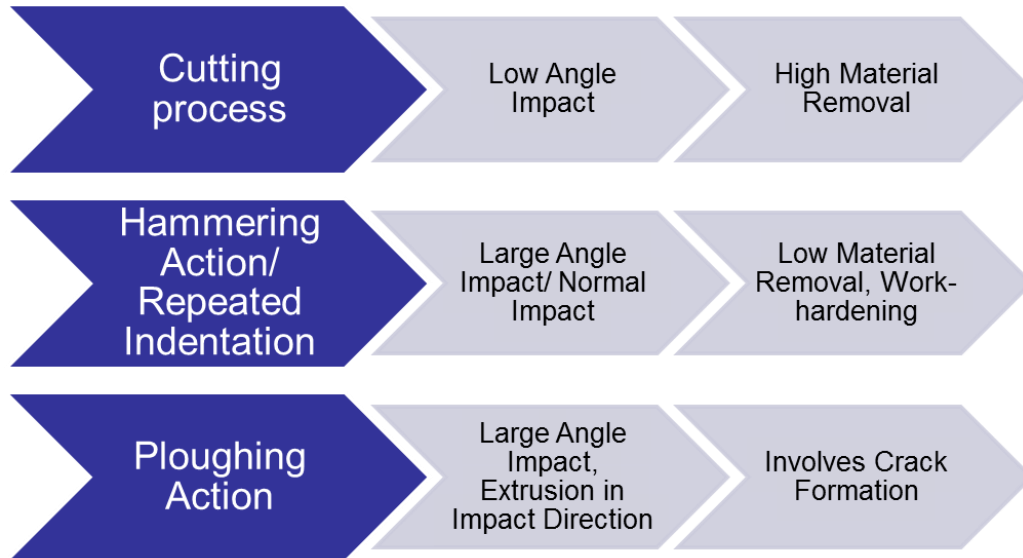
Fig 2.3: Possible material removal mechanisms in ductile mode machining

2.3.1.3 Existing Models to Predict MRR in Erosion Process

Based on different mechanisms shown in Figure 2.3, models have been developed to predict the material removal rate as a function of parameters evaluated from experimental tests. The factors which affect the ductile mode material removal include particle size, impact velocity, angle of impact and the workpiece hardness. Literature suggests that the macro-mechanical properties of workpiece such as fracture toughness (K_{Cw}) and elastic modulus (E_w) do not greatly influence the material removal during ductile mode machining [85]. Most of the earlier models developed to predict the material removal rate assumed that the volume removed by a single particle is proportional to the cylindrical volume given by the radius of the crack and its depth [78]. Based on empirical equations using linear regression data analysis, various models have been developed to estimate the material removal rate [76, 78, 83, 89, 90]. In these studies, the material removal rate is described as a function of the abrasive particle characteristics (velocity, radius,

16

density), and the mechanical properties of the target material properties (hardness, toughness, Young's modulus).

The material removal in the VANILA process is attributed to the impacts of abrasive grains on the surface of brittle workpiece. The material removal is similar to that of erosion process of brittle materials due to solid particle impact [77, 91] and machining processes including abrasive jet machining process [92], non-contact ultrasonic abrasive machining (NUAM) [79] and impact lithography process [58]. Removal of material by impact of solid particles is often classified as wear or erosion and it is a complex phenomenon consisting of several simultaneous and interacting processes, typically involving mechanical, chemical and material parameters as well as complex mechanisms [77].

Material removal in ductile mode erosion was attributed to a mechanical process termed as cutting wear due to micro-cutting [84, 93]. The material removal model developed based on micro-cutting process [84] predicted that no erosion would occur at normal angle of impact which was contrary to the experimental evidence [85]. Subsequent investigations revealed that an additional mechanism was operative during erosion at normal or large angle impacts which was termed as deformation wear due to repeated hammering action [86]. Studies also revealed that several complex phenomena would occur due to the repeated hammering [77, 94] which include heating/melting of the target and work-hardening [87] and crack development [86]. Other phenomena which could affect the material removal mechanism in ductile mode are thermal softening, lip formation due to extrusion, flake formation, effect of abrasive grain fragmentation, fatigue due to plastic strain reversals and annealing effects [95, 96].

17

Based on these mechanisms, models were developed to predict the material removal rate as a function of parameters evaluated from experimental tests. The factors which affect the ductile mode material removal include particle size, impact velocity, angle of impact and the workpiece hardness. The studies also suggest that the macro-mechanical properties of workpiece such as fracture toughness (K_{Cw}) and elastic modulus (E_w) do not greatly influence the material removal during ductile mode machining [85]. Various models to estimate the material removal rate have been theoretically derived by Evans et al., [76], Marshall et al., [83], Aquaro and Fontani [89], Wakuda et al., [78], and Wiederhorn and Hockey [90] based on empirical equations using linear regression data analysis. In all the models, the material removal rate are described as a function in terms of the characteristics of the particle (velocity, radius, density) and the mechanical properties of the target material properties (hardness, toughness, Young's modulus) which are the main variables affecting the material removal rate. Thus from the literature review, we learn that the material removal in brittle materials can occur in different regimes depending on the impact conditions [75, 76]. The damage in ductile regime is strongly influenced by material hardness (H_w) of the workpiece.

2.4 Tool Wear Study

Several studies on tool wear in nanomachining processes [97] and in particular, the wear of AFM tip have been reported in literature [98-100]. The wear phenomena in nanomachining processes involve deformation in only a few atomic layers and often occur at very short time scales which does not permit any direct observation of the actual process. In-situ experimental studies would be quite challenging and often cannot be relied upon to understand the basic theory of the tool

wear mechanism. However, several techniques to study the tool wear mechanism and to quantify the wear rate have been developed based on experimentation, theoretical modeling, and simulation.

2.4.1 Methods to Study Tip Wear

The following section of literature survey focuses on some of the approaches used to understand the tool wear at nanoscale.

2.4.1.1 Theoretical Approach and Modeling of Tool Wear

There have been several attempts to analytically model the wear behavior of an AFM probe in operation in order to identify the mechanism of wear and to predict the tool profile and height loss of the tip [100-102]. The degree of tip wear rates during contact mode operation were usually assessed using Archard's wear equation in which the friction coefficient is assumed constant and the dissipated energy is proportional to the product of normal load, sliding distance, and friction coefficient [103]. Some studies have proposed an energy dissipation-based models to predict wear rates at macroscale [104] which could be used for tapping (or intermittent contact) mode operations; however, their direct applicability is not clear and straightforward. The reasons being at nanoscale, other forces such as adhesive, capillarity, etc. become prominent [105] and also the wear length is extremely small often in the range of the surface roughness of the specimen [106]. Several other models to estimate the tool wear have been reported, nonetheless, no broadly applicable model exist which can predict the evolution of wear at nanoscale [105].

2.4.1.2 Tool Wear Study using Experimentation

The wear of an AFM tip has been estimated experimentally through various methods such as inverse imaging of the tip [98, 107], using blind tip reconstruction [108], direct imaging in AFM [109] and from high resolution microscope images taken before and after wear scans. Even though these methods have demonstrated their capability to show the AFM tip wear to some extent, there are several significant limitations. The microscope characterization techniques using Field Emission SEM and High Resolution Transmission Electron Microscope (HRTEM) [98, 108, 110, 111] are able to correlate the tip deterioration with the image quality, but does not provide an in-depth analysis of how the actual tool worn shape is formed. AFM-based techniques such as blind tip reconstruction and inverse imaging are limited by the fact that both the tip and the workpiece undergo wear which adds complexities and inaccuracies.

2.4.1.3 Simulation Approach based on Molecular Dynamics

Unlike theoretical modeling and experimentation, simulation has the capability to bring out the underlying mechanisms behind the tool wear in a nanoscale process. The use of such an approach could also potentially reduce a large number of experimental investigations and associated costs such as expensive AFM probes [112]. However, at such small governing length scales; the continuum representation of the problem becomes questionable. In the past, molecular dynamics (MD) simulation based approach has been employed to study nanoscale machining considering its capability to analyze and visualize the atomic-scale wear phenomenon [113]. MD simulations have been widely utilized to study the tool wear in nanometric cutting process using a diamond tool [100, 113, 114].

2.4.2 Effect of Tip Shape and Size

Researchers have found that the tip shape of the AFM probe significantly influences the deformation behaviors at nanoscales [115-117]. Most studies reported have used MD simulation based approach in which a blunt hemispherical indenter and a sharp pyramidal shaped indenter are compared to investigate the effect of tip shape on the material removal process. The hemispherical indenters were found to cause point defects deep into the substrates, while the pyramidal indenters only introduces the disorder of the atoms around the indenter [115, 117]. Additionally, the effect of tip size (radius), known as *size effect* could have a significant influence on the nanoscale wear process affecting onset and evolution of different phases during the indentation process [118].

2.4.3 Tool Wear Mechanisms

AFM tip wear occurs through multiple wear mechanisms [98, 100, 106] such as abrasive and adhesive wear [109], low-cycle fatigue and material fracture [109], gradual wear due to atom-by-atom attrition [119], plastic deformation [107], coating failure, tribochemical wear [107], and thermo-chemical wear [113] depending on the operating conditions. It was revealed that in contact mode operation, classical laws which describe the wear as macroscopic tribological phenomena do not necessarily hold at nanoscale [99, 119]. Instead the nanoscale wear of the AFM tip often seemed to proceed as a smooth and gradual continuous process of atom-by-atom attrition without any indication of fracture [100, 119]. The attrition is attributed to the breaking of individual bonds described by a thermally activated process [119], while the tip wear rate is found to decrease as the tip becomes blunter since the contact stresses become lesser [98, 119].

The nanoscale tool wear, as investigated using MD simulations, is found to happen primarily through thermo-chemical wear, micro-delamination [113] and phase transformation [120, 121]. These simulation studies have mostly focused on the wear of single point diamond tool during nanoscale cutting of silicon based substrates. It has been reported that at nanoscale, the diamond tool wear depends on the cutting temperature, because the cutting heat will decrease the cohesion energy of carbon and weaken the bonding of C-C leading to high pressure phase transformation and graphitization [120, 121].

In addition, there are several other mechanisms which govern the atomistic wear of an AFM tip such as inter-diffusion and re-adhesion caused by the interaction of the workpiece atoms and the tool atoms [114]. An overview of possible mechanisms affecting the AFM tip wear is listed in table 2.3.

Table 2.3: Possible mechanisms affecting AFM tip wear

Studied Processes	Possible Mechanisms of AFM Tip Wear
AFM Scanning – Contact Mode	Abrasive and adhesive wear [109], Low-cycle fatigue and material fracture [109], Plastic deformation [107], Coating failure [98], Tribo-chemical wear [107]
Nanoscratching, Nanometric Cutting, Single Point Diamond Turning	Gradual wear due to atom-by-atom attrition [119], Thermo-chemical wear and micro-delamination [113], High pressure phase transformation of material [120], Inter-diffusion of the workpiece and tool atoms [114], Re-adhesion of the worn particles to the tool [114]
Nanoindentation	Plastic deformation [121], High pressure phase transformation of material [121]

2.4.4 Choice of Potential Function for MD Simulation

Molecular dynamics simulation depends strongly on the choice of the potential function best suited to represent the physics of the system. In this section, a detailed literature review is done with an aim to find the suitable potential function for the simulation of tool wear during VANILA process which essentially involves interactions between a diamond abrasive grain and a silicon workpiece. There are several inter-atomic potentials which have been used in the past for MD simulations to model the deformations mechanisms in bulk silicon material. Most popular among them are Stillinger-Weber (SW), Tersoff, Embedded-Atom Method (EAM),

Environment-Dependent Interatomic Potential (EDIP), ReaxFF, REBO and modified forms of these potentials [122].

Among these, Tersoff potential [123] is the most suitable semi-empirical model for providing realistic description of covalently-bonded materials like silicon and carbon. It is computationally less expensive and is based on the bond order concept where the bond strengths, angle and directionality are affected by the presence of surrounding atoms. Literature study reveals that Tersoff potential can well describe the properties of silicon and has thus been extensively employed to predict silicon's mechanical behavior including lattice dynamics, point defects, crack initiation [52, 124, 125], crack propagation [126], micro-crack formation [50, 127], ductile fracture [122], ductile-to-brittle transitions [122], and phase transformations [128].

It is worth noting that most of these semi-empirical potentials have short cut-off radius and often do not provide a good description of brittle fracture [129, 130]. A larger cut-off radius would be necessary to make these potentials more suitable for such a long-range and ultra-fast process such as brittle fracture. The deficiencies of all these semi-empirical models are quantitative in nature where the failure strengths are often over-estimated. Long range potentials are able to overcome this problem of explaining brittle fracture, however, they are very poor at elastic and plastic regimes and also fail to predict compressive strains [131]. It is generally accepted that none of the available potential functions for silicon are capable of accurately describing its mechanical behavior close to reality [129]. Although, in recent years, there have been numerous attempts using hybrid approaches; the search for an accurate potential function for silicon without increasing much computational cost, still remains of great relevance.

Chapter Summary

- While the single point tool based target specific processes, involve very high forces for machining and are mostly suitable to machine soft and ductile materials.

- Abrasive based process have relatively lesser force of machining, but the process is not target specific and hence are being applied for large surface modification operations such as grinding or polishing applications of brittle materials.

- The literature review on molecular dynamics simulation reveals that the suitability of Tersoff potential function for VANILA process simulation of impact of diamond nanoparticles on silicon substrates.

- The literature study on theoretical modeling suggests that the material removal in brittle materials can occur in different regimes depending on the impact conditions.

- While damage in ductile regime is strongly influenced by material hardness (H_w), the brittle regime is primarily governed by the material's critical stress intensity factor or fracture toughness (K_{Cw}).

- Molecular Dynamics simulation technique is a potential tool to analyze the mechanism of tool wear in the VANILA process.

- The AFM tip wear mechanisms depend on the process and operating conditions and thus multiple mechanisms could dominate the wear process in a nanomachining process.

- The size effect between the interacting materials (tip and workpiece) also needs to be considered for the better understanding of the wear progress.

- It is clear that even with so many potentials for silicon, it is unfortunate that none is particularly superior over others. Thus there is no clear choice of potential for studying the material behavior of silicon.

- Based on its suitability for covalently bonded materials such as silicon and diamond, *Tersoff potential* is selected in this study to dictate the interaction between the Si-Si, Si-C and C-C atoms. Although, the Tersoff potential may not include forces required to simulate brittle fracture within the bulk silicon, it should be possible to observe some of the significant wear mechanisms such as plastic deformation and crack development at nanoscale, at least qualitatively.

Chapter 3: Feasibility Studies

In this research, the target specific machining capability of single point tool based processes is combined with the hard and brittle material machining abilities of abrasives, to develop Vibration Assisted Nano Impact-machining by Loose Abrasives (VANILA process) - a innovative hybrid nanomachining process that uses a *single-point AFM probe* with *loose abrasives* and *vibration assistance* to perform target specific impact-based machining of nanoscale features on hard and brittle materials as shown figure 3.1.
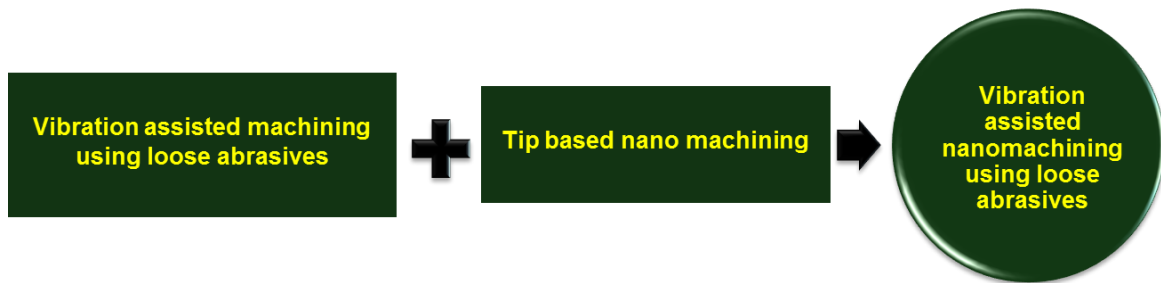
Fig 3.1: Research Hypothesis

3.1 Principle of VANILA Process

VANILA process is a tip-based nanomachining process that uses a single-point AFM probe with loose abrasives and vibration assistance and can be used to perform target specific impact-based machining of brittle materials at nanoscale [132, 133]. The VANILA process is conducted on an atomic force microscope (AFM) as the platform and a slurry of nano diamond powders smaller than 10 nm which is introduced between the tool and the workpiece. The tool used is a tapping mode AFM tip and it is vibrated constantly while maintaining a constant distance from the workpiece as shown in figure 3.2a. This results in continuous hammering of suspended nano

diamond powders which in turn impact the impact the workpiece surface repeatedly resulting in nanoscale material removal (figures 3.2b and 3.2c).
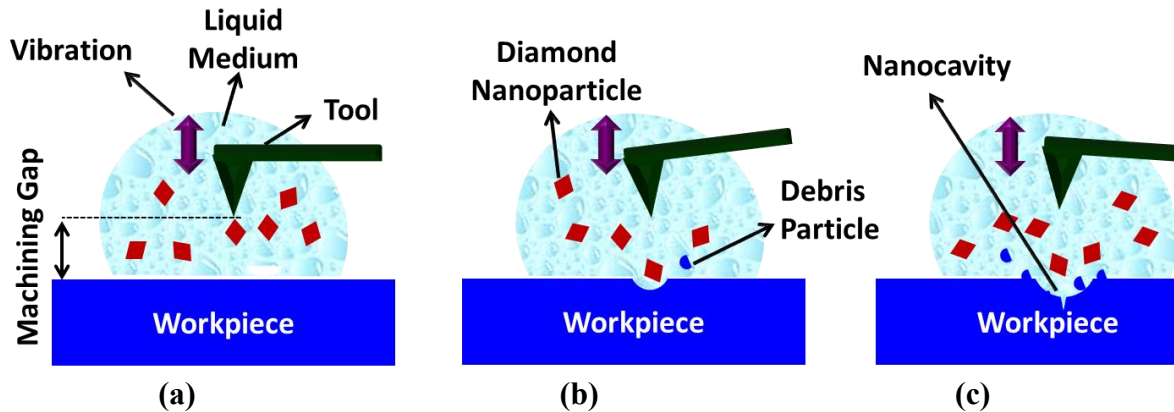
Figure 3.2: Schematic Diagram of the VANILA process a) Vibrating tool hammers the diamond nanoparticles b) Nanoparticle impact the workpiece surface causing material removal c) Repeated impacts of diamond nanoparticles resulting in Nanocavity formation on workpiece surface [134]

3.2 Feasibility model

Analytical studies of VANILA process has been studied based on fracture models, indentation models, impact models, erosion studies etc. Theoretical model based on Hertzian impact theory have been developed and suggests that the process is capable of nanomachining hard and brittle materials. The mathematical model developed to predict the feasibility of VANILA process is described in this section.

3.2.1 Assumptions

The simplification assumptions are listed below:

1. Earlier studies on a closely related process (indentation) report that impact by blunt indenters result in elastic deformation, while impact by sharp indenters cause plastic damage [82, 135]. Thus the shape of the abrasive grain is expected to affects the mode of material removal. Though impacting abrasive grains will not normally be spherical, self-impacts prior to impingement onto the workpiece surface will generally reduce them to a roughly spherical shape [136]. Therefore, for simplification, effect of non-sphericity is not considered in this model and all diamond abrasive particles are assumed to be identical spheres.

2. The tool tip and abrasive particles are considered to have equal hardness, while the workpiece is softer than the abrasive particles.

3. The collision between tool tip and abrasive particles is considered to be perfectly elastic.

4. The abrasive particle and the workpiece surface while in contact are frictionless and non-conforming i.e., the workpiece surface, being softer than abrasive grains, deforms while in contact. The abrasive particles do not undergo any shape change and the particles remain intact throughout the machining process.

5. The workpiece is assumed to be stationary before and after the impact of the abrasive particles.

6. Energy loss due to the presence of liquid medium is neglected. The dynamic behavior of abrasive grain motion in fluid medium and its impact on the workpiece surface could be possibly affected by several variables such as instantaneous fluid velocity, fluid viscosity and temperature [84]. The effect of liquid medium and subsequent energy loss due to drag would make the theoretical model closer to the actual process. However, this is beyond scope of this section and hence not considered in the model developed here.

7. *Abrasive* grains impacts perpendicularly (impact angle α= 90°) onto the workpiece surface. Studies show that the nature and extent of damage due to solid particle impact depends on the angle of particle impingement [84]. In VANILA process, the tool tip could strike the particles on the workpiece surface at an angle which is not necessarily perpendicular to the workpiece surface, but at an inclined angle. The simplest case of particle striking in perpendicular direction [84] is considered in the model developed here.

8. The workpiece is not atomically flat and its surface is assumed to have flaws at nanoscale.

3.2.2 Mathematical Model for verifying the Feasibility of the process

The material removal in VANILA process consists of several simultaneous collisions as depicted in Figure 3.2. Initially, the tool probe which is vibrating at high frequency impacts with the loosely suspended abrasive grains (Impact 1). This collision imparts kinetic energy to the abrasive grains which are in the machining zone. The abrasive grains with high kinetic energy then impacts the workpiece surface (Impact 2).

Impact modeling is often very difficult because impact is a complex physical phenomenon, characterized by very short duration of contact, high force levels reached, rapid dissipation of energy and large accelerations and decelerations [137]. The dynamic analysis of VANILA process is done based on the assumption that the process can be considered as discrete and that a single impact event of abrasive grain with the workpiece surface is a good understanding of the complex phenomenon of material removal due to impact damage. The VANILA process can be modeled using a simplified approach consisting of separating the effects due to the operative variables. Variables affecting the material removal in VANILA process can be broadly classified

into three categories: tool tip, abrasive grain variables and workpiece material variables as listed in Tables 3.1, 3.2 and 3.3. The following are the nomenclature used in modeling VANILA Process.

3.2.2.1 Impact 1- Impact between tool and abrasive particles

Assuming zero phase for cantilever vibration, the dynamic motion of the tool can be written as $a_t e^{i\omega t}$ [138] where a_t is the amplitude and ω is the angular frequency of vibration of the tool tip. The maximum velocity of the tool tip (V_{t1}) immediately before tip/abrasive grain impact can be expressed as [139]

$$V_{t1} = \omega * A_t = 2\pi f_t a_t \tag{3.1}$$

The tool tip and abrasive grain are made of same material and thus the impact between tool tip and abrasives is considered to be perfectly elastic collision. For a perfectly elastic collision, both momentum and kinetic energy are conserved [140]. Conservation of momentum and kinetic energy can be expressed by equations (3.2) and (3.3) respectively.

$$m_t V_{t1} + m_a V_{a1} = m_t V_{t2} + m_a V_{a2} \tag{3.2}$$

$$0.5 m_t V_{t1}^2 + 0.5 m_a V_{a1}^2 = 0.5 m_t V_{t2}^2 + 0.5 m_a V_{a2}^2 \tag{3.3}$$

where V_{a1} and V_{a2} are the velocities of abrasive particle before and after collision. V_{t2} is the velocity of the tool after collision.

The abrasive particle is considered to be stationary before collision with tool. Hence,

$$V_{a1}=0 \tag{3.4}$$

Also, while solving for V_{a2}, $m_a{}^2$ may be neglected as m_a is very small. Therefore,

$$V_{a2} = 2V_{t1} \tag{3.5}$$

From equation (3.1),

$$V_{a2} = 4\pi f_t a_t \tag{3.6}$$

3.2.2.2 Impact 2 – Impact between abrasive particles and workpiece surface

This collision involves impacts of accelerated nanoparticles on the surface of brittle workpiece. This process has close resemblance to the macroscale erosion process of brittle materials as a result of impact of solid particles which is extensively studied for many years [141]. Damage or material removal in brittle materials as examined by several investigators in great detail, is found to happen in three regimes – Elastic regime (Hertzian cone cracks), Transition zone of elastic-plastic regime, Plastic regime - depending on several impact parameters in the regime [75].

While damage in plastic regime is strongly influenced by material hardness (H), the Hertzian fracture (elastic regime) is primarily governed by the material's critical stress intensity factor or fracture toughness (K_C) [75]. The damage in the elastic-plastic transition regime is governed by a combination of variables such as material hardness (H), fracture toughness (K_C) and with the sphere (abrasive grain) diameter (d_a) [75].

The impacting of brittle material surface by small abrasive grains can lead to strength degradation and consequent material damage caused by fracture and crack formation [136]. Depending on factors such as impact velocity of the abrasive grains, thickness of workpiece material and size of existing flaws on the workpiece surface, the fractures can be classified as

Hertzian ring cracks (with or without conical fractures), median, radial and lateral cracks and in some cases star cracks [142]. The AFM tool tip speed (V_{t1}) during VANILA process is of the order of less than 1 m/s [143] and thus the speed of abrasive grain just before impact on the workpiece surface is low enough for the consequent fracture to be considered as Hertzian cone cracks [142]. The system can thus be analyzed in terms of the fundamental Griffith theory of fracture for elastic-brittle solids wherein a pre-existing crack propagates into a characteristic cone in accordance with the requirements of an energy balance condition [144].

3.2.2.3 Feasibility Criteria

Maximum force (P_m) generated during the impact of the abrasive particle and the workpiece surface can be expressed as [136]

$$P_m = \left[\left(125\pi^3/48 \right)^{1/5} \left(E_w/k \right)^{2/5} \rho_a^{3/5} \left(d_a/2 \right)^2 \right] V_{a2}^{6/5} \tag{3.7}$$

where k is the elasticity constant given by $k = \frac{9}{16} \left[(1 - v_a^2) + (1 - v_w^2) \frac{E_w}{E_a} \right]$ (3.8)

Using equation (3.6), the maximum force applied on the workpiece surface becomes

$$P_m = 7.56 * \left(E_w/k \right)^{2/5} \rho^{3/5} d_a^2 (f_t * a_t)^{6/5} \tag{3.9}$$

Critical load P_c for crack growth can be calculated using Auerbach's law [145] and Griffith energy balance condition [146] where [82]

$$P_c = K_C^2 \phi \frac{d_a}{2} k / E_w \tag{3.10}$$

where ϕ is a dimensionless material constant whose value is obtained experimentally [144] and K_C is the fracture toughness of the workpiece material.

When this critical value (P_c) is exceeded, strength degradation can occur [136] and consequent development of Hertzian cone cracks [147].   In order to understand the significance, the analytical model is tested on following hard and brittle materials: Soda-lime glass, Silicon, Borosilicate glass (Pyrex), SiO_2, Silicon Carbide and Zirconia. In this theoretical study, the abrasives used are diamond nanoparticles of 10 nm size and the value of the dimensionless material constant is taken as $5*10^{-5}$ [144]. The impact parameters along with the results of the feasibility calculations are shown in Tables 3.1, 3.2 and 3.3.

Table 3.1: Impact Parameters – Tool Tip Vibration Parameters [133]

	Resonance Frequency f_t (KHz)	Amplitude a_t (nm)	Velocity V_t (m/s)
Tool Tip Vibration	10	200	0.02512

Table 3.2: Impact Parameters – Abrasive Grain Material Properties [133]

Abrasive Grain Material	Poisson's ratio v_a	Young's Modulus E_a (N/m^2*10^{10})	Diameter d_a (nm)	Density ρ_a (Kg/m^3*10^3)
Diamond	0.07	114	10	3.5

Table 3.3: Impact Parameters – Workpiece Properties and Feasibility Study Results [133]

Workpiece Material	Poisson's ratio	Elastic Modulus	Fracture Toughness	Max. Load	Critical Load	Feasibility
	ν_w	E_w (N/m^2* 10^{10})	K_c (MPa*m$^{1/2}$)	P_{max} (N*10^{-12})	P_c (N*10^{-12})	
Soda-lime glass	0.22	7.07	0.74	1.573	1.148	**Yes**
Silicon	0.3	18.8	0.7	2.25	0.4197	**Yes**
Borosilicate glass (Pyrex)	0.198	6.27	0.63	1.503	0.9328	**Yes**
SiO$_2$	0.167	7.25	0.79	1.587	1.2794	**Yes**
Silicon carbide (SiC)	0.17	45.47	2.8	2.972	3.352	**No**
Zirconia	0.25	21	6	2.334	2.8152	**No**

3.3 Experimental Verification

The experimental setup to conduct the feasibility study of VANILA process is shown in Figure 3.3. VANILA process is conducted using a Dimension 3100 Atomic Force Microscope (AFM) with Nanoscope IIIa controller. The workpiece is placed in a machining cell and introduced between the AFM probe head and AFM sample holder plate. The probe used for machining is a Silicon Nitride tapping mode probe having a tip radius of 50 nm. A direct drive fluid cantilever holder (DDFCH) is used while conducting the machining.

The tool is vibrated at a frequency which is slightly less than its resonant frequency, typically in the range of 3-12 KHz. Figure 3 shows typical drive amplitude vs. frequency graph during the cantilever tuning. Nano diamond grains of 10 nm size are used as the abrasive material which is mixed with deionized water to form slurry. The slurry of diamond grains is introduced on the workpiece surface using a syringe before machining process.

Theoretical predictions listed in Table 3 reveal that VANILA process is feasible for Soda-lime glass, Silicon, Borosilicate glass and Silicon dioxide for the experimental conditions used in this study. Among them, single crystal silicon wafers (type 100) of rectangular shape with sharp corners is chosen as the work material in this feasibility study. The experimental conditions used are shown in Table 3.4.
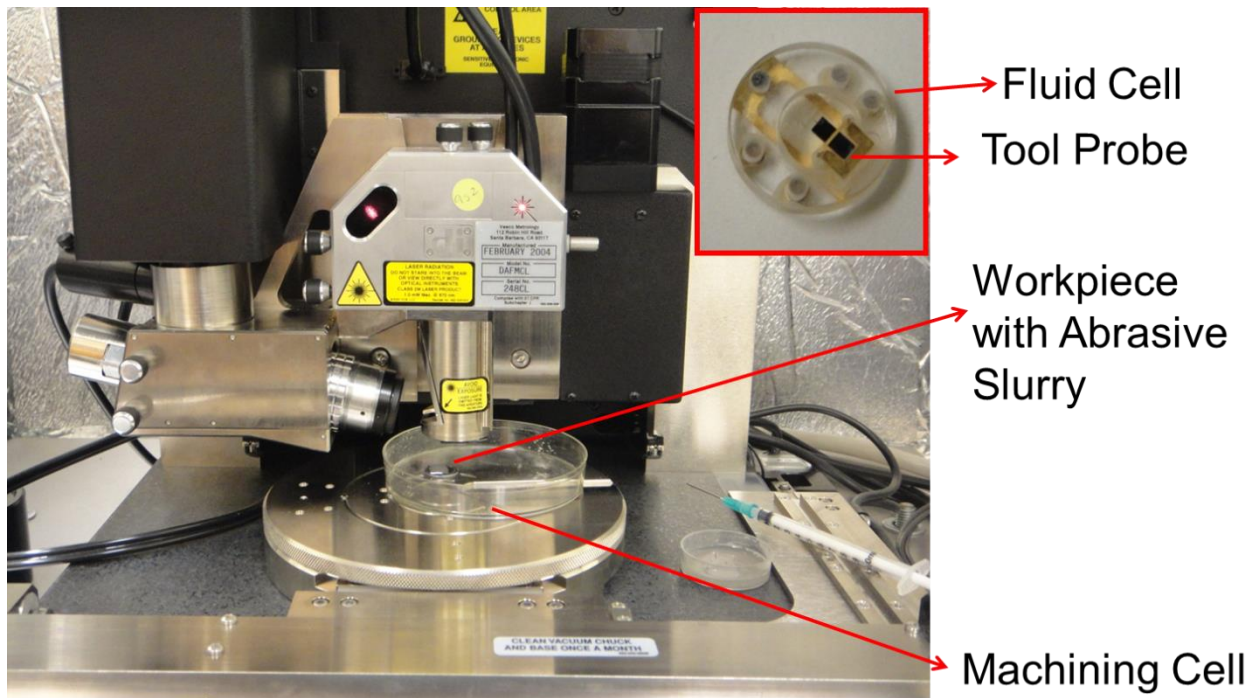
Fig 3.3: Experimental Setup (Inset: Fluid Cell) [133]

Table 3.4: Experimental Conditions for Feasibility study [133]

Workpiece Material	Single Crystal Silicon (Type 100)
Machine	AFM Dimension 3100
Abrasive	Diamond Particles less than 10 nm radius
Probe Used	NSC 19/50 (Micromasch) Tip Radius 10nm Resonant Frequency in air 161 KHz Spring Constant 40 N/m Probe Material – Silicon Nitride (Uncoated)
Liquid Medium	Deionized water

Initially the silicon wafer is cleaned repeatedly with acetone, dried using dry air and placed firmly in the machining cell. Target surface details before machining are acquired by scanning the sample in air in tapping mode. The machining spot is identified along with its distance from the corner points and sides in order to facilitate locating the machined nano features during post-machining scans. Then the scanning probe is replaced with the tool probe which is placed in the probe holder (DDFCH) and using a syringe, a slurry mixture of deionized water and diamond nano particles is introduced between the tool probe and the sample. The machining is done in tapping mode while the tip is raised by about 100- 200 nm to avoid direct contact with the workpiece surface. Once the machining is done, the sample along with the machining cell is removed, cleaned thoroughly in an ultrasonic cleaner (Branson 5510MT) using acetone and dried

in air. The machined sample is placed on the AFM and the machined area is carefully located using navigation screen (available in Nanoscope IIIa software) along with the previously recorded information of the distances from corner points and sides and then scanned using the scanning probe to obtain details of the machined features. Figure 3.4 shows a single nano-cavity (1) of circular shape (diameter 102.3 nm and depth 63.7 nm) machined on Silicon substrate a duration of 20 seconds. Figure 3.5 shows another single nano-cavity (2) with diameter 100 nm and depth 150 nm.

3.3.1 Pattern Machining

To examine the repeatability and controllability aspect of VANILA process, nano-cavity patterns are machined. Figure 3.6 shows AFM images of a pattern of nano-cavities machined through VANILA process for duration of 20 seconds per cavity. The pattern design with 8 cavities (numbered A-H) and the sequence of machining is shown in Figure 3.6c. The resultant machined pattern (Pattern 1) has cavity depths ranging from 5-42 nm and diameters ranging from 78-276 nm as shown in Table 3.5. The distance between two consecutive cavities ranged from 3-6 μm while the goal was to create cavities with a spacing of 5 μm. To further confirm the repeatability and controllability of VANILA process, a second pattern (Pattern 2) is machined with 4 cavities (numbered A-D) machined for 20 seconds as shown in Figure 3.7a according to design shown in Figure 3.7d. The cavities obtained in pattern 2 have depths ranging from 16-38 nm and diameters in the range of 101-221 nm with inter-cavity spacing ranging from 3.6-5 μm as shown in Table 3.6.

38
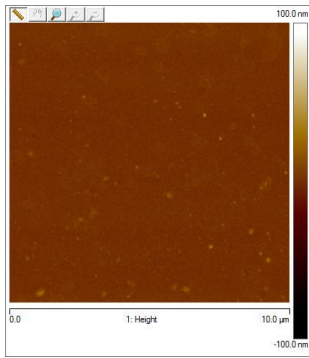
(a) Workpiece surface before VANILA Process
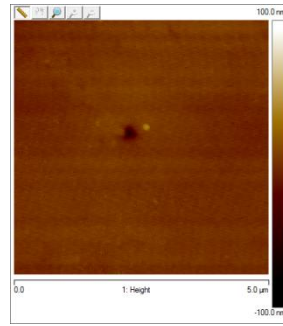
(b) Workpiece Surface after VANILA Process showing nano-cavity
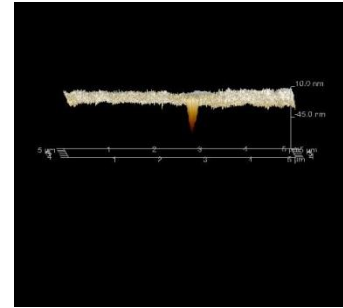
(c) 3-Dimensional View
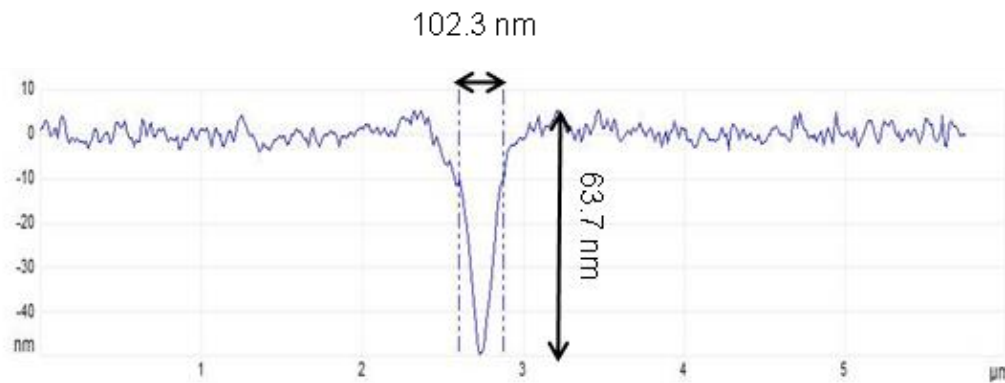
(d) Section Plot of the nano-cavity

Fig 3.4: AFM images of nano-cavity (1) machined through VANILA Process (machining time 20 seconds) [133]
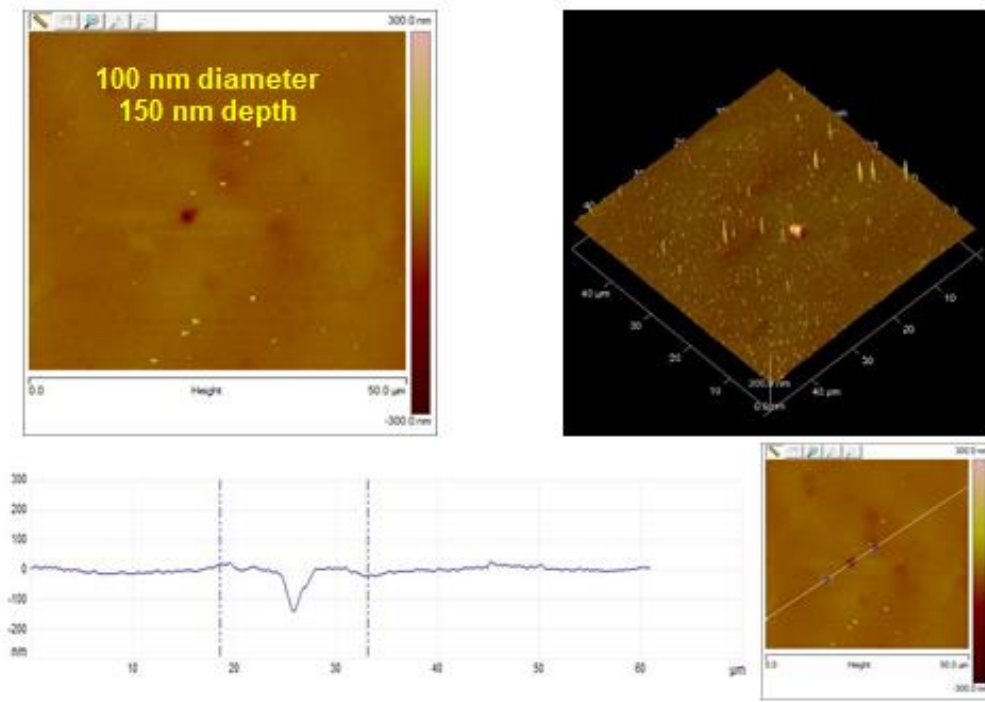
Fig 3.5: AFM images of nano-cavity (2) machined through VANILA Process (machining time 20 seconds) [133]
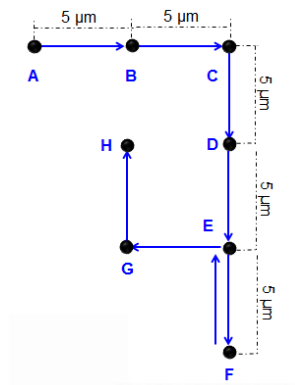
(c) Pattern Design
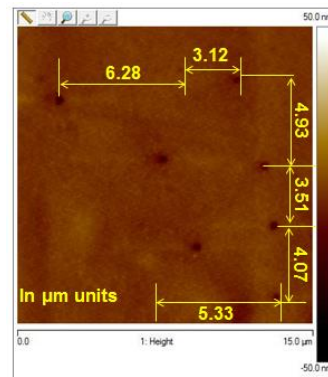
(d) Pattern of Nanoholes through VANILA Process

Fig 3.6: Topography of nanocavities (Pattern 1) [133]

Table 3.5: Dimensions of nanocavities of pattern-1 machined through VANILA process

[133]

Cavity Number	Diameter (nm)	Depth (nm)
A	275.7	35.3
B	78.5	6.8
C	110.3	17.6
D	246.6	22.4
E	223.4	28.7
F	165.4	4.8
G	198.8	41.4
H	220.6	40.6
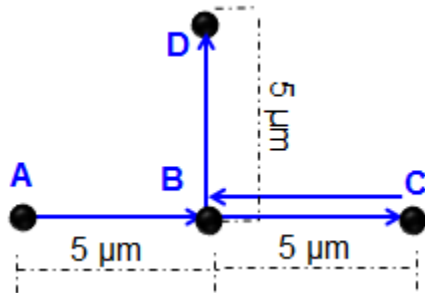
(d) Pattern Design
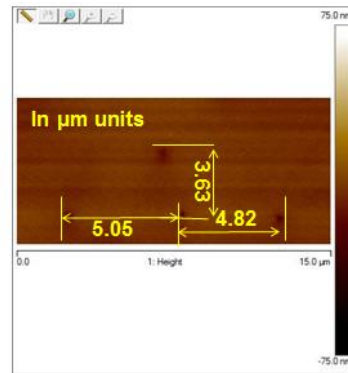
(e) Pattern of Nanoholes through

VANILA Process

Fig 3.7: Topography of nanocavities (Pattern 2) [133]

Table 3.6: Dimensions of nanocavities of pattern-2 machined through VANILA process

[133]

Cavity Number	Diameter (nm)	Depth (nm)
A	220.5	37.5
B	101.9	21.8
C	180.4	30.6
D	123.1	16.2

Chapter Summary

- Vibration Assisted Nano Impact-machining by Loose Abrasives (VANILA) that combines the principles of vibration-assisted abrasive machining and tip-based nanomachining is introduced in this work to perform target specific nano abrasive machining of hard and brittle materials.

- An analytical model based on Hertzian fracture theory is developed to evaluate the feasibility of the process for different workpiece materials.

- The feasibility of the VANILA process is experimentally verified on single crystal silicon substrate using a commercially available AFM. Nano-cavities with circular shape having depths (in the range of 6-64 nm) and diameters (in the range of 78-276 nm) are achieved.

- Patterns of nano-cavities are successfully machined to verify the controllability and repeatability aspect of the process.

Chapter 4: Material Removal Rate Studies

The objective of this chapter is to grain fundamental understanding of the material removal rate (MRR) of the VANILA process. The VANILA process machining consists of a vibrating tool, suspended nanoparticles and a workpiece which undergoes a series of impacts. MRR of the process would depend on the material properties as well as the process parameters. Before modeling the MRR of the process, it is therefore important to understand the effects of critical process parameters on the events leading to nanoparticle impacts and subsequent material removal. Since the nanoparticle is suspended in liquid medium, the behavior of nanoparticle, its dynamics and the energy loss in the liquid medium are of prime interests. Thus in the first part (4.1) of this chapter, a detailed study is conducted to understand the dynamics of the nanoparticle in the VANILA process. In the second part (4.2), the MRR of the process is modeling and experimentally verified.

4.1 Study on the Vibration Induced Transport of Nano Abrasives in Liquid Medium

Understanding the transport of diamond nanoparticles in fluid is essential to determine the effective gap between the tool and the work surface in VANILA process. In this section, various forces acting on the abrasive nanoparticle in aqueous slurry are analyzed.

The material removal during the VANILA process is happening due to the impacts of the sharp nano abrasive particles on the workpiece surface[81]. This section investigates the *forces involved* in the transport of nanoparticle in liquid to estimate the velocity of impact of the nanoparticle on the workpiece surface and determine the effective gap between the tool and the

work surface for the given machining conditions. A theoretical approach is used to model the nanoscale forces and predict the velocity and penetration depth of the nanoparticle within the liquid medium and the model is verified using a 3-D molecular dynamics simulation (MDS).

4.1.1   Prediction of nanoparticle velocity and penetration depth in liquid medium

During the VANILA process, diamond nanoparticles are dispersed in the liquid and the vibration of the tool at resonance introduces an acoustic field into the slurry medium [148, 149] which leads to movement of the nanoparticles. The combination of various forces experienced by the abrasive nanoparticle determines its motion towards the workpiece surface. Thus, to predict the behavior of the nanoparticle in suspension passing through an acoustic field, the forces experienced by the particle need to be quantified. Since the derivation of exact expressions for the forces acting on the nano abrasive particle during the machining process is too difficult and beyond the scope of this study, an order-of-magnitude estimates of the individual forces acting on the nanoabrasive grains are considered to determine their degree of influence.

4.1.2 Analysis of forces on the nanoparticle in liquid medium

Several nanoscale forces could arise due to the relative motion and also the size effect of the nano diamond abrasive grains moving within the liquid medium. The forces that could influence the motion of the abrasive nanoparticle have been identified as: Tool impact force, Acoustic Radiation Force, Acoustic Streaming Forces, Gravity force and Brownian force [150, 151]. Several other nanoscale forces such as Inertial forces, Thermophoresis, Hydrophobic effects, Van der Waals force, Electrostatic force, Casimir force and Molecular surface forces are not considered in this study as they are less significant. The modeling of individual forces is described below.

4.1.2.1 Tool Impact Force

The tool used in the VANILA process is a tapping mode AFM probe which consists of a cantilever with a conical tip having a nanoscale radius. The tool is acoustically driven by a piezoelectric element at the fundamental resonant frequency of the tip. The oscillatory motion of tool tip used in the VANILA process can be expressed as $A_t e^{i(\omega t + \pi/2)}$ as shown in figure 4.1. The phase associated with the total force is considered as $\pi/2$ due to the fact that machining is conducted at resonance frequency and since on resonance the oscillations of the cantilever follow the total force with a phase delay of $\pi/2$ [138]. The drive force will generate acceleration *(a$_t$)* at the tool tip perpendicular to the workpiece surface, resulting in impact onto particles coming into contact with the tool tip. This tool impact force *(F$_T$)* can be estimated as [152]

$$F_T = m_a a_t \tag{4.1.1}$$
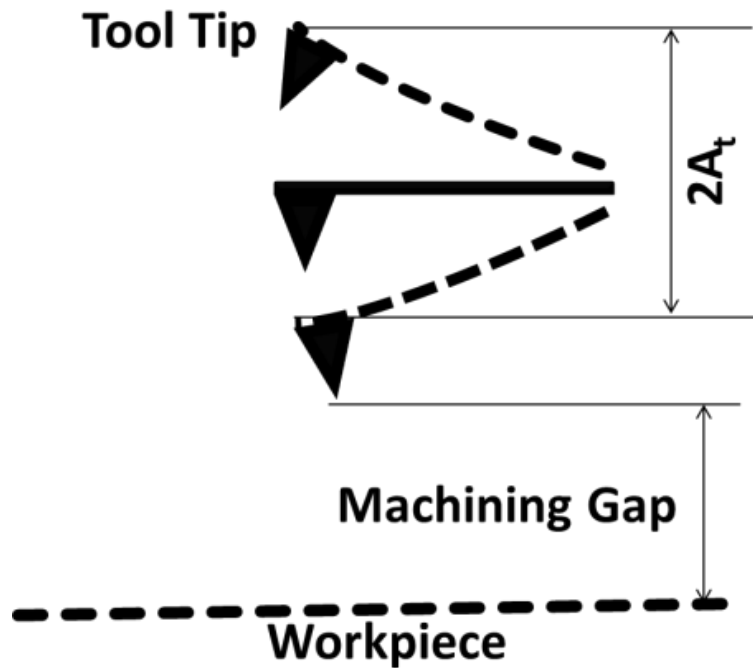
Figure 4.1: Tool Tip Dynamics during the VANILA Process [134]

As a general rule, nanoparticles having very small aspect ratio (< 2) can be considered as spherical for nanoscale force calculations. Thus, for a single particle having radius R_a, the mass of the abrasive particle m_a can be written as

$$m_a = \frac{4}{3}\pi R_a^3 \rho_a \tag{4.1.2}$$

Thus the equation below shows the maximum acceleration (a_t) at the tool tip

$$a_t = 4\pi^2 f_t^2 A_t \tag{4.1.3}$$

The resonating tool tip produces an acoustic power that can be calculated as [104]

$$P_t = \frac{\pi k_t A_t^2 f_t}{Q_t} \tag{4.1.4}$$

The intensity of vibration of acoustic waves created at tool tip can be estimated as the ratio of the acoustic power to the surface area [153].

$$I_t = P_t \Big/ (\pi R_t^2) \tag{4.1.5}$$

4.1.2.2 Acoustic Radiation Force

The mechanical vibration of the tool in the vicinity of the slurry could generate acoustic waves in the bulk of the nanofluid slurry, thus transmitting acoustic radiation through the slurry. The acoustic radiation leads to momentum transfer between the neighboring particles and consequently, every single nano abrasive grain starts to oscillate about its mean position at driving frequency. These acoustic radiation forces (F_R) affect the motion of the nanoparticles in the vicinity of the tool. The acoustic radiation force instantaneously drives the nano abrasive particles near its vicinity towards the workpiece surface with a unidirectional displacement

[154]. For particles much smaller than the wavelength of acoustic waves as in the case here, the acoustic radiation force acting on the particles can be estimated using King's [155] expression as [150],

$$F_R \sim 64\rho_{fl}\left(\frac{2\pi f t}{c}\right)^4 R_a^6 V_{fl}^2 \left[\frac{1+\frac{2}{9}\left(1-\left(\rho_{fl}/\rho_a\right)^2\right)}{\left(2+\rho_{fl}/\rho_a\right)^2}\right]$$ (4.1.6)

4.1.2.3 Acoustic Streaming

Acoustic streaming is a steady current in a fluid driven by the absorption of high amplitude acoustic oscillations[156]. During the VANILA process, resonating tool tip within the fluid medium generates acoustic streaming in the form of strong recirculating vortices near the tool tip as displayed in figure 4.2. The phenomenon of acoustic streaming is most efficient when the tool tip is excited at its resonance frequency with sufficiently high drive amplitude[157]. There are possibly two major counter-rotating streaming vortices which are generated around the tool tip along the axis of vibration [158-160] which causes nanoparticles to impact on the workpiece with high velocity as shown in figure 5a.
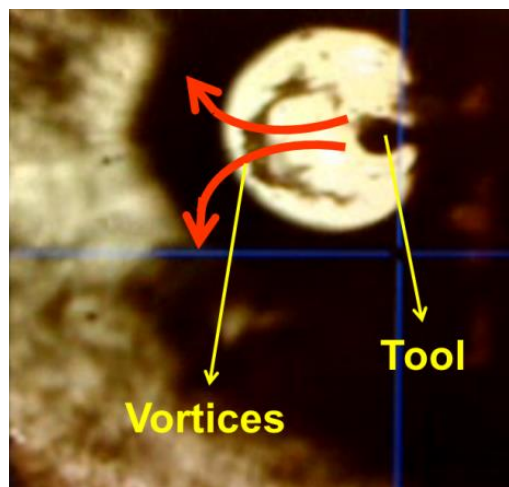
Figure 4.2: Vortices generated at near the tool tip during the VANILA process [134]

a) *Drag Force due to Acoustic Streaming (F_S)*

The acoustic streaming motion around the tool tip results in drag force caused by interaction between the fluid and the abrasive nanoparticles. This drag force carries the nanoparticles on to the workpiece surface as depicted in figure 4.3a. In laminar regime, the drag force due to acoustic streaming can be determined using the Stokes Formula which is also applicable for nanofluids[161]. The magnitude of this force is proportional to the particle's relative velocity and can be calculated as [162]

$$F_S = 6\pi\mu_{fl}R_a(V_{fl} - V_a) \tag{4.1.7}$$

where V_{fl} is the instantaneous fluid particle velocity which be estimated using the relation [150]

$$V_{fl} = \left[I_t / \rho_{fl} c \right]^{1/2} \tag{4.1.8}$$

b) *Acoustic Cavitation Force*

Acoustic cavitation refers to the formation of small bubbles and their subsequent growth and collapse within the liquid due to pressure change because of acoustic excitation [163]. During the VANILA process, the abrasive nanoparticles act as pre-existing nucleation sites [164] which require less energy to develop into bubbles and cause transient cavitation[165]. Shock waves are generated due to the implosive collapse of these instable bubbles, causing the nanoparticles to be driven at extremely high speeds as shown schematically in figure 4.3b. The acoustic cavitation force can be calculated as[166]

$$F_C = \pi P_C R_a^2 \qquad\qquad (4.1.9)$$

The nanoparticle gains the same velocity as that of the surrounding water molecules [167]. The abrasive grain velocity due to cavitation (V_C) can be approximated as [168]

$$V_C = {P_C}/{\rho_{fl} c} \qquad\qquad (4.1.10)$$

The oscillatory motion of the tool tip could result in vertical bending, lateral bending (figure 4.1), torsion and extension of the cantilever [169] which cause the axes of the vortices to be tilted from normal to the workpiece surface. The axis of the vortices would determine the eventual angle of impact of the nano abrasive grains on the workpiece surface. The impact angle is a critical factor which influences the material removal mechanism during VANILA process [81].

a) Acoustic Streaming   b) Acoustic Cavitation
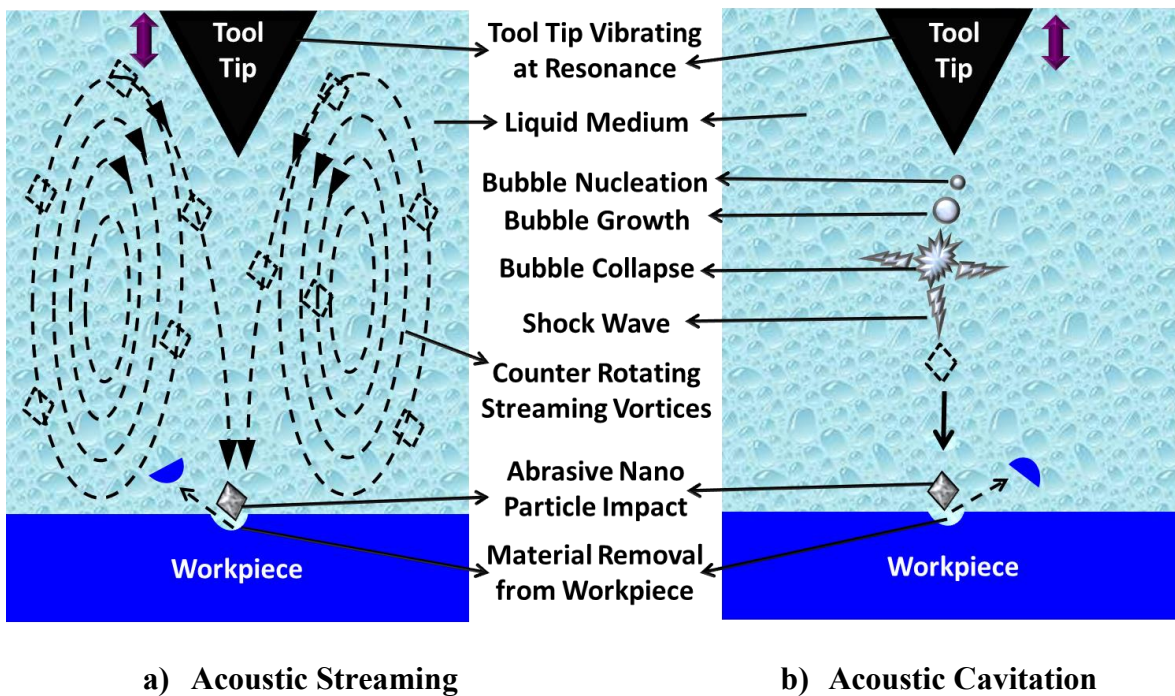
Figure 4.3: Acoustic Forces influencing Abrasive Nanoparticle Motion during VANILA Process [134]

4.1.2.4 Gravity Force

The gravity force F_G acting on the abrasive grain is proportional to its volume and the relative density of the grain and fluid [170].

$$F_G = -\frac{4\pi}{3}\left(\rho_a - \rho_{fl}\right)gR_a^3 \tag{4.1.11}$$

where g is the gravitational acceleration.

4.1.2.5 Brownian Force

Brownian motion is the random motion of the nanoparticles within the base fluid due to continuous collisions between the nanoparticles and the molecules of the base fluid[170]. On an average, the Brownian motion causes nanoparticles to vary in direction many millions of times per second [171]. Brownian motion is described by the Brownian diffusion coefficient, D_B, which is calculated using the Einstein-Stokes's equation[170, 172]:

$$D_B = \frac{k_B T}{3\pi\mu_{fl}R_a} \tag{4.1.12}$$

The Brownian force is a function of the Brownian diffusion coefficient D_B, surface area of the abrasive grain and the concentration gradient [170]. The Brownian force F_B can thus be expressed as

$$F_B = 4\pi\rho_a D_B R_a^2 V_B \nabla\phi \tag{4.1.13}$$

Where V_{Br} is the Brownian velocity which is a function of temperature and abrasive grain size

$$V_B = \frac{k_B T}{2\pi\mu_{fl}R_a^2} \tag{4.1.14}$$

4.1.3 Impact velocity of nanoparticle in liquid medium and penetration depth

The velocity of a single nano abrasive grain impinging onto the workpiece has two components; namely the velocity of nanoparticle originating from tool impact, and the velocity created by acoustic streaming – which includes acoustic cavitation and drag forces.

The equation of individual abrasive grain motion is given by

$$m_a \frac{dV_a}{dt} = -F_S \qquad (4.1.15)$$

$$m_a \frac{dV_a}{dt} = 6\pi\mu_{fl}R_a(V_{fl} - V_a) \qquad (4.1.16)$$

Solving the equation, the velocity of the abrasive grain can be calculated as below

$$\frac{dV_a}{dt} = \frac{6\pi\mu_{fl}R_aV_{fl}}{m_a} - \frac{6\pi\mu_{fl}R_aV_a}{m_a} \qquad (4.1.17)$$

$$\text{Let} = \frac{6\pi\mu_{fl}R_aV_{fl}}{m_a}, \beta = 6\pi\mu_{fl}R_a \quad \text{so} \quad {}^{\alpha}\!/_{\beta} = \frac{V_{fl}}{m_a} \quad \text{and} \qquad \frac{m_a}{\beta}\alpha = V_{fl} \qquad (4.1.18)$$

$$\frac{dV_a}{dt} = \alpha - \frac{\beta}{m_a}V_a \qquad (4.1.19)$$

$$\frac{dV_a}{\alpha - \frac{\beta}{m_a}V_a} = dt \qquad (4.1.20)$$

$$\frac{dV_a}{V_a - \frac{m_a}{\beta}\alpha} = -\frac{\beta}{m_a}dt \qquad (4.1.21)$$

$$\int_0^V \frac{dV_a}{V_a - \frac{m_a}{\beta}\alpha} = -\frac{\beta}{m_a}\int_0^t dt \tag{4.1.22}$$

$$\ln\left[V_a - \frac{m_a}{\beta}\alpha\right] - \ln\left[V_{a0} - \frac{m_a}{\beta}\alpha\right] = -\frac{\beta}{m_a}\Delta t \tag{4.1.23}$$

Boundary conditions, at t=0, $V_{a0} = V_T + V_C$

$$\ln\left[V_a - \frac{m_a}{\beta}\alpha\right] - \ln\left[V_T + V_C - \frac{m_a}{\beta}\alpha\right] = -\frac{\beta}{m_a}\Delta t \tag{4.1.24}$$

$$\ln\frac{\left[V_a - \frac{m_a}{\beta}\alpha\right]}{\left[V_T + V_C - \frac{m_a}{\beta}\alpha\right]} = -\frac{\beta}{m_a}\Delta t \tag{4.1.25}$$

$$V_a - V_f = \left[V_T + V_C - V_{fl}\right]\left[e^{-\frac{\beta}{m_a}\Delta t}\right] \tag{4.1.26}$$

$$V_a = V_{fl} + \left[V_T + V_C - V_{fl}\right]\left[e^{-\frac{\beta}{m_a}\Delta t}\right] \tag{4.1.27}$$

Replacing α and β terms and replacing $m_a = \frac{4}{3}\pi R_a^3 \rho_a$

$$V_a = \frac{m_a}{6\pi\mu_{fl}R_a}\frac{6\pi\mu_{fl}R_a V_{fl}}{m_a} + \left[V_T + V_C - \frac{m_a}{6\pi\mu_{fl}R_a}\frac{6\pi\mu_{fl}R_a V_{fl}}{m_a}\right]\left[e^{-\frac{6\pi\mu_{fl}R_a}{\frac{4}{3}\pi R_a^3 \rho_a}\Delta t}\right] \tag{4.1.28}$$

$$V_a = V_{fl} + \left[V_T + V_C - V_{fl}\right]\left[e^{-\frac{9\mu_{fl}\Delta t}{2\rho_a R_a^2}}\right] \tag{4.1.29}$$

where Δt is the duration of motion of the abrasive grain within the slurry.

In this study this distance is termed as *penetration depth* which is defined as the distance that the abrasive grain penetrates through the surrounding fluid after the impact from the tool and until its kinetic energy falls below 0.1 KeV, approximate impact kinetic energy required for nanoscale

material removal [133]. The theoretical penetration depth is determined as follows. The duration of motion (Δt) at which the kinetic energy falls below 0.1 KeV is estimated. The penetration depth is then calculated as the product of the average velocity (half of maximum abrasive velocity) and the duration of motion.

4.1.4 Prediction of impact velocity and penetration depth of nanoparticle in liquid medium for the given experimental conditions

The order of magnitude of the forces is estimated for the experimental conditions of the VANILA process. The abrasive used for the VANILA process is 10 nm sized diamond nanoparticles which is suspended in water slurry. The diamond material properties used are elastic modulus 1140 GPa, Poisson's ratio of 0.07 and density (ρ_a) = 3500 Kg/m^3 [173]. The tool used is commercially available tapping mode AFM probe which is made of silicon having a tip diameter of 10 nm. The tool is excited at its resonance frequency (5-50 KHz).

The tool impact force $F_T \sim R_a{}^3$ has a magnitude in the order of 10^{-5} pN (1 pN = 10^{-12} N) and the vibration intensity of the acoustic waves is $I \sim 0.9 \times 10^5$ W/m^2. The acoustic radiation force is $F_R \sim R_a{}^6$ and is negligibly small for the diamond nanoabrasive used in the experiments. The instantaneous fluid particle velocity is approximately in the range of 0.2-0.5 m/s. The drag force due to acoustic streaming $F_S \sim R_a$ is found to be in the range of 25-100 pN. To find the transient acoustic cavitation force, an estimate of the shock wave pressure due to bubble collapse is required. Shock wave pressure in the range of 100 MPa to 10^{4}MPa has been reported in for

acoustic cavitation in nanofluids [158, 174]. Taking the conservative value of 100 MPa for the shockwave pressure, the acoustic cavitation force $F_C \sim R_a^2$ in the order of 10^3 pN.

The gravitational force $F_G \sim R_a^3$ acting on the 10 nm sized diamond abrasive grain in water is negligibly small and hence not considered for velocity calculations. The Brownian force is a random force caused by the fluid particle collision on the nanoparticle. However, the continuous collisions of the fluid molecules on the nanoparticles do not have a preferred direction and hence the ensemble average of the random Brownian force vanishes [175].

Table 1 shows the summary of forces involved in the VANILA process along with their degree of influence. The maximum velocity of impact of the nano diamond abrasive grain during the VANILA process can be estimated using equation 2.2o. The collision time Δt is found to be 2×10^{-10} s for mean free path (λ) of 300 nm. Thus the approximate velocity of impact V_a of the nano abrasive grain is found to be in the order of 100-200 m/s. It is also estimated that the machining gap should be maintained less than 200 nm so that the impacting abrasive grain has sufficient kinetic energy to cause material removal.

Table 4.1: Forces Involved in the VANILA process [134]

Force Type	Model	Order of Magnitude
Tool Impact Force	$F_T = m_a a_t$	$\sim 10^{-5}$ pN
Acoustic Radiation Force	$F_R \sim 64\rho_f \left(\frac{2\pi f_t}{c}\right)^4 R_a^6 u_f^2 \left[\frac{1 + \frac{2}{9}\left(1 - \left(\rho_f/\rho_a\right)^2\right)}{\left(2 + \rho_f/\rho_a\right)^2}\right]$	Negligible
Drag Force due to Acoustic Streaming	$F_S = 6\pi\mu_f R_a(V_f - V_a)$	25-100 pN
Acoustic Cavitation Force	$F_C = \pi P_C R_a^2$	$\sim 10^3$ pN
Gravity Force	$F_G = -\frac{4\pi}{3}(\rho_a - \rho_f)g R_a^3$	Negligible
Brownian Force	$F_B = 4\pi\rho_a D_B R_a^2 V_B \nabla\phi$	Vanishes

4.1.5   Verification Using Molecular Dynamics Simulation

The molecular dynamics simulation (MDS) is used in this study to verify the predicted impact velocity and penetration depth of nanoparticle in liquid medium. The tool tip vibrates continuously and repeatedly impacts the diamond nanoparticles suspended in water to provide the motion of a single diamond abrasive grain moving in a droplet of water with a starting velocity. The study aims to understand the interaction forces between the diamond nanoparticle and the water molecules in the nanofluid, thereby determining the penetration depth of the nano abrasive grain in water. In these MDS studies, a three-dimensional MD simulation model has been implemented using LAMMPS [176] to determine the impact velocity and the appropriate machining gap to be maintained between the tool and the workpiece.

In order to determine the impact velocity and the machining gap, the MDS study considers a vibrating tool and a spherical abrasive grain within the simulation box. The tool is made of silicon and is conical in shape consisting of approximately 20,000 atoms and is vibrating in the z-direction. The diamond abrasive grain consists of carbon atoms (lattice constant 3.57 Å) within a rigid sphere of specified radius. Periodic boundary conditions are used along x, y and z axes. Tersoff potential is used to describe the interactions between the tool and the abrasive grain. Numerical integration is performed using the Velocity Verlet integration algorithm with a timestep of 1 picosecond (1.0×10^{-15} s) for simulation duration of 1 nanosecond. The tool temperature is maintained by rescaling the temperature after every 10 timestep. Energies and other particle information were recorded every 10 timestep. The simulation conditions used to determine the machining gap are listed in table 4.2. The schematic of the MD simulation model is depicted in figure 4.4.
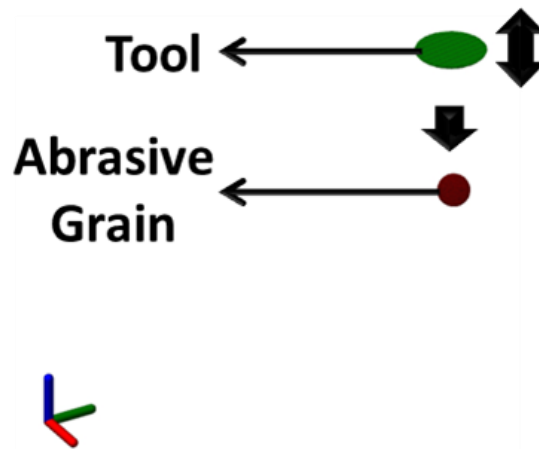
Figure 4.4: Schematic of Molecular Dynamics Study of Abrasive Grain Motion [134]

Table 4.2: MDS Conditions for VANILA process Abrasive Grain Motion Study [134]

Tool	Material	Silicon
	Shape and Size	Cone Tip Radius 20 nm
	No. of Atoms	20,000
Abrasive Grain	Material	Diamond Carbon
	Size and Shape	Sphere Radius (5-20 nm)
	No. of Atoms	160,000
Simulation Conditions	Potential Used	SiC.tersoff
	Temperature	300 K
	Time step	1 ps
	Duration	1 ns

The abrasive grain is given an initial velocity in negative z-direction which is equivalent to the acoustic cavitation velocity as estimated from the theoretical modeling. The tool impacts the abrasive grain which gains kinetic energy. The viscous drag effect of water on the abrasive grains is considered using a Langevin thermostat which maintains a temperature of 300 K. The Langevin thermostat considers the viscous drag force F_{drag} using a user specified damping factor term *'damp'*. F_{drag} is proportional to the particle's velocity and is calculated as following

$$F_{drag} = -\gamma V_a \tag{4.1.30}$$

where γ is the proportionality constant termed as damping coefficient and is computed as

$$\gamma = 6\pi\mu_{fl}R_a \tag{4.1.31}$$

'damp' is inversely proportional to γ and is related as

$$\gamma = {}^{m_a}\!/_{damp} \qquad (4.1.32)$$

where m_a is the mass of the abrasive grain. After the impact with tool, the kinetic energy of the abrasive grain increases and penetrates into the bulk water. However, due to viscosity, drag force absorbs the kinetic energy of the grain and the grain continues to move with the fluid. The VANILA process is feasible only if the workpiece is placed within a distance at which the abrasive grain still have sufficient kinetic energy to cause material removal. To understand the effect of abrasive grain on the penetration depth, the motion of a range of abrasive grains between 5nm to 20 nm are analyzed with a tool vibration frequency of 10 KHz. Figure 4.5 shows the initial and final (after 1 ns) positions of the tool and the abrasive grain.

(1a)　　　　　　　(1b)　　　　　　　(1c)　　　　　　　(1d)

(2a)　　　　　　　(2b)　　　　　　　(2c)　　　　　　　(2d)
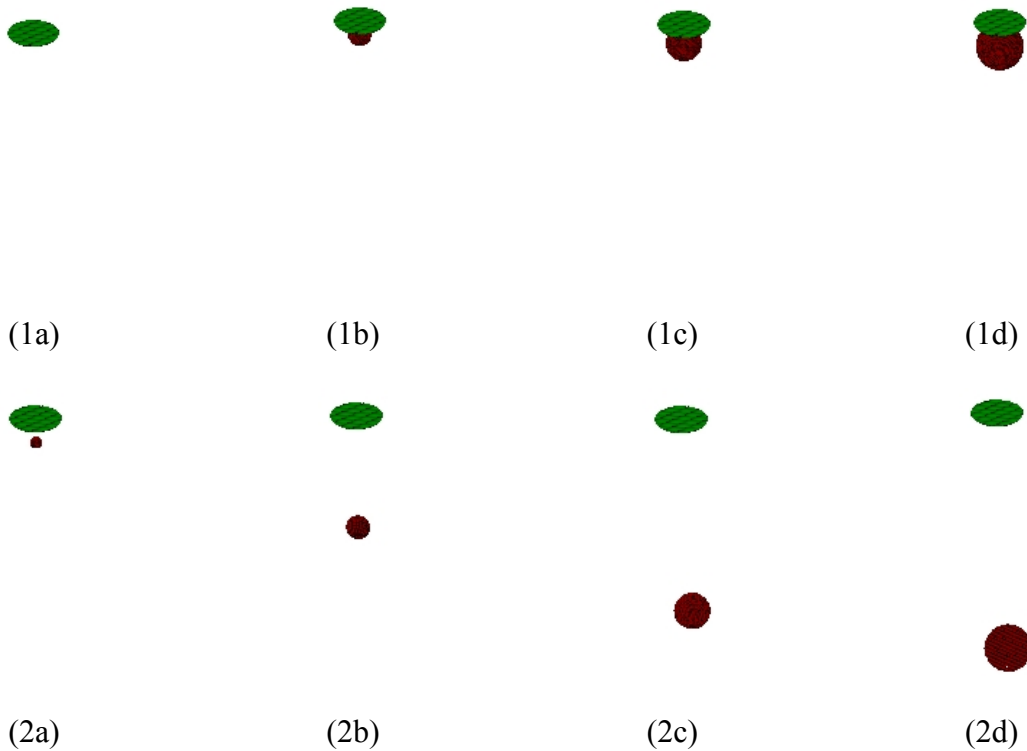
Figure 4.5: Results of MDS of Effect of Abrasive Size on Penetration Depth 1) Initial position and 2) Final position for Grain Sizes a) 5 nm b) 10 nm c) 15 nm d) 20 nm [134]

The results of this MDS study are compared with the results obtained using the previously discussed theoretical model as shown in figure 4.6. From the results it is seen that the penetration depth increases with the size of the abrasive grain. This can be explained by the fact that energy gained by the abrasive grain due to the interaction with the tool increases with the size of the abrasive, at the same time, the increase in viscous drag force is not considerably higher and hence the grain is able to penetrate larger distances. It is seen that for the size range of abrasive grains considered in this study, the workpiece should be placed within a machining gap of 200 nm for machining to happen.
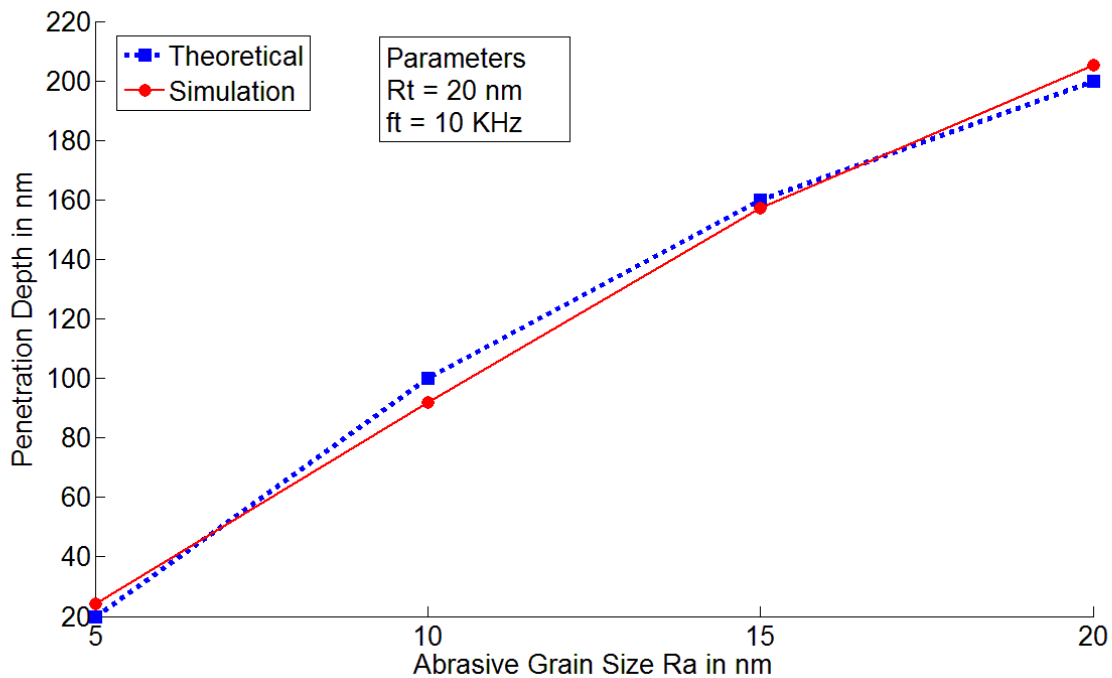
Figure 4.6: Comparison of Theoretical and MDS study results on the Effect of Abrasive Grain Size on Penetration depth [134]

4.2 Study of the Material Removal Rate

This study aims to construct an analytical model to find the material removal rate (MRR) in the VANILA process. The experimental machining results reveal that the material removal mainly happens due to plastic deformation. A model for estimating MRR during the VANILA process is developed based on elasto-plastic impact theory for vertical impacts. The model is validated through a series of experiments which verifies that the model is capable of predicting the machining results within 10% error.

4.2.1 Motivation for MRR Study

The material removal rate (MRR), defined as the volume of workpiece material removed per unit time, is one of the most important quantities for a machining process [177, 178]. To exploit the potentials of VANILA process for use in industrial applications, the MRR of the VANILA process has to become more efficient and predictable. In this section, analytical models to predict the MRR in the VANILA process are developed. The model is established as a function of the impact parameters and material properties which affect the material removal process.

Experimental results reveal that the material removal during the VANILA process happens primarily in ductile mode due to repeated impacts of the abrasive grains. Representative cross-sectional images of nanocavities machined on silicon and borosilicate glass are shown in Figure 4.7 a and b respectively. There are no noticeable ridges or pile-ups near the edges of the nanocavities. It could be also possible that the pileups at the edges of the cavities are removed by repeated impact.
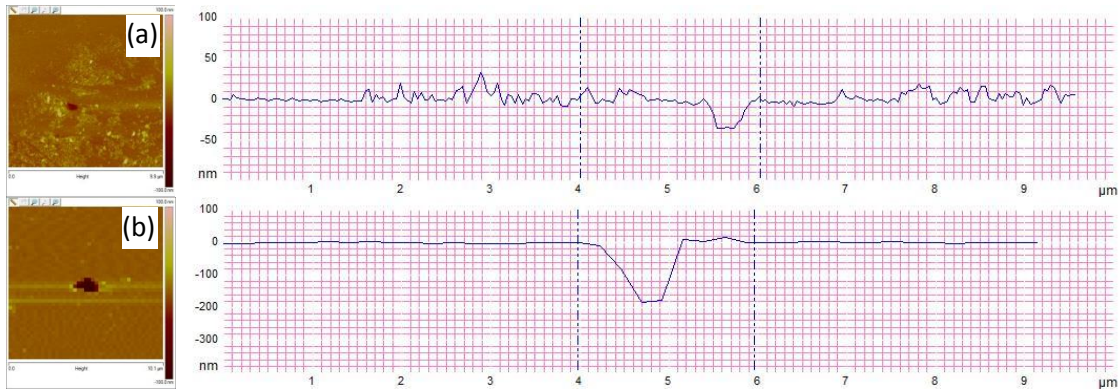
Figure 4.7: Topography and cross-section of the machined nanocavities on a) Silicon and b) Borosilicate glass [179]

4.2.2   Modeling The Material Removal In VANILA Process

The vibration of the tool at resonance introduces an acoustic field into the slurry medium [148, 149] which leads to acceleration of the nanoparticles towards the workpiece surface [180]. The successive impacts of nano abrasive grains with considerable kinetic energy on the hard and brittle workpiece material result in nanoscale material removal. Impact modeling is often very difficult because of the inherent complexities, characterized by very short duration of contact, rapid dissipation of energy and large accelerations and decelerations [137]. For the analytical modeling purpose of the material removal process during the VANILA process, the following simplification assumptions are made.

a) The classical impact mechanics is suitable for analyzing the nanoparticle impacts.

b) The tool tip and abrasive particles are considered to have equal hardness, while the workpiece is softer than the abrasive particles.

c) The workpiece surface is assumed to be plastic solid.

d) Abrasives and workpiece surface are electrically and chemically neutral and the electrostatic effects during impact are not considered in this study.

61

The magnitude of the overall impact velocity (V_I) of a single nano abrasive grain at the instant of impact has two coincident components (1) velocity of particle due to the tool impact (V_T) and (2) velocity due to acoustic streaming (V_S) which include acoustic cavitation [181] and acoustic drag components. The maximum velocity of impact of the single particle on the workpiece surface is cumulative of the two individual components of velocities.

$$V_I = V_T + V_s \tag{4.2.1}$$

The tool used in the VANILA process is a tapping mode AFM probe which consists of a cantilever with a conical tip having a nanoscale radius. The tool is acoustically driven by a piezoelectric element at the fundamental resonant frequency of the tip. The oscillatory motion of tool tip used in the VANILA process can be expressed as $A_t e^{i(\omega t + \pi/2)}$. The phase associated with the total force is considered as $\pi/2$ due to the fact that machining is conducted at resonance frequency and since on resonance the oscillations of the cantilever follow the total force with a phase delay of $\pi/2$ [138]. The drive force will generate acceleration at the tool tip perpendicular to the workpiece surface, resulting in impact onto particles coming into contact with the tool tip. The tool tip and abrasive grain are made of same material and thus the impact between tool tip and abrasives is considered to be perfectly elastic collision. For a perfectly elastic collision, both momentum and kinetic energy are conserved [140] and hence the maximum abrasive grain velocity due to impact with tool (V_T) will be twice the tool tip velocity which is the product of vibration amplitude and frequency.

$$V_T = 4\pi f_t A_t \tag{4.2.2}$$

Thus the impact velocity due to impact of single abrasive grain can be expressed as

$$V_I = 4\pi f_t A_t + V_s \tag{4.2.3}$$

Depending on the impact angle θ, the abrasive grain velocity will have 2 components, V_{IN} is the normal component ($V_{IN} = V_I \cos\theta$) and V_{IT} is the tangential component ($V_{IT} = V_I \sin\theta$). For the conditions used in the VANILA process experimentation, the grain velocity due to tool impact *(V_T)* is in the range of 0.01-1 m/s and the grain velocity due to streaming is in the range of 100-200 m/s. Thus the overall impact velocity of the abrasive grain *(V_I)* is in considered to be in the range of 100-200 m/s. Based on the estimated impact velocity values, the kinetic energy of the impacting abrasive grains is not large enough to produce fractures on the workpiece surface, so brittle removal is not expected to happen during the VANILA process as witnessed in the previous experimental observations. The abrasive particle impacts the workpiece normally with an impact velocity of V_{IN} with a normal impact force (F_{IN}). According to the law of conservation of momentum, the impact force exerted on the surface caused by the nanoparticle can be expressed by [182]

$$F_{IN} = \frac{m_a V_I \sin\theta}{\Delta t} \tag{4.2.4}$$

where Δt is response time .

$$\Delta t = \frac{2\rho_{fl}R_a^2}{9\rho_a v_{fl}} \tag{4.2.5}$$

It is a measure of the time for the abrasive grain to change direction within the bulk fluid [182].

The framework used to model the impact of abrasive nanoparticle on the hard and brittle workpiece in VANILA process is schematically shown in figure 4.8 [183]. In the elastic zone, the abrasive particle impact induces surfaces stresses on the workpiece surface as a result of elastic deformations; however material removal does not occur. As the normal impact force F_{IN} exceeds a critical value F_{pl}, plastic deformation occurs on the workpiece resulting in material removal.
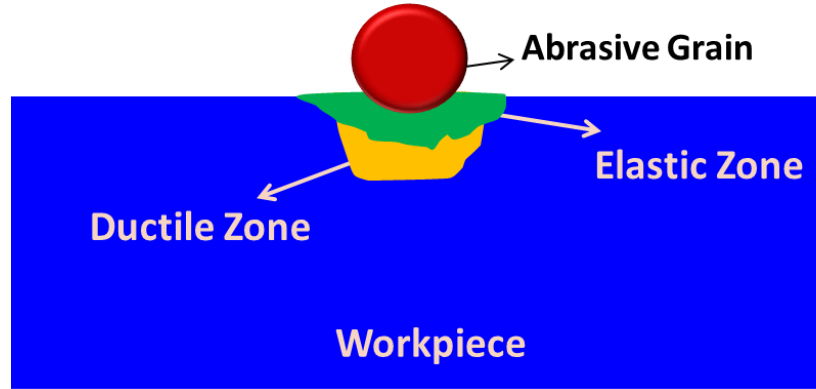
Figure 4.8: Schematic of Material Removal in VANILA process[179]

This critical force F_{pl} can be written as [184]

$$F_{pl} = \frac{9}{2}\left(\frac{R_a}{E^*}\right)^2 (\pi H_w)^3 \qquad\qquad (4.2.6)$$

The dynamic analysis of VANILA process is done based on the assumption that the process can be considered as discrete and that a single impact event of abrasive grain with the workpiece surface is a good representation of the complex phenomenon of material removal due to impact damage. [82]. MRR can be expressed as the function of the frequency of impact f, multiplied by number of active abrasive grains [185] and the volume removed by single impact τ.

$$MRR = \eta * \tau * n_a * f \qquad\qquad (4.2.7)$$

It should be noted that not all particles which impact the workpiece surface will have sufficient energy to removal the material. Some of the abrasive nanoparticles collide with each other while others are not involved in the material removal. An efficiency factor η is thus introduced to account for this phenomenon. The frequency f of impact of abrasive particles can be considered to be equal to the tool vibration frequency f_t. n_a is the number of abrasive grains participating in

the machining process which can be derived as following. The vibrating tool impacts the suspended nanoparticles contained in an assumed cylindrical region as depicted in figure 4.9.
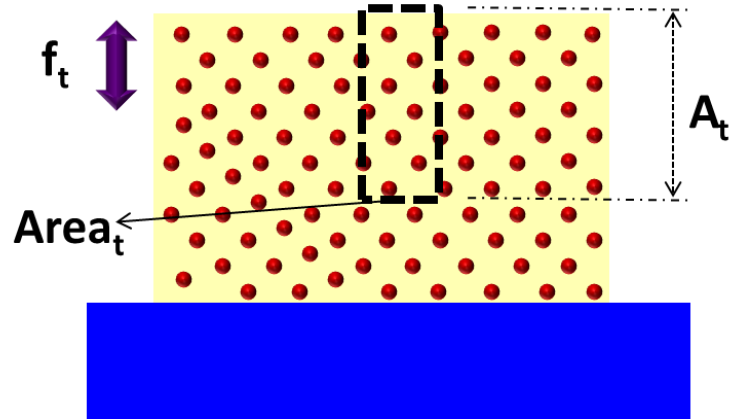
Figure 4.9: Zone of machining in VANILA Process [179]

The volume of this assumed region can be written as

$$Volume = Area_t A_t c_z \tag{4.2.8}$$

where c_z is volume concentration of diamond nanoparticles, $Area_t$ is area of cross-section of tool tip and A_t is vibration amplitude.

The volume of the cylindrical region can be as well written as the product of the number of abrasive nanoparticles (n_a) within the assumed region and volume of one grain.

$$Volume = n_a * \frac{4\pi R_a^3}{3} \tag{4.2.9}$$

Equating the above two equations, n_a can be calculated as

$$n_a = (3 Area_t A_t c_z)/(4\pi R_a^3) \tag{4.2.10}$$

τ refers to the volume of workpiece material removed by the impact of a single particle during the VANILA process. The material removal in this case depends on several factors including impact conditions, abrasive grain properties and workpiece parameters as displayed in figure 6. Literature suggests that during ductile mode machining, the material damage is strongly

influenced by material hardness (H_w) [90] and that other macro-mechanical properties of workpiece such as fracture toughness and elastic modulus do not greatly influence the material removal [85].
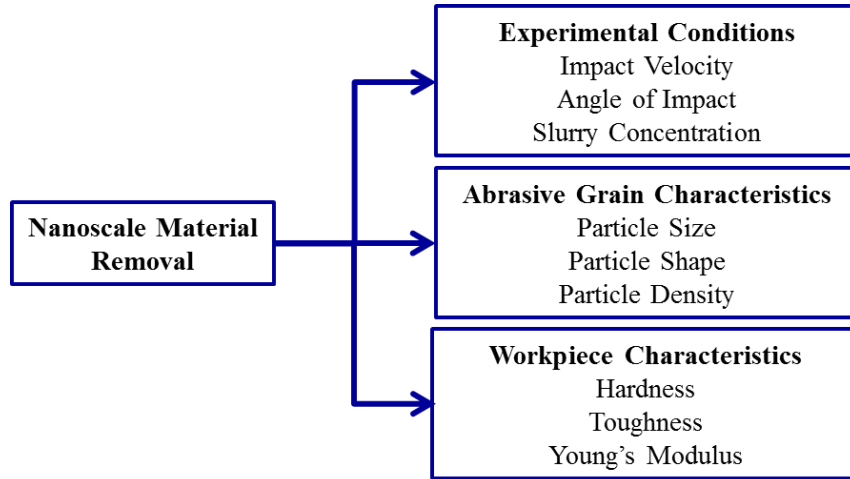
Figure 4.10: Factors affecting material removal during VANILA process [179]

During a ductile mode machining involving normally impact of abrasive particles on the workpiece surface, the volume of material removed per single abrasive grain impact during the impact process can be written as [77]

$$\tau = K_D * R_a^3 V_{IN}^3 \rho_a^{1.5} H_w^{-1.5} \tag{4.2.11}$$

where K_D is the material independent constant.

Thus, the material removal rate MRR during the VANILA process can be expressed as

$$\mathbf{MRR} = \frac{3}{4\pi}\boldsymbol{\eta} * \mathbf{K_D} * \boldsymbol{Area_t}\mathbf{f_t}\mathbf{A_t}\mathbf{c_z}V_{IN}^3 \left(\frac{\rho_a}{H_w}\right)^{3/2} \tag{4.2.12}$$

4.2.3   Experimentation Verification

VANILA process experiments are performed on silicon and borosilicate glass substrates. A commericial AFM is used for developing the machining setup. A machining cell is introduced between the AFM probe head and sample holder stage in order to conduct the nanomachining in the presence of homogeneously mixed abrasive slurry. A tapping mode probe having a tip radius of 10 nm with a spring constant of 40 N/m is used. The conditions used in experiments for this study are displayed in table 1.

Table 4.3: Experimental Conditions for VANILA Process [179]

Workpiece Material	Silicon, Borosilicate Glass
Machine	AFM Dimension 3100
Abrasive	10 nm sized diamond nanoparticles
Probe Used	NSC 16/50 (*Mikromasch*), Uncoated tip radius 10 nm, Probe Material – Silicon Nitride Coated with Cr-Au, Air Resonant Frequency 161 KHz, Spring Constant 40 N/m
Liquid Medium	Deionized water
Slurry Concentration	0.5 vol.conc %

The MRR model is verified by machining several nanocavities under different experimental conditions for machining duration of 60 seconds. For Silicon workpiece, theoretical critical force value for plastic deformation (F_{pl}) is calculated to be 1125 nN. For Borosilicate glass workpiece, the force F_{pl} is found to be 706 nN. The impact force of the diamond abrasive particle is found to

be approximately 1385 nN which is higher than the threshold force required for failure through ductile mode suggesting that the material removal will happen through plastic deformation and yielding.

The volumes of the nanocavities are measured using the bearing analysis function in Nanoscope IIIa software. Bearing analysis function is a method of calculating how much of a surface lies above or below a user-specified reference plane. In using this function, all the data points of the image considered as above the reference plane are distinguished from the surface. The software then calculates the total area covered by these points and further estimates the volume between the data points and the reference plane. A detailed illustration of the bearing analysis function is presented in figure 4.11.
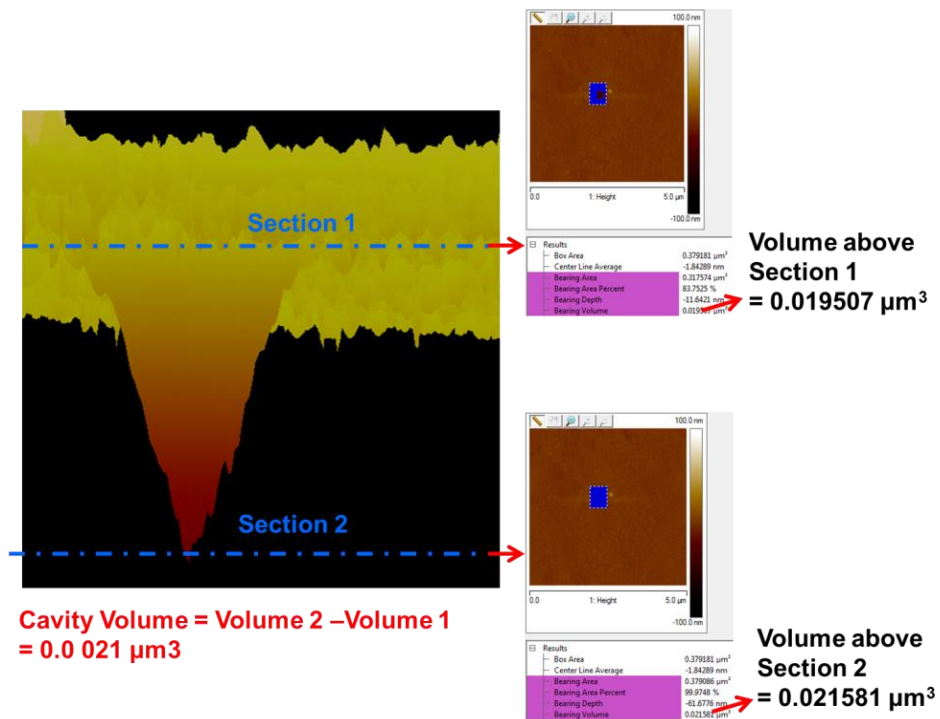
Figure 4.11: Illustration of using Nanoscope Software's Bearing Analysis Function [179]

The value of material independent constant K_D is evaluated using the experimental results as described below. A set of experiment trials are conducted on silicon and borosilicate glass substrates and volumes are measured and experimental MRR is calculated. The machining time is kept constant at 60 seconds. Individual K_D values are then calculated for each of these machined cavities by using their experimental MRR (volumes obtained from bearing analysis function) and theoretical MRR (assuming $K_D = 1$). An efficiency factor $\eta = 0.7$ is used as suggested in literature for abrasive jet machining process which also involves accelerated abrasive grains impacting a substrate within a fluid stream [186].

The experimental MRR values for the nanocavities machined during these trials are 45800, 55900, 39900, 41900 and 52700 nm^3/s. The corresponding theoretical MRR value (assuming K_D = 1) is 30500 nm^3/s. The individual K_D values are calculated as the ratio of respective experimental and theoretical MRR values (In this case are 15.00, 18.32, 13.09, 13.72 and 17.26 respectively). The average of these individual K_D values (15.48 approximated as 15) is then considered as the final K_D value for the model. Estimating the value of the material independent constant K_D in this method would help include the effects of several factors neglected in the simplification assumption during modeling and thus provide more accuracy the MRR model. Several experimental trials are further conducted on silicon and borosilicate glass substrates in order to test the validity of the model. Figure 4.12 a and b respective shows the comparison of theoretical and experimental MRR values of silicon and borosilicate glass. The MRR model is predicting the experimental values within 10 % deviation for both the materials.
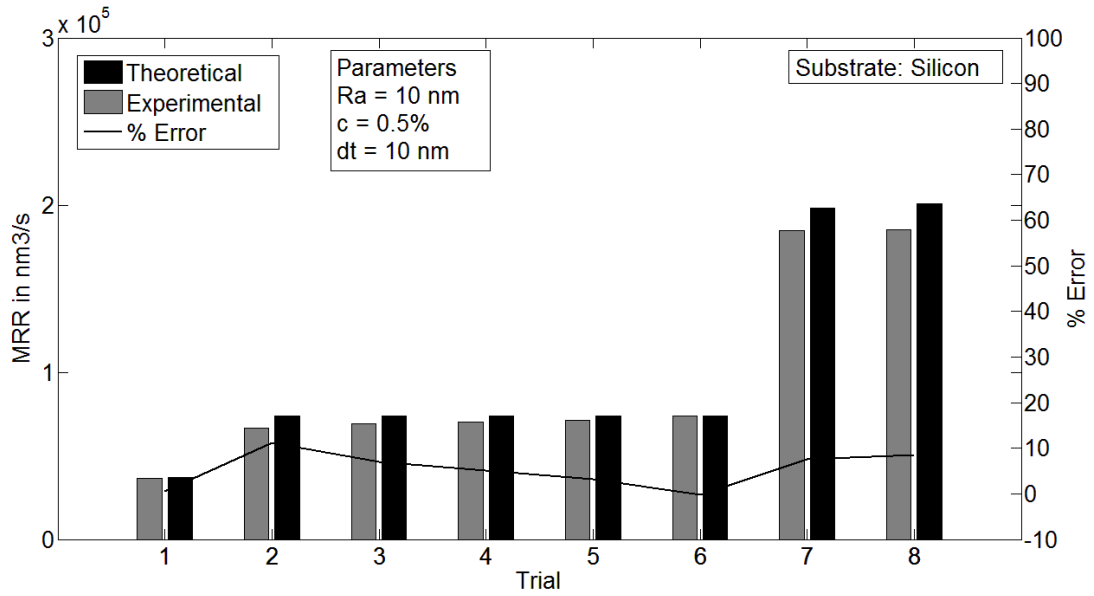
Figure 4.12a: Comparison of Theoretical and Experimental MRR for Silicon Substrate

[179]
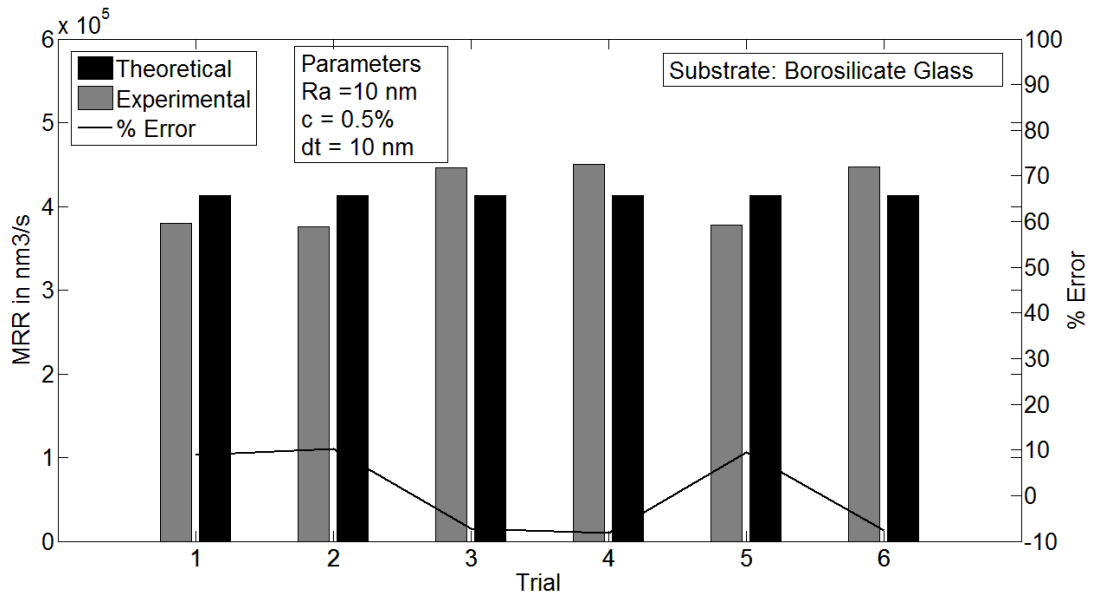
Figure 4.12b: Comparison of Theoretical and Experimental MRR for Borosilicate Glass

Substrate [179]

Chapter Summary

An analytical modeling based force analysis is conducted to understand the effect of significant forces acting on a nano particle moving in liquid medium. A theoretical model is developed to predict the velocity and penetration depth of nanoparticle within the nanofluid. A 3-D molecular dynamics based study is conducted to verify the theoretical predictions. Based on this study, following conclusions are made:

- Among the several forces involved, transient acoustic cavitation force and acoustic streaming force are the two forces that have dominant effect on the velocity of nanoparticle in liquid.
- The penetration depth of the nanoparticle increases as the size of the abrasive grain increases and the theoretical predictions of are conforming to the molecular dynamics study results.
- It is found that during the machining process, an impact velocity in the order of 10^2 m/s is achieved.
- The effective machining gap between the tool and the work surface is determined to be less than 200 nm for the size range of abrasive grains used in this study.

Material removal rate in VANILA process is studied analytically. The experiments show that the material removal occurs mainly in ductile mode due to plastic yielding and repeated deformation, which happens at near vertical impacts.

- A model based on impact mechanics is developed for predicting the MRR during the VANILA process for vertical impacts and is verified through experimentation performed on

silicon and borosilicate glass substrates. The experimental results confirm that the analytical

model is able to predict the results within 10% error.

Chapter 5: Material Removal Mechanism Studies

Fundamental understanding of material removal mechanism of the VANLA process is critical to improve its efficiency and effectively control the nanoscale features. The process essentially involves repeated impacts of hard diamond nanoparticles on solid substrate surface at various impact conditions. The tool used in the VANILA process is a tapping mode AFM probe which consists of a cantilever with a conical tip having a nanoscale radius. The tool is acoustically driven by a piezoelectric element at the fundamental resonant frequency of the tip. This provides an oscillatory motion to the tool tip during the machining process while impacting the suspended diamond nanoparticles in the liquid medium. The oscillatory motion would thus play a significant role in determining the kinetic energy of impact and the angle with which the nanoparticles impact the workpiece surface. Further, the direction of impact is also affected by the motion of fluid molecules within the machining zone. It is thus understood that the various impact conditions are involved during the VANILA process and thus the material removal mechanism would be complicated.

Literature suggests that Molecular Dynamics Simulation (MDS) is the appropriate tool for the fundamental understanding of the process characteristics of the materials at nanoscales [50]. In this chapter, MDS study of the VANILA process is conducted with an aim to understand the underlying material removal mechanisms. The first part of this chapter describes the preliminary study to understand the influence of critical process parameters on nanoscale impact process. This is followed by a three-dimensional MDS study in part 2 which explains the nanoscale material removal mechanism.

5.1 Molecular Dynamics Simulation Study of Effect of Process Parameters on Material Removal

5.1.1 Motivation for MD based Simulation of VANILA Process

The VANILA process is developed primarily for nanomachining of hard and brittle substrates. Nanoscale material removal could happen in brittle mode via crack propagation or ductile mode via plastic deformation or by a combination of both i.e. brittle/ductile transition phenomena. Fundamental understanding of material removal mechanism of a nanomachining process is critical to improve its efficiency and effectively control the nanoscale features. Theoretical study of the VANILA process based on fracture mechanics involves a degree of uncertainty because of the simplification assumptions typically used in the model developments, and therefore, the effect of process parameters and material removal mechanism cannot be entirely clarified. Usage of in-situ experimental observations for this purpose is also quite challenging due to the limitation of techniques to capture the phenomena such as sub-surface intrinsic atomic/molecular scale deformations and displacements happening in a very short time period in the VANILA process.

Numerical simulation techniques such as Finite Element Method (FEM) and Molecular Dynamics (MD) are some of the other options to study such problems. However, process simulation at the nanoscale is a challenging task because the material properties at the nanoscale differ significantly from those at the macroscale. Since the nanomachining occurs in a very small region (a few layers of atoms), the continuum theory based FEM approach is also not suitable for

studying nanoscale machining processes. Consequently, an MD-based simulation tool is required for the fundamental understanding of the process characteristics such as crack propagation and plastic flow of the material at nanoscales. Molecular dynamics simulation approach is used in this study to investigate the effect of critical process parameters, viz. impact velocity and the angle of impact of the abrasive grain, and understand the material removal mechanism in the VANILA process. Classical MD simulation is implemented using Large-scale Atomic/Molecular Massively Parallel Simulator (LAMMPS) [176]. This study reports on the results obtained through the MD simulations of the VANILA process for machining single crystal silicon substrate using nano diamond abrasive grains.

5.1.2 VANILA Process Simulation Model

The MD simulation in this study is performed using LAMMPS [176], in which the VANILA process is considered as an impact of a very small rigid sphere on the surface of workpiece. The simulation system consists of a workpiece made of single crystal silicon and a diamond abrasive grain which is modeled as a rigid body. The initial atomic configuration of the workpiece material is created from diamond lattice structure of silicon and consists of 11,425 Si atoms. The size of the workpiece is 500 Å x 200 Å with a lattice spacing of 5.43 Å. The diamond abrasive grain is made of a sphere of carbon atoms arranged in cubic lattice structure with a lattice spacing of 3.57 Å. The pictorial view of the model used for VANILA process simulation is shown in figure 5.1. The conditions used in the VANILA process simulation are given in Table 5.1. The interatomic forces between the Si-diamond atoms, Si-Si and C-C diamond atoms are calculated using Tersoff many-body potential, a suitable potential for the simulations of covalent

bonding materials like silicon. The Velocity-Verlet algorithm is employed to calculate the position and velocity of the atoms.
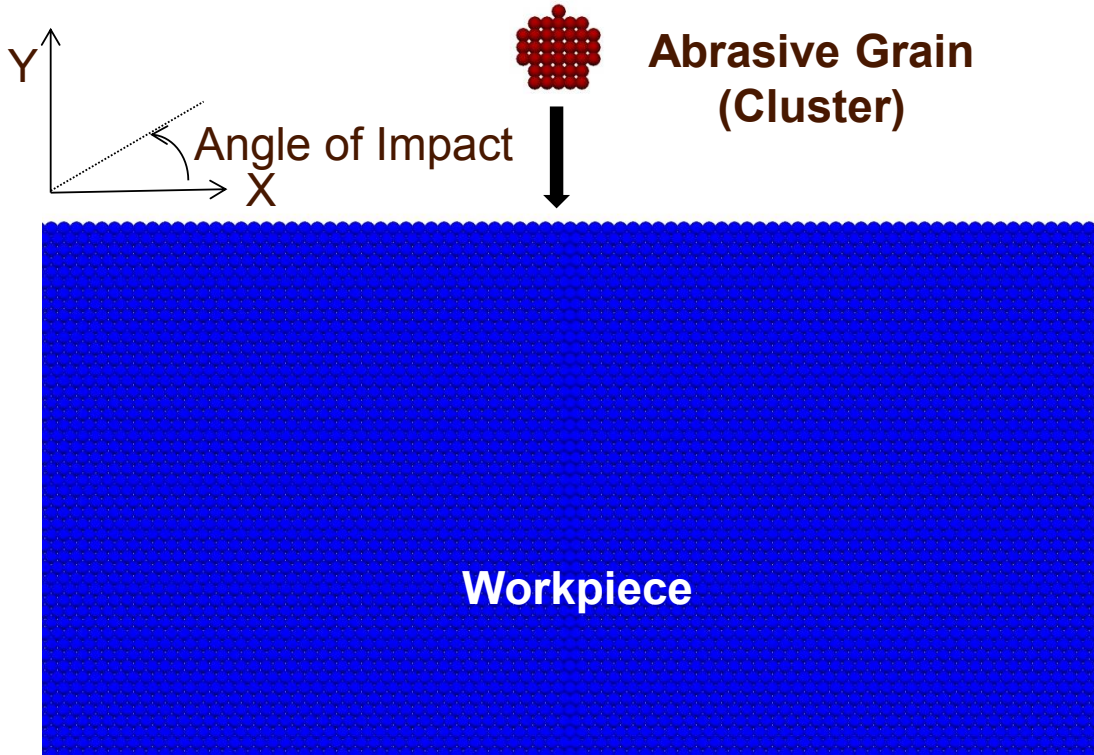
Fig 5.1: Schematic of MD Simulation Model of VANILA process [81]

Table 5.1: Simulation Conditions used in the MD Simulation of VANILA process [81]

Materials	Work Material	Silicon (500 Å x 200 Å)
	Abrasive Material	Diamond Sphere (Diameter Range 1-30 Å)
Machining Conditions	Bulk Temperature	300 K
	Initial Machining Gap	20 Å
	Time step	0.001 ps (picoseconds)
	Duration of Simulation	0.5 ps

5.1.3 Results and Discussion

All the results reported in this work refer to data obtained after 0.5 ps of simulation. A representative deformation behavior of the workpiece molecules during the VANILA process for an impact velocity of 5.5 nm/ps for 90° angle of impact is shown in figure 5.2. The atoms are color-coded based on the displacement from its initial configuration with blue showing the least (zero) displacement and red showing the displacements above 5.43 Å (figure 5.2 (a)), which is the lattice constant of silicon workpiece material. Several displaced workpiece atoms are seen around the abrasive grain (colored maroon) after collision between the cluster and the workpiece atoms. The displaced atoms consequently move away and form crater on the surface as shown in figure 5.2 (b).
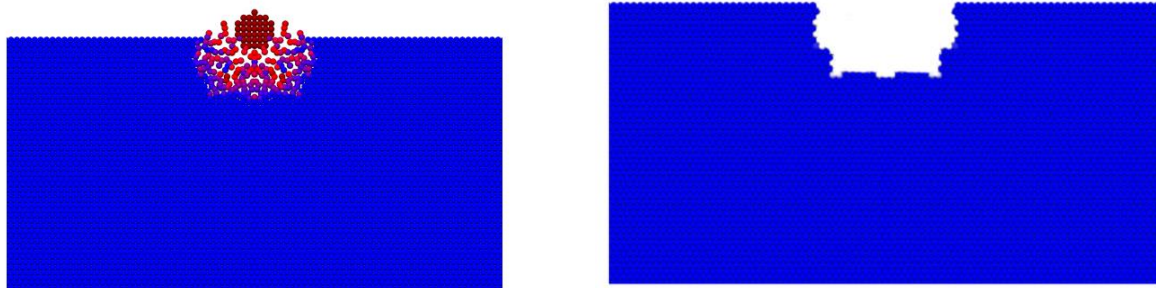
(a) Displacement of workpiece atoms for an abrasive impact velocity of 5.5 nm/ps

(b) Crater formed after the displacement of atoms

Fig 5.2: Representative atomic configuration during the MDS of VANILA process [81]

The MD simulation of VANILA process revealed different modes of material removals (figure 5.3) under different process conditions viz., impact velocities, particle sizes and angles of impact. The modes are classified as pure brittle mode - cone crack only (figure 5.3a), pure ductile mode - plastic deformation only (figure 5.3b), combination of ductile-brittle modes - plastic deformation + cone crack (figure 5.3c), plastic deformation + cone crack + lateral crack (figure 5.3d), cone crack + Lateral crack (figure 5.3e) and transition (figure 5.3f). The material removal mechanism

during impact process of brittle material by solid particles is governed by a combination of variables such as workpiece characteristics, abrasive particle characteristics and environmental effects as displayed in Table 5.2. This study focusses on the effects of impact velocity of abrasive particle, particle size, and angle of impact of the abrasive grain on *Net Depth* during the VANILA process. The output parameter Net Depth (d_n) considered in this study is the difference between the crater depth (d_c) and the abrasive grain penetration depth (d_p).

(a) Cone crack

(b) Plastic deformation

(c) Plastic deformation + Cone crack

(d) Plastic deformation + Cone crack+ Lateral crack

(e) Cone crack + Lateral crack

(f) Transition
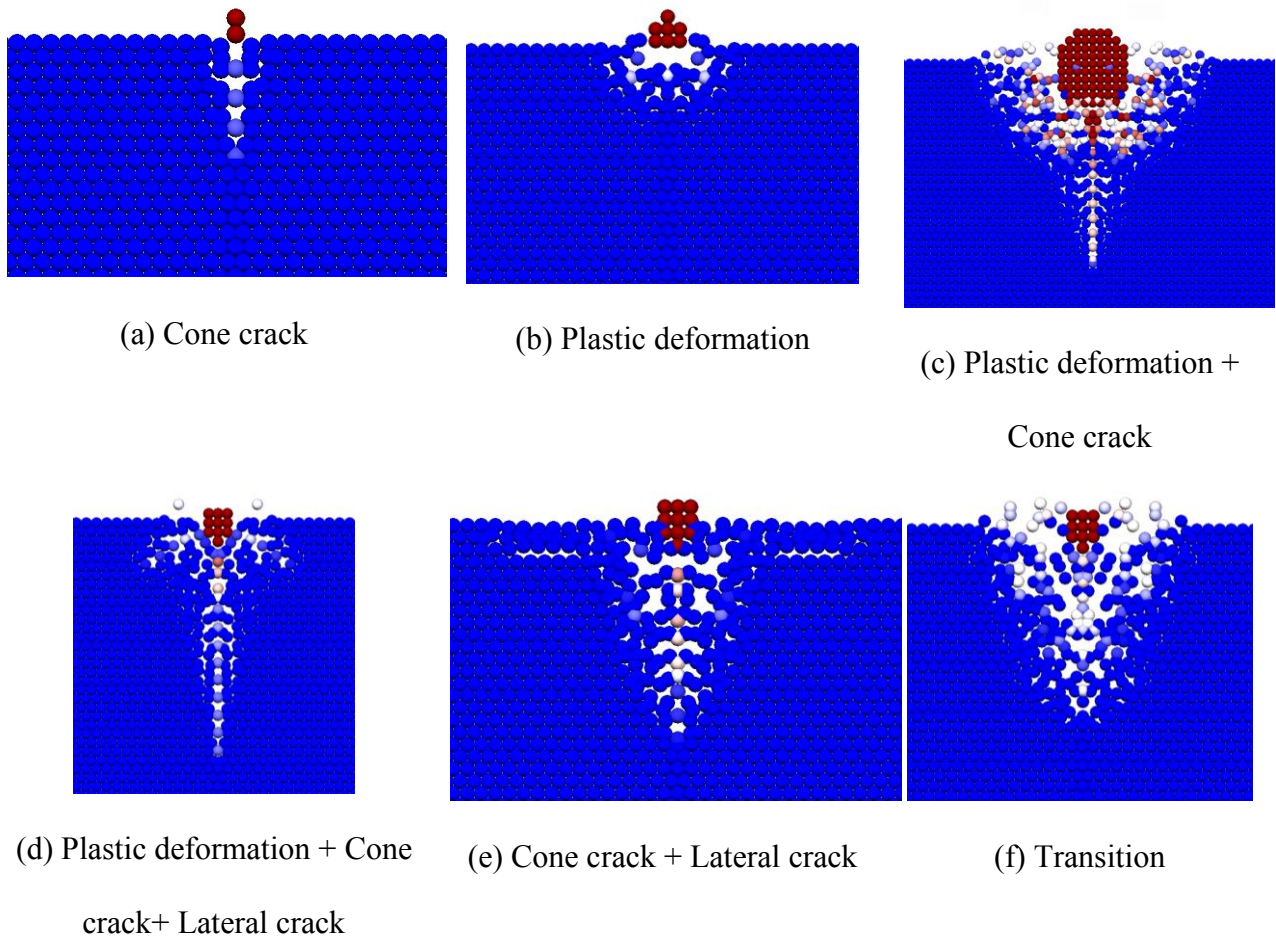
Fig 5.3: Modes of material removal during VANILA process obtained through MD Simulation [81]

Table 5.2: Critical factors affecting material removal mechanism in impact-based processes

[81]

Workpiece Characteristics	Abrasive grain Characteristics	Environmental Effects
Dynamics Hardness (H)	Impact velocity	Bulk temperature during impact
Dynamic Fracture Toughness (K_c)	Particle Size (Diameter)	Abrasive grain bonding to workpiece surface
Young's modulus (E)	Particle shape (round/blunt or sharp/angular)	Atmospheric reaction
Surface structure	Density	

5.1.4 Effect of Impact Velocity of the abrasive grain

The variation in net depth (d_n) produced for impact velocities ranging from 1-40 nm/ps for an abrasive grain size diameter of 10 Å and an initial gap of 20 Å between the abrasive grain and substrate is depicted in figure 5.4. At very low impact velocities, crack initiation and propagation are not feasible and the abrasive grain will only plastically deform the target surface. However, with increasing values of impact velocity, contact area of the brittle workpiece material is deformed due to crack formation of different kinds such as radial cracks, median crack and lateral cracks, resulting in gradual increase in the net depth of machining.

5.1.5 Effect of Particle Size on material removal process

For an impact velocity of 10 nm/ps and an initial gap of 20 Å between abrasive grain and the workpiece surface, figure 5.5 shows the variation of net depth with respect to the abrasive grain size ranging from 1-30 Å in diameter for different impact velocities (10 nm/ps, 20 nm/ps and 30 nm/ps). It is seen that the net depth (d_n) increases with abrasive grain size till 15 Å and then remains almost constant. The variations are possible due to the different modes of material removal shown in figure 5.3. Further studies have been conducted (described in the next section) to know the effect of this.
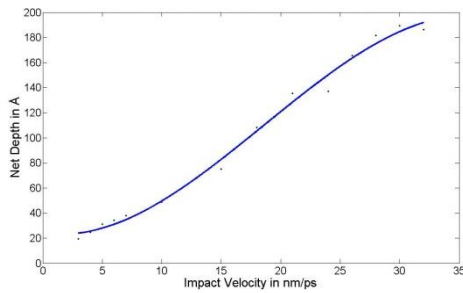
Fig 5.4: Effect of Impact Velocity on Net Depth in VANILA process for normal impact (angle of impact 90° and abrasive grain diameter 20 Å [81]
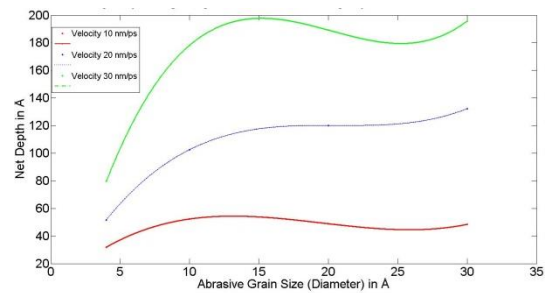
Fig 5.5: Effect of Particle Size on Net Depth in VANILA process for normal impact (angle of impact 90° and impact velocity 10 nm/ps) [81]

5.1.6 Material Removal Mechanism in VANILA process

In order to develop an understanding of the material removal behavior in VANILA process, MD simulations have been performed for a range of impact velocities from 1 to 40 nm/ps, and particle sizes in the range of 1-30 Å. Investigations reveal that in addition to the threshold effects reported in literature [16] i.e., transitions in material removal behavior from brittle to ductile modes, the material removal in VANILA process is also influenced by the pattern of the cracks

formed due to the impact of abrasive particle. A material removal mechanism map showing the effects of impact velocity and abrasive grain size on the occurrence of transitions between plasticity-dominated and fracture-dominated behavior during VANILA process is shown in figure 5.6, which indicates different regimes of material removal mechanisms and their transitions.
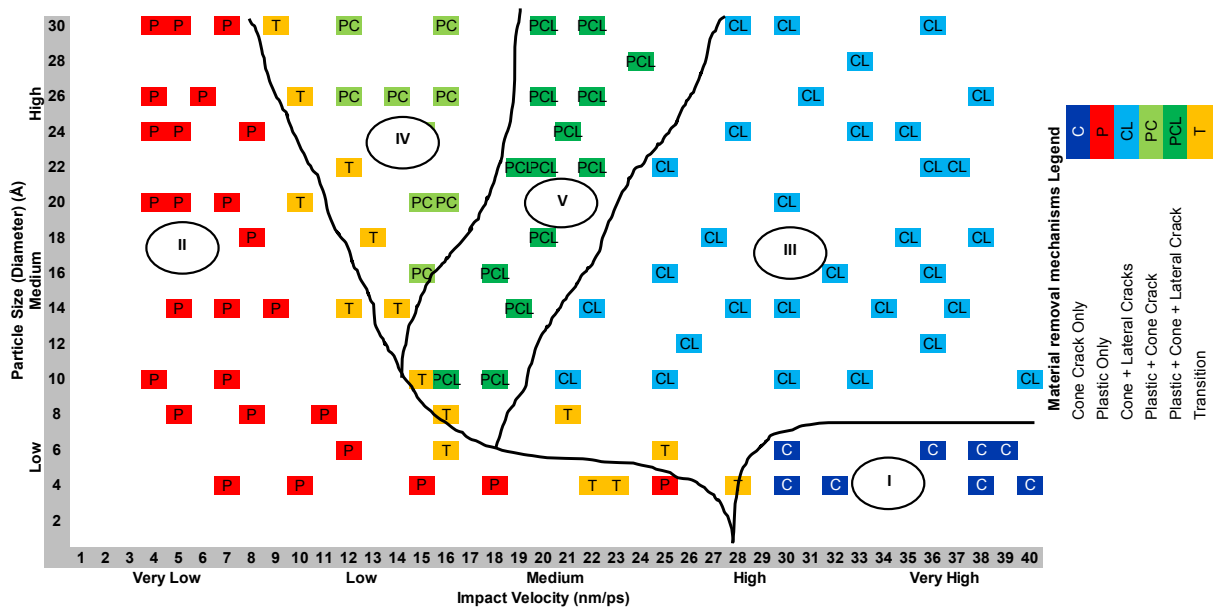
Fig 5.6: Different regimes of material removal mechanisms in VANILA process [81]

It is observed that in regime II which corresponds to low impact velocities (range 3-16 nm/ps) the material removal process is dominated by plastic deformation under ductile mode. For small abrasive grain sizes, when the impact velocity exceeds more than 28 nm/ps (regime I), the material removal mechanism is dominated by pure conical crack formation. For medium impact velocities ranging from 10-28 nm/ps, a plastic deformation is partially accompanied by conical and lateral crack formations (regimes IV and V). With further increase in the impact velocities, the material removal mechanism is dominated by brittle-mode involving conical and lateral crack

formations (regime III) without involving significant plastic deformation. A transition zone is observed along the regimes II (pure plastic) and regimes IV, V and III (crack formation).

5.1.7 Confirmation Study

In addition to the abrasive size, and impact velocity, material removal may also be influenced by the angle of impact of the abrasive grain on the workpiece surface. This effect of angle of impact on material removal was studied to confirm the earlier results of brittle and ductile mode machining. As per literature, peak material removal occurs in the range of 80-90° in the case of brittle machining and at 20-30° for ductile machining. This clear difference in the range of angle of impacts for peak material removal can be used to confirm the occurrence of brittle and ductile mode machining in VANILA process. Thus, MD simulations are conducted with parameters given in Table 5.3 for brittle and ductile regimes. Results of brittle and ductile mode machining are shown in figures 5.8 and 5.9 respectively.

Table 5.3: Process parameters and their values used in confirmation study [81]

Process parameter	Brittle machining	Ductile machining
Abrasive particle size	Diameter 16 Å	Diameter 10 Å
Impact velocity	32 nm/ps	7 nm/ps
Angle of impact range	0° to 90°	0° to 90°
Time steps	500	500
Duration	0.5 ps	0.5 ps

(a) Effect of angle of impact   (b) 90° Angle of impact   (c) 30° Angle of impact
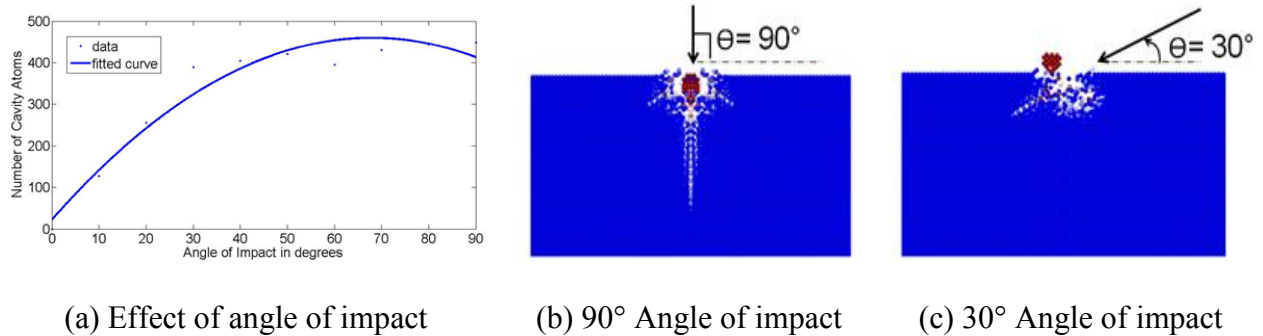
Fig 5.7: Brittle mode machining in VANILA process [81]

In brittle mode machining, relatively a higher material removal in the range of 50 to 500 atoms is observed with the peak material removal occurring for high angle of impacts in the range of 60 to 90° as displayed in figure 5.7 (a). Material removal at higher angle of impact happens through median or radial cracks as seen in figure 5.7 (b), resulting in large fragment formation and results in high material removal. As the angle of impact decreases, there is considerable decrease in the localized surface cracking [4], and the cracks produced during low angle impact are predominantly lateral type as seen in figure 5.7 (c). This transition from median/radial cracks to lateral crack formation results in decrease in material removal at lower angle of impacts.

(a) Effect of angle of impact   (b) 90° Angle of impact   (c) 30° Angle of impact
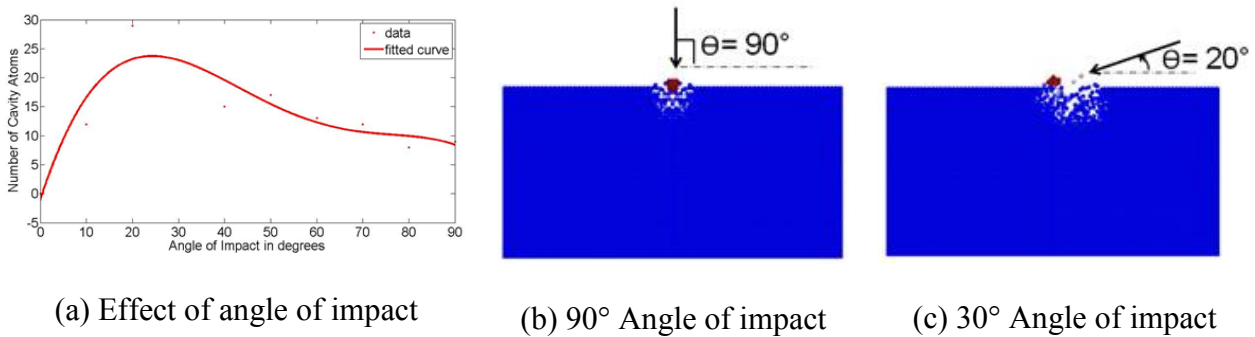
Fig 5.8: Ductile mode machining in VANILA process [81]

In ductile mode machining, a relatively lower material removal in the range of 5 to 25 atoms is seen with the maximum removal happening at low impact angles (15° to 30°) as displayed in figure 5.8 (a). For lower angles of impact between 0° and 45°, shearing of workpiece material occurs due to the horizontal component of the impact energy. For larger angles of impact in ductile machining, the material removal decreases as the mechanism of material removal is dominated by plastic deformation of the workpiece surface by repeated hammering or indenting due to the vertical component of the impact energy . The Atomic configurations for plastic deformation and shearing are shown in figures 5.8 (b) and (c) respectively.

5.2 Molecular Dynamics Simulation Study of Effect of Material Removal Mechanisms in the VANILA process

The preliminary MDS study [81] found that impact angle and velocity of the nanoparticle determine the extent of material damage on the substrate. However, that study used a two-dimensional simulation and did not consider the drag effects of liquid medium on the abrasive grain motion. Additionally, that study used an impact energy scale which is much higher than theoretically estimated impact energy levels of 100-1000 eV. The present section reports a three-dimensional MDS study on the material removal mechanism during the VANILA process using more realistic impact conditions including the drag effects of liquid medium.

5.2.1 Simulation Model

In this section, three-dimensional MDS study is performed using large-scale atomic/molecular massively parallel simulator (LAMMPS) [176] and Visual molecular dynamics (VMD) as the post processing tool. The simulation system consists of a workpiece made of single crystal silicon <100> and a single diamond abrasive grain which is modeled as a rigid body. Silicon atoms of the substrate are initially arranged in a diamond cubic lattice structure with a lattice constant of 5.43 Å at a temperature of 293 K. The substrate consists of about 75,000 Si atoms in total with a size of 150 x 150 x 60 Å. The outer layers (2 Å) of the substrate are fixed in space except the top surface. A thin layer (3 Å) of thermostat atoms are kept at 293 K and is used to ensure the reasonable heat conduction away from the impact region of the workpiece. The diamond nanoparticle is made of a sphere of 10 Å diameter and about 100 carbon atoms arranged in diamond cubic structure. The simulation model assumes that a single impact event of diamond nanoparticle with the workpiece surface is a good understanding of the complex phenomenon of material removal due to impact damage. The effect of percussive impact has not considered in this simulation studies. The schematic representation of the MDS model used for VANILA process simulation is shown in figure 5.9.

The viscous drag effect of the liquid water is provided by the addition of a Langevin thermostat which models interaction of the nanoparticle with a background implicit solvent. The Langevin thermostat considers the viscous drag force F_{drag} using a user specified damping factor term *'damp'*. F_{drag} is proportional to the particle's velocity V_a and is calculated as following

$$F_{drag} = -\gamma V_a \tag{5.2.1}$$

where γ is the proportionality constant termed as damping coefficient and is computed as

$$\gamma = 3\pi\mu d_a \qquad (5.2.2)$$

where d_a is the diameter of the diamond abrasive grain and μ is the dynamic viscosity of the fluid. *'damp'* is inversely proportional to γ and is related as

$$\gamma = {}^{m_a}\!/_{damp} \qquad (5.2.3)$$

where m_a is the mass of the abrasive grain. For the conditions used in this study (i.e, diameter of nanoparticle d_a = 10 Å and dynamic viscosity of water μ = 0.00064 kg/m-s), the *damp* value is estimated to be about 400. Periodic boundary conditions are maintained on all the atoms along the x, y and z directions. The interatomic forces between the Si-diamond atoms and Si-Si atoms are calculated using Tersoff many-body potential, a suitable potential for the simulations of covalent bonding materials like silicon [55]. The Velocity-Verlet algorithm is employed to calculate the position and velocity of the atoms. In order to study the material removal mechanism during the VANILA process, a series of simulations are performed under different impact conditions including angle of impact (θ) and initial kinetic energy of impact. The initial kinetic energy of the nanoparticle is varied between 100 eV and 900 eV which is approximately the range of value estimated through theoretical calculations. Impact angle (θ) in this study is defined as the angle between the incident direction and the Y-axis. The impact angle is varied between 30° and 90° considering number of impacts at angles lower than 30° to be insignificant.

(a)   (b)
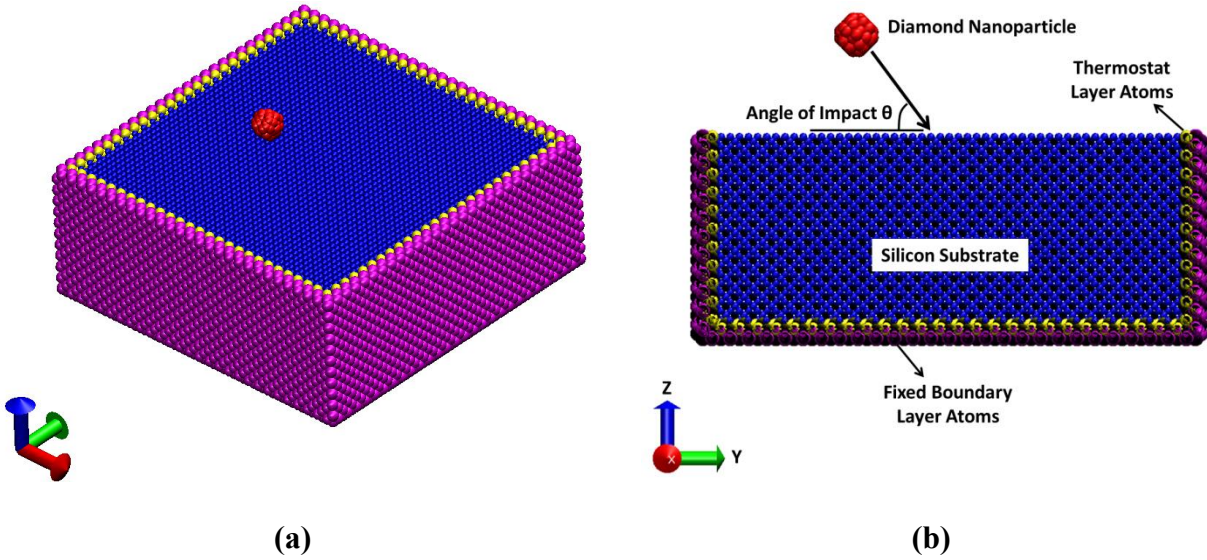
Figure 5.9: Schematic of MDS model of VANILA Process a) 3-Dimensional view b)

Sectional view

Table 5.4: Simulation Conditions used in the MDS study of VANILA process

Materials	Workpiece Material	Silicon (150 Å x 150 Å x 60 Å) Type <100>
	Abrasive Material	Diamond Sphere (Diameter 10 Å)
	Liquid Medium	Background implicit solvent
Machining Conditions	Angle of Impact (θ)	30°, 40°, 50°, 60°, 70°, 80°, 90°
	Initial Kinetic Energy of Abrasive	100, 200, 300 400, 500, 600, 700, 800, 900 eV
	Potential Used	Tersoff (SiC.Tersoff)
	Bulk Temperature	293 K
	Initial Machining Gap	10 Å
	Time step	0.001 ps (picoseconds)
	Duration of Simulation	1 ps

5.2.2   Simulation Results And Discussion

5.2.2.1 Material Removal Mechanisms

The MDS study is conducted for a range of angles of impact and initial kinetic energy of the nanoparticle. The cross-sectional views of the machined substrate across the impact zone are then analyzed using the VMD tool. The simulation results revealed that there are three distinct mechanisms dominating the material removal process namely – a) nanocutting in which cutting is significant, b) nanoplowing in which plowing is dominant and nanocracking in which radial crack formation happens. Several simulation results show that these nanoscale mechanisms coexist – that means they occur simultaneously. The characteristics of the three material mechanisms found in this study are described below.

a) *Nanocutting:* This mechanism of material removal is characterized by chip formation due to cutting of substrate material. Considering the nanoscale material removal chip in this study refers to small fragments of substrate molecules which are completely removed from the substrate surface. The machined cavities have a shallow but wider profile and also show signs of amorphous phase transformation. The cross-section view of the substrate machined through nanocutting mechanism for an impact initial kinetic energy of 700 eV, angle of impact of 30° and duration of 1 ps is shown in figure 5.10a.
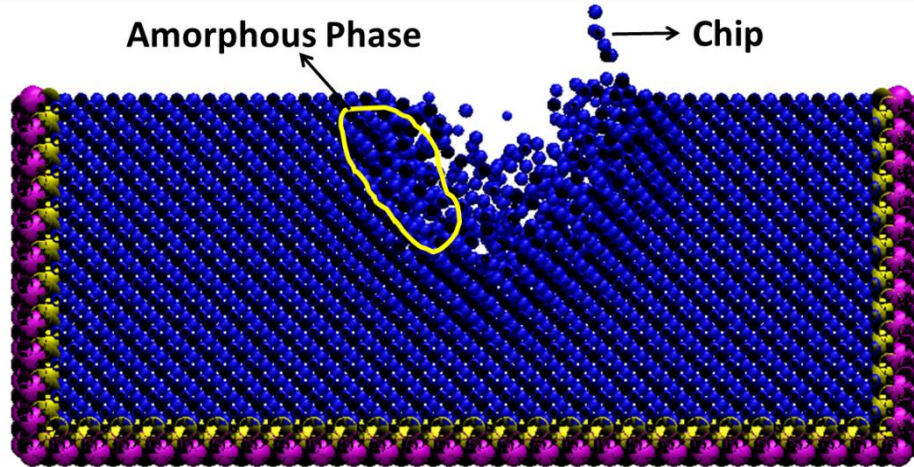
Figure 5.10a: Cross-sectional view of substrate machined through nanocutting mechanism – (Initial kinetic energy 700 eV, Angle of impact 30°, Duration 1 ps)

b) *Nanoplowing:* This mechanism of material removal is characterized by plastic deformation with amorphous phase transformation, but no chip type substrate fragments are formed during machining. The material is plowed to the sides of the machined cavity resulting in formation of occasional pileups of substrate molecules. The cavity depth is found to be more than that during the nanocutting mechanism. A representative cross-section view of substrate machined through nanoplowing mechanism for an initial kinetic energy of 500 eV, angle of impact of 90° and duration of 1 ps is shown in figure 5.10b.
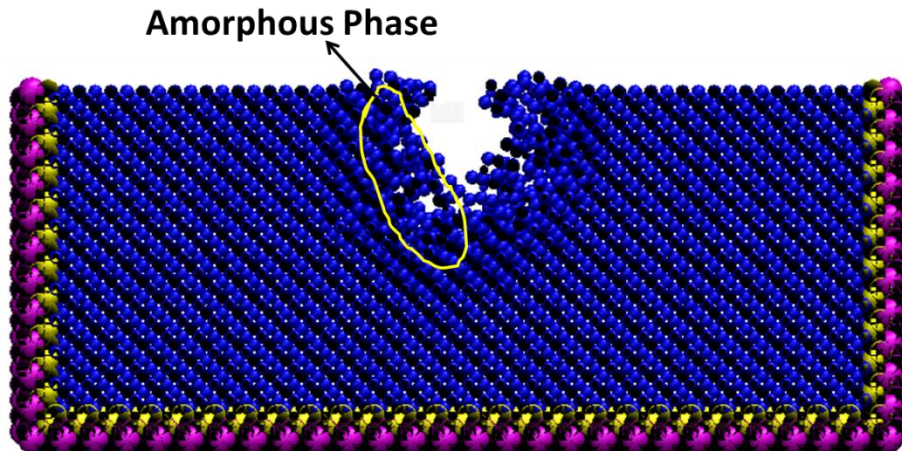
Figure 5.10b: Cross-sectional view of substrate machined through nanoplowing mechanism – (Initial kinetic energy 500 eV, Angle of impact 90°, Duration 1 ps)

c) *Nanocracking:* Material removal due to nanocracking mechanism happens when small radial cracks form at the lowest point of the cavity. The nanocracks run radially into the bulk of the substrate causing eventually causing small scale fracture in the substrate. For the conditions used in this study, nanocracking was the least probable among the three mechanisms of material removal. A representative cross-section view of the substrate with machined through nanocracking for an initial kinetic energy of 900 eV, angle of impact of 70° and duration of 1 ps is shown in figure 5.10c.
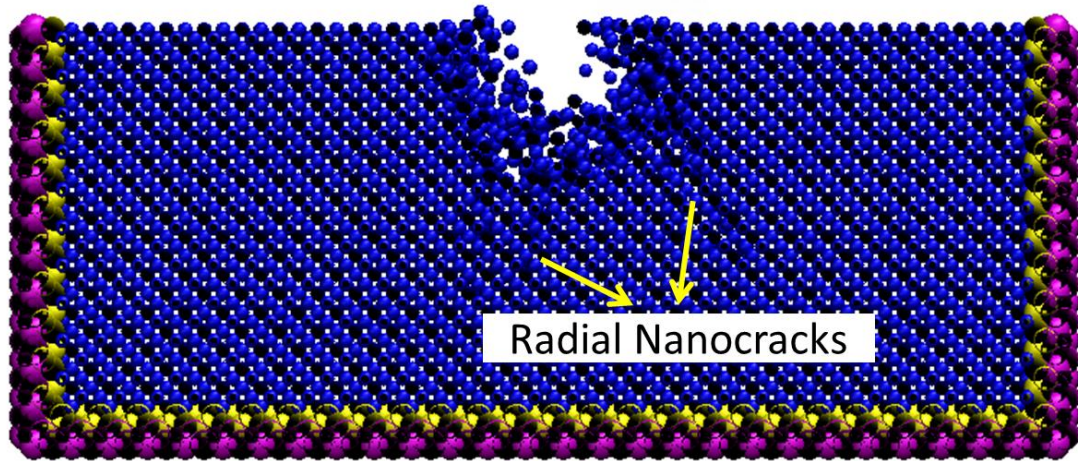
Figure 5.10c: Cross-sectional view of substrate machined through nanocracking mechanism – (Initial kinetic energy 900 eV, Angle of impact 70°, Duration 1 ps)

5.2.2.2 Effect of Angle of Impact

Angle of impact of the particle is one of the most important factors in impact based material removal processes [81]. In order to understand effect of angle of impact on the material removal mechanisms, simulation studies are done by keeping the kinetic energy of the nanoparticle constant and varying the angles of impact from 30° to 90°. The specified angles of impact are achieved by adjusting the magnitudes of the Y and Z components of initial particle velocity. It is seen that for angles of impact within the range of 30° to 60°, nanocutting mechanism dominate the material removal process. Additionally, the abrasive nanoparticle pushes the material in the direction of motion resulting in formation of small lips on the substrate.

As the angle of impact is increased (between 60° to 90°), the nanoplowing mechanism is significant. There is no chip-type substrate fragments found and the substrate molecules undergo amorphous phase transformation. Cross-sectional views of substrates impacted at low and high

angles of impact are shown in figure 5.11 – a) 40° and b) 80° for an initial kinetic energy of 500 eV and duration of simulation of 1 ps. It is seen that the low angle impacts result in nanocutting while high angle impacts result in nanoplowing.

(a)   (b)
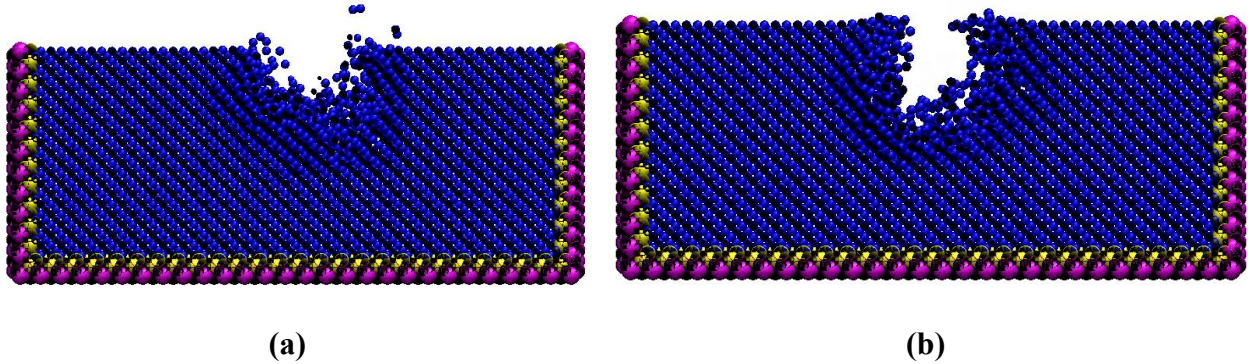
Figure 5.11: Effect of angle of impact (θ) on the material removal mechanism in the VANILA process - Angle of impact a) 40° and b) 80° for an initial kinetic energy of 500 eV and duration of 1 ps

5.2.2.3 Effect of Initial Kinetic Energy of Nanoparticle

The initial kinetic energy of the diamond nanoparticle is calculated as $\frac{1}{2} m_a V_a^2$ where m_a and V_a are the mass and initial velocity of the nanoparticle respectively. This energy is similar to the translational kinetic energy of the group of molecules comprising the diamond nanoparticle. Clearly, the kinetic energy is affected by both the mass and the initial velocity of the particle. For the purpose of simplicity, the mass or in turn the size of the particle is kept constant (10 Å diameter) for most of the simulations unless otherwise mentioned. The initial velocities are thus varied for the simulation studies; the range of velocities used are 1,000 m/s to 10,000 which is much higher than the actual range of impact velocities calculated theoretically (100 m/s -200 m/s). However, for this combination of mass and initial velocities the initial kinetic energy is in

the range of 100 eV to 1000 eV which is very close to the theoretically estimated range. This justifies the use of a higher velocity range for this simulation study.

The simulation results show that by increasing the initial kinetic energies of the nanoparticle, the material removal mechanism changes from nanocutting and nanoplowing mechanisms to nanocracking mechanism. Within a low range of initial kinetic energies (100-600 eV), the material dominated by shallow nanocutting or nanoplowing mechanisms with amorphous phase transformation. For higher initial kinetic energies (600-900 eV), the nanocracking mechanism begin to dominate the material removal process. Figure 5.12 shows the cross-sections views of substrates impacted by nanoparticles with different initial kinetic energies – a) 200 eV and b) 800 eV for angle of impact of 70° and duration of simulation of 1 ps. From the figure, it is seen that as lower initial kinetic energies result in shallow nanocutting whereas increasing the kinetic energies above 600 eV results in nanocracking through radial nanocrack formation.

(a)   (b)
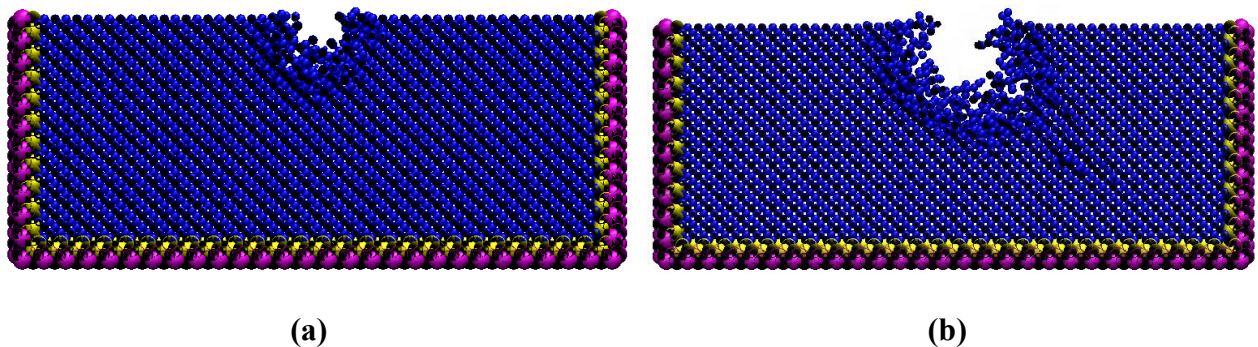
Figure 5.12: Effect of Initial kinetic energy on material removal mechanism in the VANILA process – Initial kinetic energy a) 200 eV and b) 800 eV for an angle of impact of 70° and duration of 1 ps

5.2.2.4 Material Removal Mechanism Map

Based on the series of simulations, a mechanism map capturing the effects of angle of impact (θ) and initial kinetic energy on the three dominant nanoscale material removal mechanisms is built as represented in figure 5.13. The initial kinetic energy values are varied between 100 eV and 900 eV while the angles of impact are varied from 30° to 90°. The map reveals that nanocutting mechanism is dominant for low initial kinetic energies and low angles of impact. Above 60° angle of impact, the mechanism is dominated by nanoplowing with no chip formation during material removal. Nanoplowing is observed for high impact angles are relatively low values of initial kinetic energies. As the initial kinetic energy of the diamond nanoabrasive increases above 600-700 eV, radial nanocrack begins to form and nanocracking mechanism dominates this impact condition.

It is also seen that one or more of these nanoscale material removal mechanisms coexists during the impact machining, even though one of those mechanisms dominate the material removal process. The transition zone from nanocutting to nanoplowing is observed at angle of impact of near 60° while the transition from the nanocutting and nanoplowing mechanisms to nanocracking mechanism is observed for initial abrasive kinetic energies of about 600-700 eV. As mentioned earlier, for this study the initial kinetic energy of the abrasive grains are achieved by keeping the size of abrasive constant and varying the initial velocity values. However, in order to confirm the mechanism map, few more simulations were conducted by varying the abrasive grain size while still maintaining the initial kinetic energy (by adjusting initial velocities accordingly). The results are still in accordance with the mechanism map in figure 7 thus proving that the initial kinetic energy is suitable parameter for constructing the mechanism map.
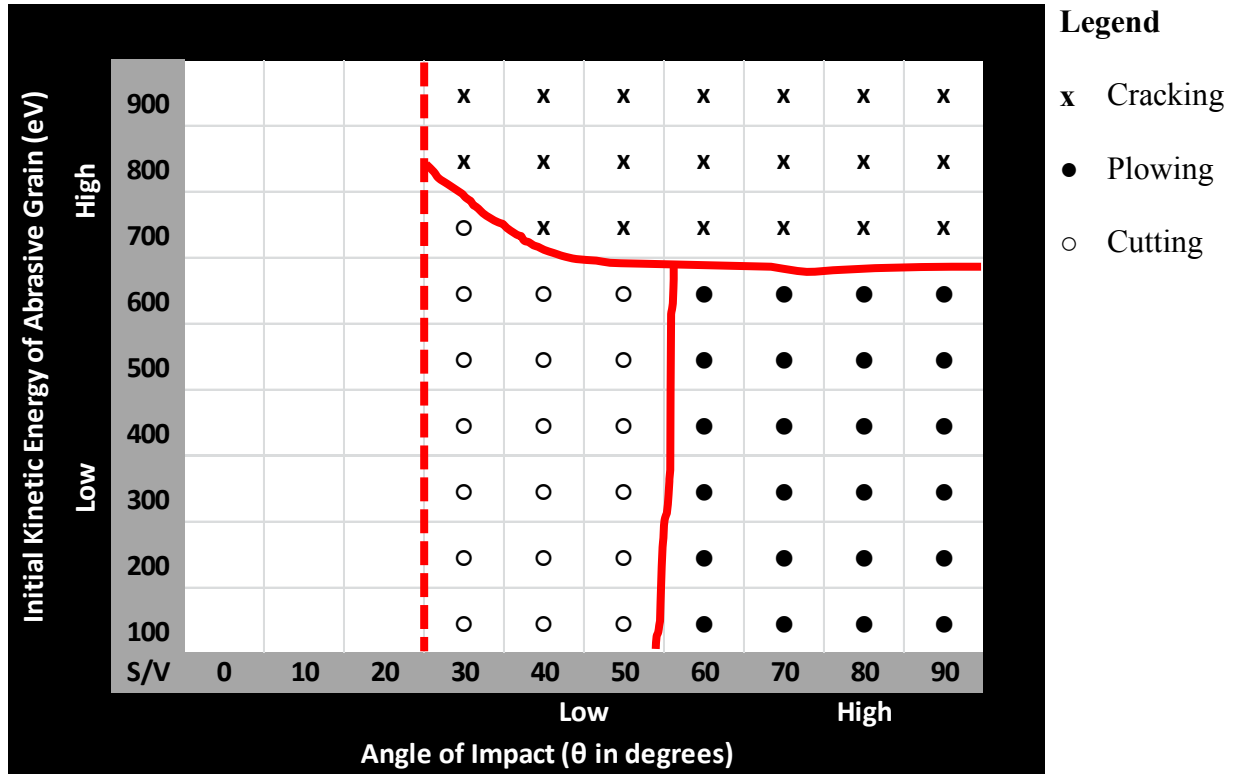
Figure 5.13: Map showing various material removal mechanisms

5.2.3   Experimental Observations

In order to experimentally confirm the findings of the MDS study, the VANILA process experiments are conducted on silicon and borosilicate glass substrates. AFM (Veeco Dimension 3100 with Nanoscope III) is used for developing the machining setup. A machining cell is introduced between the AFM probe head and sample holder stage in order to conduct the nanomachining in the presence of homogeneously mixed abrasive slurry. A tapping mode probe having a tip radius of 10 nm with a spring constant of 40 N/m is used. The common experimental conditions are listed in table 5.5.

Table 5.5: Experimental Conditions for VANILA Process Mechanism Study

Workpiece Material	Silicon, Borosilicate Glass
Machine	AFM Dimension 3100 (Veeco Instruments, Inc.)
Abrasive	10 nm sized diamond nanoparticles
Probe Used	NSC 16/50 (*Mikromasch*), Uncoated tip radius 10 nm, Probe Material – Silicon Nitride Coated with Cr-Au, Air Resonant Frequency 161 KHz, Spring Constant 40 N/m
Liquid Medium	Deionized water
Slurry Concentration	0.6 vol.conc %

The purpose of the experimentations in this study is to observe the various mechanisms of wear, even though a direct comparison between the simulation results and experimental results are not appropriate since the experimentation is conducted for multiple cycles of impact. Several nanocavities are machined under different experimental conditions for machining duration of 60 seconds. The cross-sections of the machined substrates are then analyzed using the Nanoscope III software (version 1.40). Representative cross-sectional images of nanocavities machined on silicon and borosilicate glass are shown in figures 5.14 a and b respectively.

Comparing with the MDS study results, it appears that the material removal during the VANILA process happens primarily through *nanoplowing* mechanism. This could be explained by the fact the majority of the impacts happens at near normal angles of impact, causing the nanoparticles to hammer the substrate surface, digging into it and plowing away material to the sides.

Additionally, there are no noticeable ridges or pile-ups near the edges of the nanocavities. It could be possible that the pileups at the edges of the cavities are removed by repeated impact. The material removal rates observed in machining these cavities are in the order of 10^4 nm^3/s for silicon and 10^5 nm^3/s for borosilicate glass substrates.
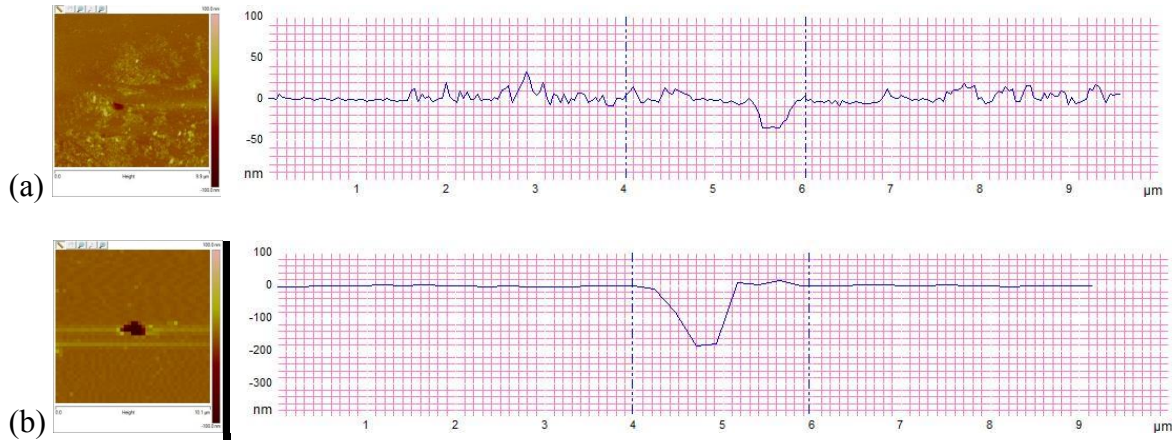
Figure 5.14: Nanoplowing machining results on a) Silicon and b) Borosilicate Glass

However, further investigation of the cross-sections of the machined nanocavities revealed that two other mechanisms happen occasionally. Comparing with the MDS studies, these nanoscale material removal mechanisms are identified as nanocutting and nanocracking. The additional mechanisms during the VANILA process experiment could be explained by the fact that the individual nanoparticles can impact the substrate in different orientations at various angles due to the vertical and lateral deflections of the tool and also the particles are in a size range rather than an explicit single size.

From the MDS studies, it is understood nanocutting mechanism arises due to the glancing impact (angle of impact less than 60°) of the abrasive particles on the workpiece surface. The material

should remove through cutting process resulting in small fragments of the substrate, even though observation of nanoscale chips during experiments is not possible because it is difficult to distinguish the silicon chip from diamond nanoparticles in the slurry. However, the cross-sectional information showed that the deformed region is shallow and has slight lip formation near the edges of the nanocavities suggesting low angle impacts. The material removal rates are in the order of 10^3 nm^3/s for silicon and 10^4 nm^3/s for borosilicate glass substrates which is lesser than that observed during material removal through nanoplowing mechanism. The relatively lower value of MRR through this mechanism can be explained by the fact that the number of active abrasive grains impacting the surface at oblique angles could be very less. Figure 5.15 a and b shows representative cross-sectional images of nanocavities machined on silicon and borosilicate glass through nanocracking mechanism.

Figure 5.15: Nanocutting machining results on a) Silicon and b) Borosilicate Glass

From the MDS studies, nanocracking mechanism is identified with formation of small radial cracks under the plastic zone. Figure 5.16 a and b show representative cross-sectional images of nanocavities machined on silicon and borosilicate glass through nanocracking mechanism. Nanocracking mechanism could happen due to pre-existing flaws or heterogeneities under the

plastic zone which can lead to nanocrack development within the bulk of the workpiece. The resulting MRR during the nanocracking mechanism is found to be in the order of 10^5 nm^3/s for silicon and 10^6 nm^3/s for borosilicate glass substrates which is relatively higher than that observed during material removal through other mechanisms.
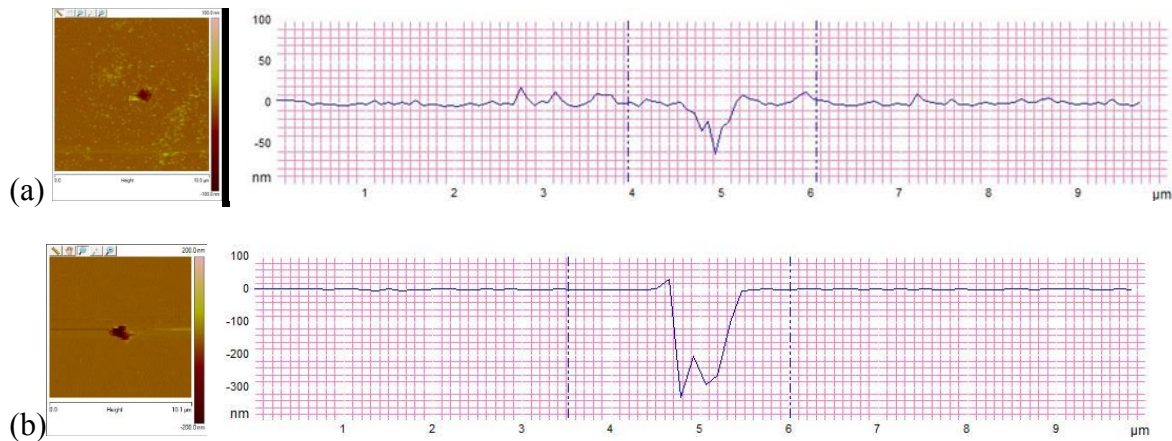
Figure 5.16: Nanocracking machining results on a) Silicon and b) Borosilicate Glass

The material removal mechanisms found in this study is in line with macro scale elastic–plastic material deformation as presented by different authors [187]. It is widely accepted that during an actual impact process owing to the stream of particles, all these modes are present, irrespective of the angle of impact of the stream. However, the coupling between various material removal mechanisms has not been analyzed in this study. In addition, it could be possible that that several complex phenomena would occur due to the repeated hammering that include heating/melting of the target and work-hardening. Other phenomena which could affect the material removal mechanism in ductile mode are thermal softening, flake formation, effect of abrasive grain fragmentation, fatigue due to plastic strain reversals and annealing effects. Thus the actual material removal during nanoscale impact may happen due to a different mechanism which requires further studies.

Chapter Summary

In the first part of this study, molecular dynamics simulations have been performed to gain fundamental understanding of material removal mechanisms involved in the VANILA process. A material removal mechanism map is constructed to capture the effects of critical process parameters – angle of impact and initial kinetic energy of the abrasive grain on the material removal mechanism. Experimentations are conducted on silicon and borosilicate glass substrates and the results are analyzed to confirm the findings of the simulation study. The following specific conclusions are drawn in regards to the understanding of the material removal process in the VANILA process.

i)   MD simulation results of the VANILA process reveals that process parameters, viz., impact velocity of the abrasive grain, abrasive size and angle of impact of the abrasive grain have significant effect on the material removal behavior.

ii)   Depending on the process conditions, material removal in VANILA process occurs in brittle mode, or ductile mode, or their combination. At low impact velocities (range 3-16 nm/ps) the material removal process is dominated by plastic deformation under ductile mode machining. At higher impact velocities (range 30-40 nm/ps), the material removal mechanism is dominated by brittle-mode involving crack formations. Investigations reveal that in addition to the threshold effects i.e., transitions in material removal behavior from brittle to ductile modes, the material removal in VANILA process is also

influenced by the pattern of the cracks formed due to the impact of abrasive particle. Confirmatory tests reveal that in brittle mode machining, material removal is seen to be relative larger with the highest material removal occurring for large angle of impacts in the range of 60 to 90°. On the other hand, in ductile mode machining, the peak is seen for low angle of impacts (range of 15 to 30°), even though the relative material removal is less.

In the second part of this study, molecular dynamics simulations have been performed to gain fundamental understanding of material removal mechanisms involved in the VANILA process. A material removal mechanism map is constructed to capture the effects of critical process parameters – angle of impact and initial kinetic energy of the abrasive grain on the material removal mechanism. Experimentations are conducted on silicon and borosilicate glass substrates and the results are analyzed to confirm the findings of the simulation study. The following specific conclusions are drawn in regards to the understanding of the material removal process in the VANILA process.

i) The MDS results reveal that the material removal happens primarily in ductile mode and there are three distinct nanoscale mechanisms involved in the material removal process – nanocutting, nanoplowing and nanocracking. Amorphous phase transformation of the impact zone along with occasional lip formation and material pileup are also observed.

ii) Material removal mechanism map showed that low angles of impact (30° to 60°) and low initial kinetic energy (100-500 eV) of abrasive grains result in material removal through nanocutting mechanism which is characterized by formation of chip-type substrate molecules. Nanoplowing dominates when the angle of impact is high (60° to 90°) and the

initial kinetic energy of abrasive grain is low (100-500 eV). Nanoplowing mechanism involved plastic deformation and amorphous phase transformation, but does not have chip formation. Higher initial kinetic energies (600-900 eV) results in material removal through nanocracking mechanism due to the formation of nanoscale radial cracks in the bulk of the substrate.

iii)   Experimental results revealed that material removal happen during the VANILA process happens primarily through nanoplowing mechanisms. In addition, two more material removal mechanisms - nanocutting and nanocracking are also observed occasionally.

iv)   Material removal rates values are found to be highest when the material is removed through nanocracking mechanism and is found to be lowest when the material removal happens through nanocutting mechanism.

v)   Both simulation and experimentation suggests that more than one mechanism could dominate the material removal process and the actual material removal could be due to coupled mechanisms.

Chapter 6: Tool Wear Studies

The tool used in VANILA process is an AFM probe which has a nanoscale tip radius. Earlier observations using Scanning Electron Microscopy (SEM) have shown that the tool wear in the VANILA process is lower than that in well-known contact nanomachining processes such as nanoscratching and nanoindentation involving direct tool contact with the workpiece [133]. However, the experimental study based on SEM is inadequate to completely understand the mechanism of the tool wear, quantification and how the actual tool worn shape is formed. The objective of this chapter to understand the tool wear mechanism involved in the VANILA process. The first part of this chapter explains the MDS study conducted for this purpose. The second part explains the analytical modeling for quantifying the extent of tool wear for various operating conditions during the VANILA process.

6.1 Tool Wear Mechanism Study

In this study a MDS based approach is used to understand the tool wear process. The results show that the tool wear is affected by the impact velocity of the abrasives and the effective tool tip radius. It is seen that based on the process conditions, the wear occurs through different distinct mechanisms such as gradual atom-by-atom loss, plastic yielding and fracture. Experimental findings provide some hint of tool wear by aforementioned mechanisms in VANILA process.

6.1.1   Motivation For Tool Wear Study in VANILA Process

The level of precision of the nanomachined features continuously degrade during machining as the tool wear is unavoidable [105]. Determining the point at which the tool is considered worn is important, since after this point, machining cannot be continued since machined features dimensions are no longer accurate [188]. In addition, certain tool materials have shown repeatable wear characteristics, which allows for compensation through tool or a timely replacement of the tool [189]. Thus characterization of tool wear to get a fundamental understanding of the underlying physical processes and predicting the extent of the nanoscale wear is of great significance. The objective of this study is to investigate the tool wear in the VANILA process in order to understand its underlying mechanisms.

6.1.2 Molecular Dynamics Simulation of Tool Wear in VANILA Process

In this study, the tool wear process is simulated using a tool and randomly generated abrasives grains which are given an initially velocity towards the tool tip. The abrasive grains impact the stationary tool tip with high velocity causing wear of tool tip while the grains remain intact. For this, a two-dimensional MD simulation model has been implemented using LAMMPS [176]. The two-dimensional assumption can be justified by the axisymmetric geometry of the tool tip. The model consists of randomly generated spherical abrasive grains (diamond material) and a conical tool (silicon material) having dimensions proportional to actual AFM probe used in the VANILA process experimentation.

The initial atomic configuration of the tool material consists of approximately 3000 silicon atoms (lattice constant 5.43 Å). The tool tip radius and height are 2.5 Å and 300 Å respectively. The simulation is performed in the x-y plane with the tool axis aligned in the y-axis direction. The geometry does have a small finite thickness in the z-direction. The reason for the finite thickness is LAMMPS specific - in 2D, the particles will still be spheres or ellipsoids, not circular disks or ellipses, meaning their moment of inertia will be the same as in 3D. The boundary atoms in the top two layers of workpiece atoms are fixed.

Each diamond abrasive grains consists of carbon atoms (lattice constant 3.57 Å) within a rigid sphere of radius in the range of 1-10 Å. A non-periodic and shrink wrapped boundary condition is used along x and y axes while, a periodic boundary condition is applied along z–axis. Shrink wrapped is a style of boundary command in LAMMPS in which the position of the respective boundary is set so as to encompass the atoms in that dimension irrespective of the distance moved by the atoms. Even though such a model does not represent the exact experimental conditions, it is used to reduce the computational processing time.

The interatomic forces between the Si-diamond atoms and Si-Si atoms are calculated using Tersoff potential [123]. The Velocity-Verlet algorithm is employed to calculate the position and velocity of the atoms. The conditions used in the simulation study are given in Table 6.1. The schematic of the tool wear simulation model is displayed in figure 6.1.
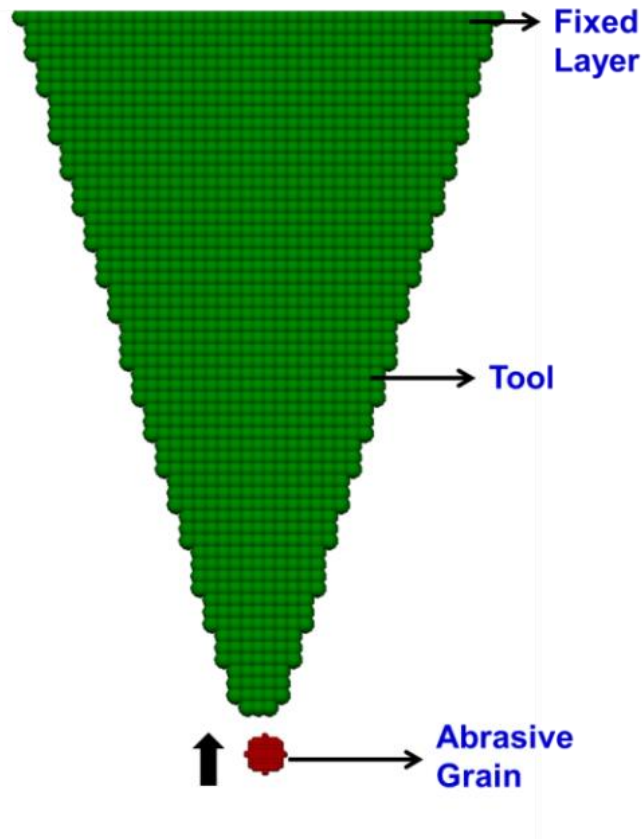
Figure 6.1: Schematic of MDS model to study tool tip wear during VANILA process

Simplification Assumptions

i)   Owing to computational complexity, this simulation study does not include the liquid medium.

ii)   The process can be considered as discrete and that a single impact event of abrasive grain with the tool is a good understanding of the complex phenomenon of wear process due to impact damage.

Table 6.1: Simulation Conditions used in the MDS Study of VANILA process Tool Wear

Tool	Material	Silicon
	Size and Shape	Conical Tip Radius 1-100 Å Tip Height 300 Å
	No. of Atoms	Approx. 3000
Abrasive Grains	Size and Shape	Diamond Carbon
	Dimension	Sphere 5 Å Radius
	No. of Atoms/ Grain	13
Simulation Condition	Potential Used	Si.tersoff Si Si SiC.tersoff Si C
	Temperature	300 K
	Initial Gap	10 Å
	Impact velocity	10^4 m/s unless otherwise specified
	Time step	0.001 ps
	Duration of Simulation	1 ps

iii)   The effect of temperature rise is neglected in this study. For the range of temperature rise suggested by the simulation, the liquid should rapidly evaporate. However this is not witnessed during the experimentation. Hence the assumption is justified.

iv)   Various crystalline structures of silicon could affect the wear behavior, however, this is not included as a parameter in this study.

v)   The tool and the abrasive grains are considered to be chemically inert and any possible chemical reactions are not considered in this study.

vi)   High pressure phase transformation (HPPT) of silicon is not considered in this study. This can be justified by the fact that a critical hydrostatic pressure of at least 11 GPa is required for HPPT to happen [190] while during the VANILA process tool wear, the pressures are theoretically calculated to be in the range of only 10-100 MPa.

A representative deformation behavior of the tool molecules during the VANILA process is displayed in figure 6.2. The atoms are color-coded with green color showing tool atoms and maroon color showing abrasive grains. The number of tool atoms removed is calculated as ensemble of tool atoms which are displaced more than 5.43 Å from their respective initial positions.

Figure 6.2: MD simulation of tool wear in VANILA process a) before impact b) after impact

One of the critical factors which is involved in the tool wear process in VANILA process is the relative sizes of the tool and the abrasive grain. Initially, the tool tip size is comparable to the abrasive grain size, however, as the wear progresses the relative size varies significantly. In this study, this size effect phenomenon is captured using the *Effective tool tip radius* R^* which is defined as suggested in literature on classical Hertzian contact theory to determine the contact radius between the impacting bodies as [191, 192]

$$R^* = \left(1/R_a + 1/R_t\right)^{-1} \qquad (6.1.1)$$

where R_t is the radius of tool tip and R_a is the radius of abrasive grain. The effective radius term would help study the tool wear in the VANILA process using tool tips with different curvature. This usage of R^* is typical used in classical contact mechanics to estimate the contact radius between the impacting bodies

6.1.3 Mechanism of Tool Wear in VANILA Process

Several MD simulations using the conditions listed in Table 6.1 are performed for various combinations of effective radii and abrasive impact velocities. The impact velocities considered in this simulation study are higher order than the theoretically estimated impact velocity values (in range of 10^2 to 10^3 m/s). This is due to the limitation of computing power and time. The timestep used is 0.001 ps which is recommended by LAMMPS for this conditions used in this simulation. MD simulation results depicting the various tool wear mechanisms are shown in figure 6.3. The various failure mechanisms are identified based on visual inspection and the number of atoms removed. Figure 6.4 plots a mechanism map for the wear process for different impact velocities and effective radii. For low values of effective radius R^*, the wear is found to

109

happen through a succession of mechanisms starting from atom-by-atom loss followed by ductile mode material removal. At large effective radius values, the tool wear rate is observed to be very high. On the other hand, impact velocity is the factor which influences the transition between ductile and brittle material removal modes. High impact velocities result in brittle mode dominating the material removal process with the onset of radial and lateral cracking.

| (a) | (b) | (c) |
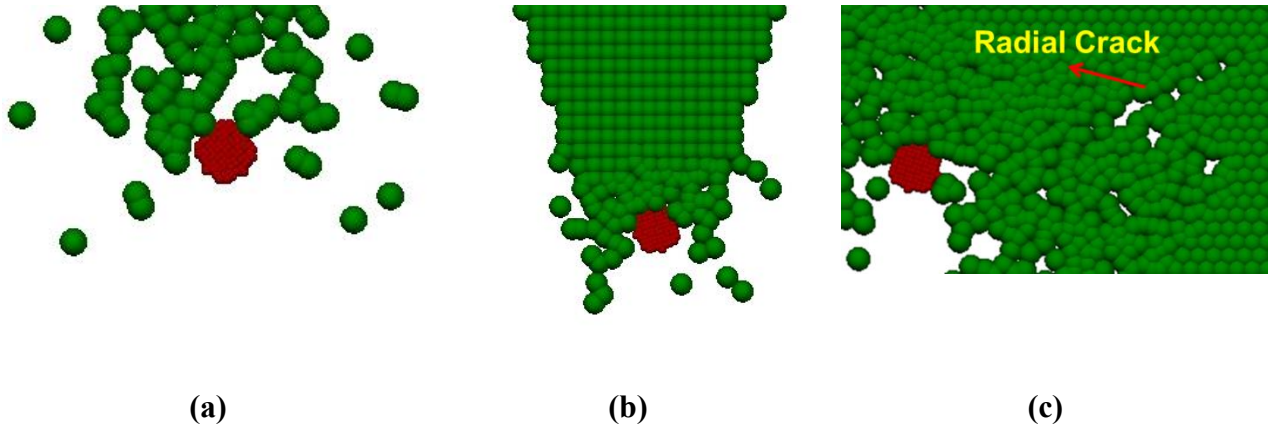
Figure 6.3: Various Tool Wear Mechanisms involved in the VANILA process a) Atom-by-Atom attrition b) Ductile Mode and c) Radial Cracking [193]

6.1.4 Effects of Process Parameters

The following section discusses the effects of critical process parameters on the tool wear in the VANILA process.

6.1.4.1 Number of Atoms Removed versus Impact Velocity

The number of atoms removed from the tool with respect to the impact velocity for simulation duration of 1 ps is shown in figure 6.5. The simulation duration of 1 ps is taken as a standard for

comparison purpose, even though the wear rate does not reach zero at this timestep. Figure 5
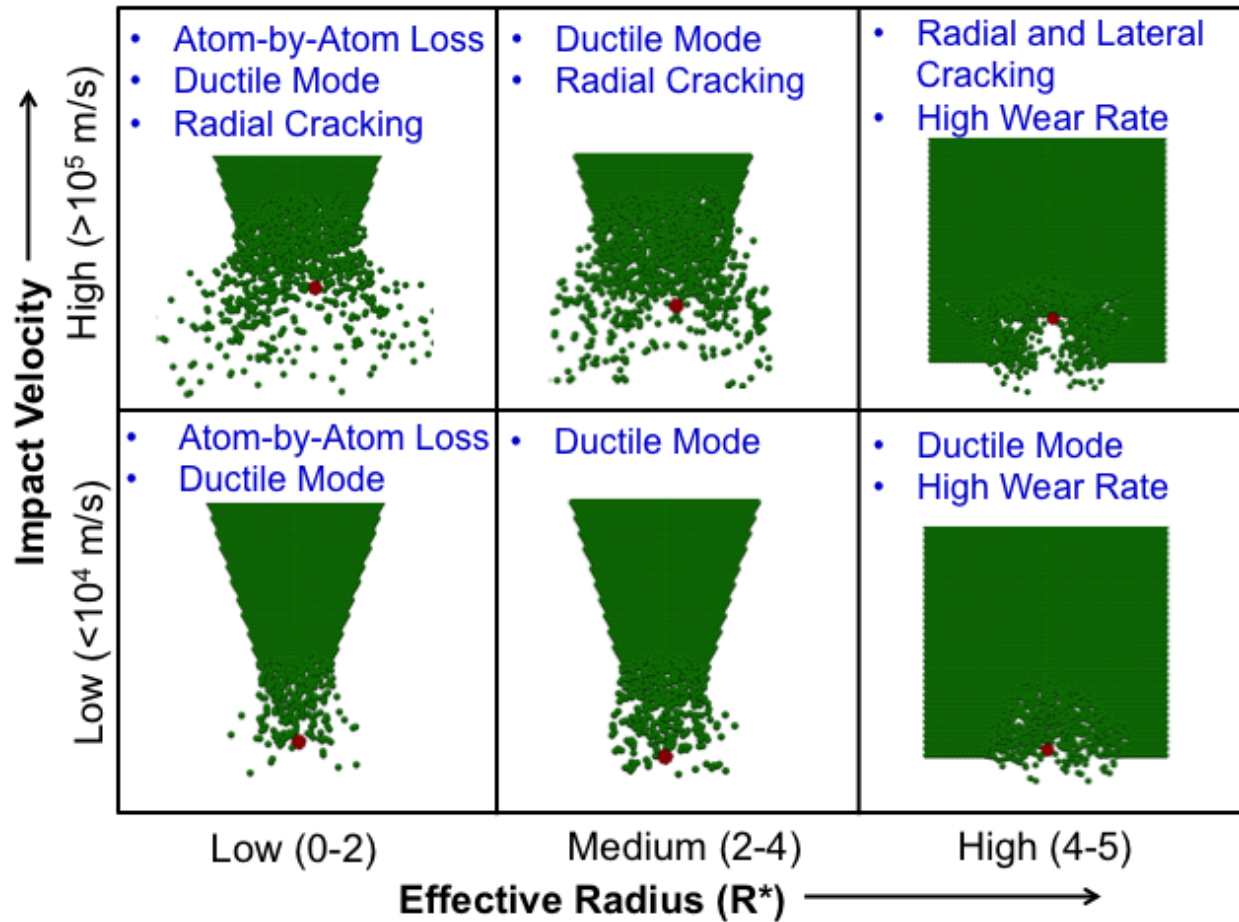
Figure 6.4: Tool Wear Mechanism Map [193]

helps us understand the various modes of material removal – in particular the brittle fracture

mode which is prominent at higher velocities. The abrasive grain size diameter used is 5 Å with

an initial gap of 10 Å between the abrasive grain and tool tip. It is seen that at the number of tool

atoms removed steadily increases with respect to impact velocity of the abrasive grain.

At low impact velocities, it is seen that the tool tip wears through ductile mode through plastic

yielding. However, with increasing values of impact velocity, the tool wears due to crack

formation of different kinds such as radial and lateral cracks, resulting in increase in the number of tool atoms removed. It is noted that impact velocity considered to plot this graph is in the low velocity range according to figure 6.4. For very high velocities ($> 10^5$ m/s), the wear rate is considerably high since the significant wear happens through brittle fracture. The tool geometry considered in this study is very small to conduct simulation for duration of 1 ps for these very high velocities and hence this range of high velocities is not plotted in this graph.
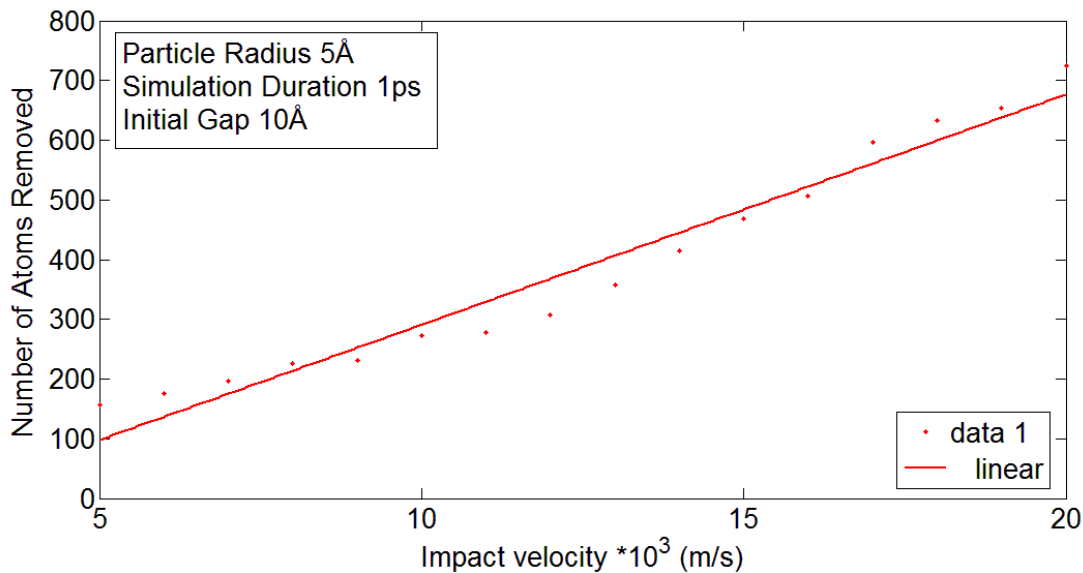
Figure 6.5: Number of Atoms Removed vs. Impact Velocity

6.1.4.2 Number of Atoms Removed versus Abrasive Grain Size

Figure 6.6 shows the variation of number of atoms removed from the tool with respect to the abrasive grain size for duration of 1 ps for the impact velocity of 10^4 m/s with an initial gap of 10 Å between the abrasive grain and tool tip. The velocity range focused in this study is of 0 to $2*10^4$ m/s which corresponds to the low/medium impact velocity zone according to figure 5b. An average value of 10^4 m/s is thus chosen for plotting this graph. It is seen that the tool tip wear

steadily increases with the grain size. This can be explained by the fact that as the grain size increases, the kinetic energy increases and causes more tool damage.
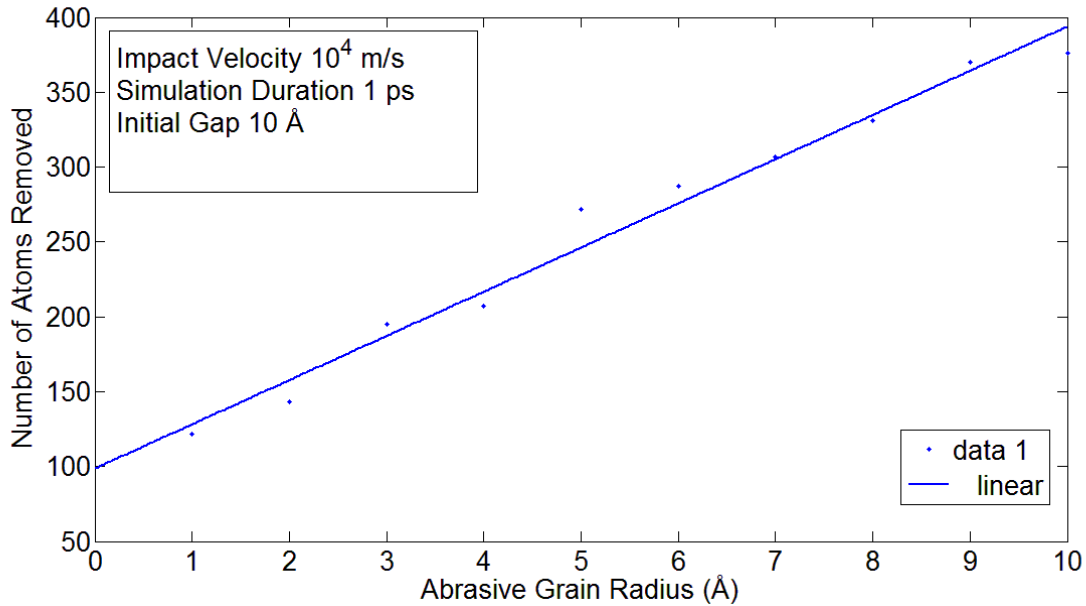
Figure 6.6: Number of Atoms Removed vs. Abrasive Grain Size

6.1.4.3 Number of Atoms Removed versus Effective Tip Radius

The variation in number of atoms removed from the tool with respect to effective tip radius is shown in figure 6.7. The study used an abrasive grain impact velocity of 10^4 m/s with an initial gap of 10 Å between the abrasive grain and tool tip. In this plot, the abrasive grain is kept constant at 5 Å, which essentially means only a single combination of the tool tip and abrasive grain radius will give a specified effective radius value.

During experiments, it is the tool tip that undergoes radius change due to wear and the abrasive grain radius remains constant which justifies the rationale for this plot. Four distinct zones can be identified in the figure. Initially (zone I) a small slope is observed which is relatively constant and material removal happens through atom-by-atom loss. In this regime the tip radius is smaller than the abrasive grain size. As the wear progresses (zone II), the slope increases indicating the removal of larger number of tool atoms. The material removal mainly happens through ductile mode. As the tool become further blunt (zone III), the slope increases drastically and the material removal is caused by radial and lateral cracking. Further, the number of tool atoms removed remains steady with increases of the effective radius (zone IV).
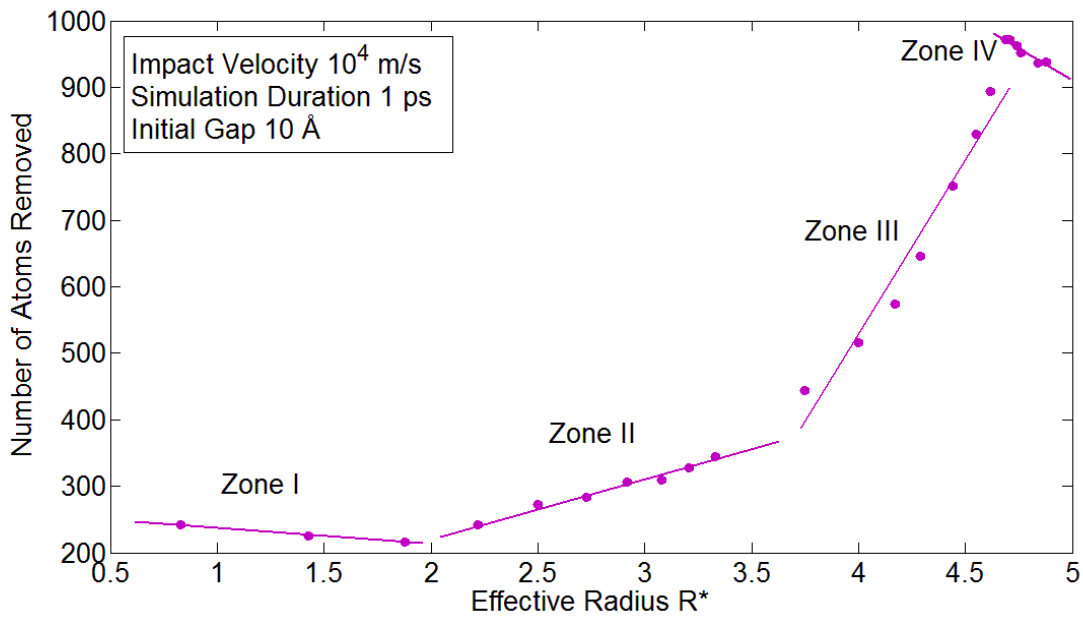
Figure 6.7: Number of Atoms Removed vs. Effective Tip Radius

Figure 6.8 shows a schematic of the tool showing four distinct wear zones during the VANILA process and the tool wear may happen through any of the three possible mechanisms viz., i) atom-by-atom loss ii) ductile mode through plastic deformation and iii) brittle mode as shown in figure 5a. The wear zones are distinguished based on the wear mechanism and the number of tool atoms removed. The concept of wear zones is introduced with the objective of relating the effective tool tip radius with corresponding wear mechanism.
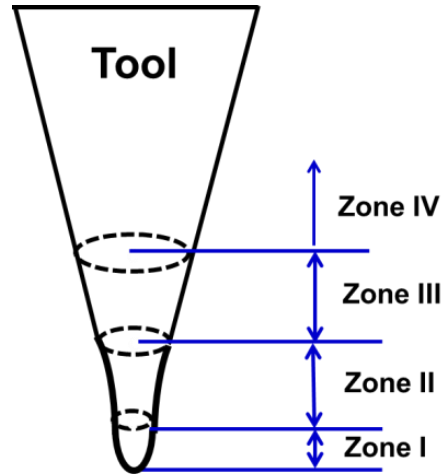
Figure 6.8: Tool Tip Showing Wear Zones

6.1.5 Experimental Observations

In order to experimentally confirm the findings of the MD simulation, the VANILA process experiments are conducted on silicon and glass substrates using different silicon tool tips and 10 nm sized diamond nanoparticles on a commercial AFM. The machining is conducted for different durations and the tool tips are observed using an SEM in order to assess the tip wear. The results obtained are shown in Figure 6.9. The experimental results confirm the predictions by MDS that the tip could undergo wear primarily through three wear mechanisms – a) atom-by-atom loss, b) plastic deformation and c) brittle fracture due to the impact with the diamond abrasive grains. The purpose of the experimentations in this study is to observe the various modes of wear, even though a direct comparison between the simulation results and experimental results are not appropriate since the experimentation is conducted for multiple cycles of impact.

Before machining   **After machining**

Side view

Bottom view

(a) Atom-by-Atom   (b) Plastic   (c) Brittle

Loss   Deformation   Fracture
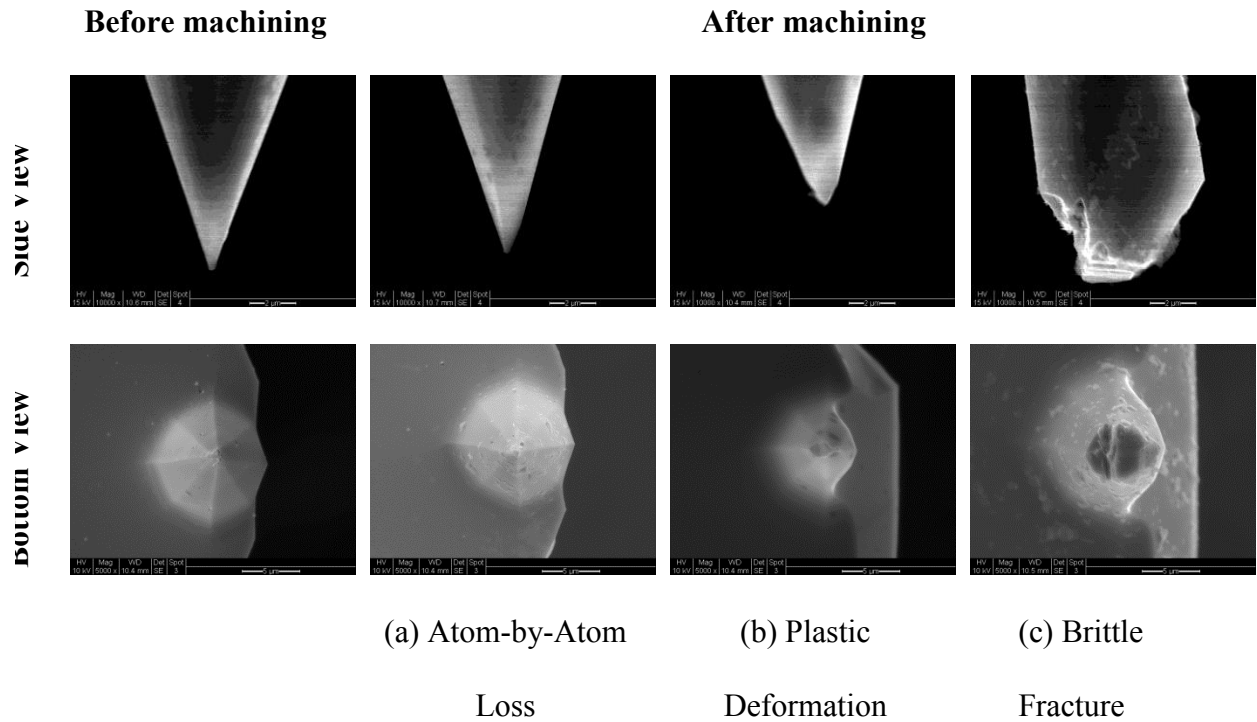
Figure 6.9: Scanning Electron Microscopy analysis results showing Tool Wear

6.2 Mathematical Modeling of Tool Wear

The tool wear rate in the VANILA process is theoretically modeled in this section. The wear is caused due to the impact of abrasive grains on the tool tip surface. Earlier studies using Scanning Electron Microscopy (SEM) imaging have shown that tool wear in the VANILA process is comparatively lower than that in other nanomachining processes such as nanoscratching and nanoindentation involving direct tool contact with the workpiece (figure 3) [133]. The critical factors determining the machining accuracy in a tip-based nanomachining process is the sharpness, material and the geometry of the tool tip [105]. The level of precision of the

nanomachined features continuously degrade during the machining process [105]. Determining the point at which the tool is worn is critical since the machinated features won't be within required accuracy after this point [188]. Thus it is important to estimate the tool wear rate and also the tool life. This study aims to develop a theoretical model to estimate the degree of tool wear rate involved in the VANILA process.

6.2.1 Mechanism Of Tool Wear During VANILA Process

A review of the available literature reveals that that AFM tip wear occurs through multiple wear mechanisms [98, 100] such as abrasive and adhesive wear [109], low-cycle fatigue and material fracture [109], plastic deformation [107], coating failure, corrosive wear, tribo-chemical wear [107], and thermo-chemical wear [113]. The wear of AFM probes has been studied at nanoscale during nanoscratching process and it is found that the damaged surface is smoothly modified [103]. The mechanism is termed as gradual atom-by-atom attrition in which atoms are removed one at a time from the tool periphery.

In VANILA process, the tool is subject to continuously strikes by nanoparticles in the slurry. The frequent impacts at the nanoscale often lead to considerable size effects both in the length and time scales. Also at nanoscale, the energy required to break the atomic bonds decrease due to bond stretching [119]. Based on the literature study, it is clear that among the various mechanisms involved; wear due to gradual atomic attrition would be the most significant mechanism. The tool wear model is thus analytically developed in order estimate the amount of tool material that gets removed by the successive impacts of the abrasive grains.

117

6.2.2   Modeling of Tool Wear in VANILA Process

The tool wear in the VANILA process is attributed to the interaction between the tool tip and the suspended diamond abrasive particles. In order to model the wear rate, the following assumptions are used.

Impact Velocity and Forces

The abrasive nanoparticles undergo dynamic motion in the in the slurry medium resulting in impact with the resonating tool. The net velocity of impact (V_I) is the resultant of two components a) tool velocity (Vt) and b) abrasive velocity (Va). The motion of tool tip can be expressed as $A_t e^{i(\omega t + \pi/2)}$. The phase associated with the total force can be considered as $\pi/2$ since on resonance the oscillations of the cantilever follow the total force with a phase delay of $\pi/2$ [138]. Average velocity of the tool tip (V_t) is calculated as

$$V_t = 0.5\omega A_t = \pi f_t A_t \qquad (6.2.1)$$

The velocity of the nanoparticles in the liquid medium can be considered to be approximately equal to the fluid molecule velocity. The acoustic streaming motion generated by the acoustic field around the tip region lead to the motion of the liquid molecules between the tool tip and the workpiece surface. The streaming fluid molecules transports the nanoparticles and causes impact with the tool tip surface. The nanoparticle velocity (V_a) can be estimated using the relation [150]

$$V_a = \left[I_t \big/ \rho_{fl} c_{fl} \right]^{1/2} \qquad (6.2.2)$$

where I_t is the vibrational intensity of the acoustic waves produced near the tip region and can be

estimated as the ratio of the acoustic power to the area of the radiating surface which is the tool

tip surface area [153].

$$I_t = P_t \big/ (\pi R_t^2) \qquad (6.2.3)$$

The acoustic power can be calculated as [104]

$$P_t = \frac{\pi k_t A_t^2 f_t}{Q_t} \qquad (6.2.4)$$

The impact velocity V_I is the resultant of the two velocity components $V_I = V_t + V_a$ $\qquad (6.2.5)$

Due to momentum conservation, the impact force (F_I). on the tool tip surface due to the impact

with the abrasive nanoparticles can be determined [182].

$$F_I = \frac{m_a V_I \sin\theta}{\Delta t} \qquad (6.2.6)$$

where θ is the angle of impact and Δt is the response time defined as

$$\Delta t = \frac{2\rho_{fl} R_a^2}{9\rho_a \nu_{fl}} \qquad (6.2.7)$$

The response time in this study is taken as the time for the nanograins to respond to changes in

the bulk liquid [182].

Establishing Threshold Criteria

When the critical pull-out force F_c, is exceeded by the tool impact force, the tool atoms are able to pass through a critical energy barrier resulting in gradual atom-by-atom attrition [119]. The critical pull-out force can be written as [194]

$$\boldsymbol{F_c} = \frac{3}{2}\pi w R^*$$
(6.2.8)

where w is the Dupré energy of adhesion and R^* is effective radius of the tip which is given by [194]

$$R^* = \left(1/R_a + 1/R_t\right)^{-1}$$
(6.2.9)

This usage of R^* is typical used in classical contact mechanics to estimate the contact radius between the impacting bodies

Estimation of Tool Wear Rate

Tool wear rate *TWR* is modeled as a function of volume τ_t removed by single impact, the total number of active abrasive grains n_a and the frequency of vibration f_t.

$$TWR \propto \tau_t * n_a * f_t$$
(6.2.10)

Using λ as constant of proportionality, the wear rate can be written as

$$TWR = \lambda * \tau_t * n_a * f_t$$
(6.2.11)

λ can be termed as wear coefficient and it is determined experimentally.

Volume Removed by Single Impact

The tool volume removed τ_t due to interaction with single nanoabrasive grain can be expressed as [101].

$$\tau_t = \Delta t * n_{atom} * w_{atom} * vol_{atom} \qquad (6.2.12)$$

where n_{atom} is the number of atoms escaping the critical limit, w_{atom} is the transition rate, vol_{atom} is the individual atomic volume. Δt corresponds to the time of interaction between the abrasive grain and the tool. The term $(n_{atom} * w_{atom})$ can be calculated using Arrhenius kinetics [195] as below [101].

$$w_{atom} * n_{atom} = f_{atom} * \bar{\rho}_t * A_c * e^{-\Delta E / k_B T} \qquad (6.2.13)$$

where ΔE = effective activation energy barrier, k_B = Boltzmann constant, $\bar{\rho}_t$ = surface atomic density of the tool, A_c = contact circular area having diameter R^* i.e. $A_c = \pi R^{*2}$. The term f_{atom} is the attempt frequency or oscillation frequency. The effective activation energy barrier ΔE is calculated as ($\Delta E = \boldsymbol{E_{act}} - \boldsymbol{E_i}$).

Number of Active Abrasives

n_a is the number of active nanoparticles within the gap between the tool and the workpiece surface. The vibrating tool impacts the abrasive grains within a assumed volume as shown in dotted line in figure 6.10.
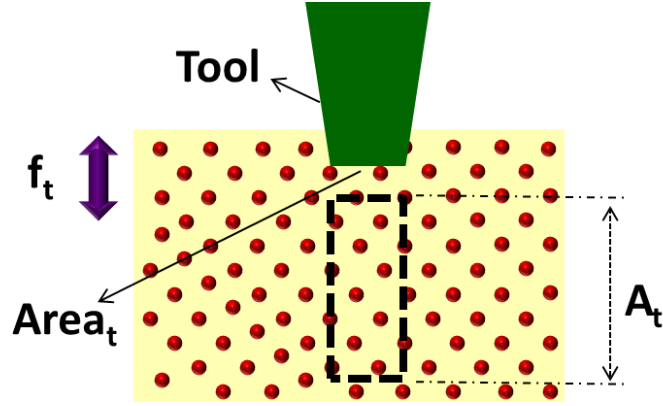
Figure 6.10: Zone of impact of tool and abrasive grains

The volume of abrasive particles within the assumed region can be written as

$$Volume = Area_t A_t c_z \qquad (6.2.14)$$

where $Area_t$ is the tool tip area given by $Area_t = \pi R_t^2$, c_z is volume concentration.

The volume of nanoparticles within the assumed region can also be written as the product of the number of abrasive nanoparticles (n_a) within the imaginary cylinder and volume of a single grain.

$$Volume = n_a * \frac{4\pi R_a^3}{3} \qquad (6.2.15)$$

Using the above equalities, n_a can be calculated as

$$n_a = (3R_t^2 A_t c_z)/(4\,R_a^3) \qquad (6.2.16)$$

Tool Wear Rate Model

Finally, the tool wear rate TWR can be expressed as

$$TWR = \frac{\pi\lambda}{6} * f_t A_t * \frac{(R_t R^*)^2}{R_a} c_z * \frac{\rho_{fl}}{\rho_a v_{fl}} * \bar{\rho}_t * f_{atom} * vol_{atom} * e^{-\Delta E / k_B T} \qquad (17)$$

6.2.3   Experimental Verification

The VANILA process experiments are performed using various commercially available tapping mode AFM probes and 10 nm sized diamond powder mixed with water. The tool is made of silicon having a tip diameter of approximately 8-10 nm and is excited at its resonance frequency (5-50 KHz range). AFM (Veeco Dimension 3100 with Nanoscope III) is used for conducting the machining process. The tool tip is vibrated at its resonant frequency. The common experimental conditions are listed in table 6.2.

Table 6.2: Experimental Conditions for VANILA Process Tool Wear Study

Machine	AFM Dimension 3100
Abrasive	10 nm sized diamond nanoparticles
Tool	Silicon with ~ 8 nm tip radius
Liquid Medium	Deionized water
Slurry Concentration	0.7 vol. conc %
Temperature	300 K

Scanning Electron Microscope (make - FEI XL30 ESEM) is used to analyze the tool tip after machining for known duration. In order to determine the wear volume with nanoscale precision, three-dimensional computer models of the tool tips are created using 3D modeling software SolidWorks™. The tip wear volume is calculated then calculated using relevant dimensions from the SEM images of the tool tip such as worn tip length and tip radius. Experimental tool wear rate (TWR) is calculated as the ratio of wear volume to the total time spent by the

resonating tip in the abrasive slurry. Figure 6.11 shows the SEM images of an unused tool tip and a tool tip used to conduct the VANILA process for 300 seconds along with a CAD model of the tip.

a) Unused Tool Tip   b) Worn Tool Tip after 300 s   c) CAD model of Tool Tip
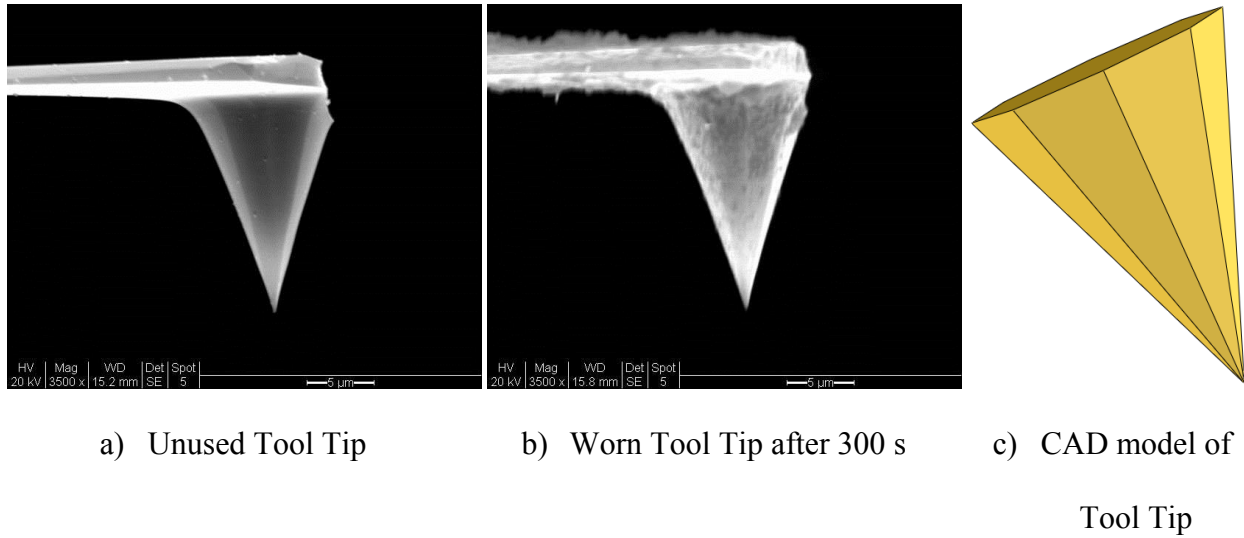
Figure 6.11: Scanning Electron Microscopy analysis results of tool wear and CAD Model of tip of the tool

Surface atomic density of the tool tip $\bar{\rho}_t$ is taken as 10^{16} atoms/cm^2 [196], the response time is approximately 10^{-12} seconds and the attempt frequency f_{atom} has typical values of 10^{13} cps for silicon [197]. The atomic volume of silicon (vol_{atom}) is taken as 0.02 nm^3 with an activation energy E_{act} value of 0.9 eV [119]. Based on these parameters, the velocity of impact is approximately in the range of 2-3 m/s while the force is estimated to be between 20-50 nN assuming the angle of impact to be normal.

A value of 4 mJ/m^2 is taken for the Dupré energy of adhesion for silicon [198] and the critical pull-out force Fc is estimated to be 0.19 nN. This force is lesser than impact force suggesting the

tool to undergo wear. Figure 6.12 depicts the comparison of theoretically predicted and the experimental values of tool wear rates for machining time ranging from 100 s to 1200 s for a λ value of 9500.
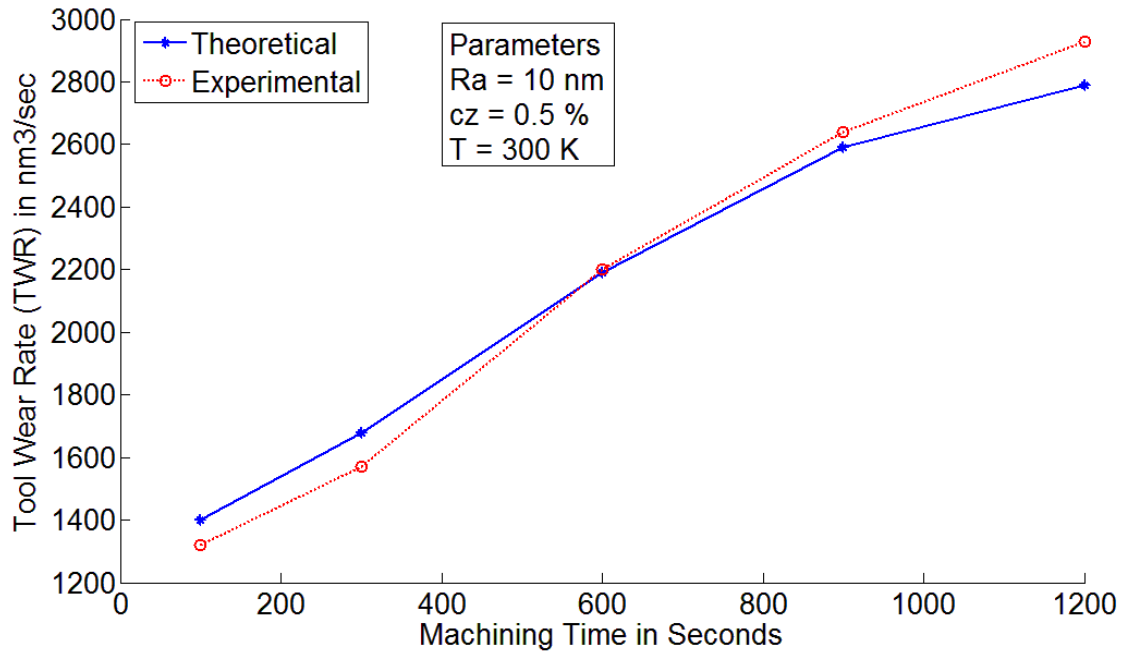
Figure 6.12: Comparison of theoretical and experimental results of tool wear rates

The graph suggests the model is capable of predicting the experimental results within 10% error. Also, the wear increases as the machining progresses. This could be due to the fact that as the machining duration increases, the more number of active abrasives interact with the tool tip surface resulting in larger wear rate.

Chapter Summary

In the first section, a two-dimensional MD simulation model has been implemented using LAMMPS and MD simulations were carried out to study the tool wear mechanism in the VANILA process.

   i.   Impact velocity of the abrasive particles and the effective tool tip radius are the most critical factors affecting the tool wear.

   ii.   It is seen that at the number of tool atoms removed proportionally increase as the velocity of impact and abrasive grain size increases. Further, the variation in number of atoms removed from the tool with respect to effective tip radius reveals four distinct wear zones suggesting that the wear process could happen through distinctive mechanism such as atom-by-atom loss, ductile mode and brittle modes.

   iii.   Experimental results confirm the predictions by MDS of tool wear by aforementioned mechanisms in VANILA process.

In the second section, the tool wear rate is modeled analytically and verified using experimental methods.

   i)   The calculated tool wear rate is of order of 10^3 nm^3/s for silicon based tools.

   ii)   Experimentation is conducted to verify the model predictions. The results show that the experimental results are accurately predicted by the analytical model within 10% deviation.

Chapter 7: Conclusion

- A new nanomachining process – Vibration Assisted Nano Impact-machining by Loose Abrasives (VANILA) that combines the principles of vibration-assisted abrasive machining and tip-based nanomachining is introduced in this work to perform target specific nano abrasive machining of hard and brittle materials.

- An analytical model based on Hertzian fracture theory is developed to evaluate the feasibility of the process for different workpiece materials.

- Nanoscale machining using the VANILA process was successfully performed experimentally on silicon and borosilicate glass substrates and nano-cavities with circular cross-sections having depths in the range of 5-100 nm and diameters in the range of 50-300 nm were achieved. In addition, patterns of nano-cavities were successfully machined to demonstrate the controllability and repeatability of the process.

- An analytical modeling based force analysis is conducted to understand the effect of significant forces acting on a nano particle moving in liquid medium. A theoretical model is developed to predict the velocity and penetration depth of nanoparticle within the nanofluid. The effective machining gap between the tool and the work surface is determined to be less than 200 nm for the size range of abrasive grains used in this study.

- A predictive model for MRR during the VANILA process based on elasto-plastic impact theory for normal angles of impact is developed and validated through a series of experiments performed on silicon and borosilicate glass substrates. The experimental results confirm that the model is capable of predicting the machining results within 10% deviation.

- Molecular dynamics simulations have been performed to evaluate the effect of critical process parameters, and study the material removal mechanism in the VANILA process. A material removal mechanism map capturing the effects of impact velocity and abrasive grain size on the occurrence and transitions between plasticity-dominated and fracture-dominated behavior during VANILA process is made, which reveals different regimes of material removal mechanisms and their transitions.

- The MDS results reveal that the material removal happens primarily in ductile mode and there are three distinct nanoscale mechanisms involved in the material removal process – nanocutting, nanoplowing and nanocracking. Amorphous phase transformation of the impact zone along with occasional lip formation and material pileup are also observed.

- Material removal mechanism map showed that low angles of impact (30° to 60°) and low initial kinetic energy (100-500 eV) of abrasive grains result in material removal through nanocutting mechanism which is characterized by formation of chip-type substrate molecules. Nanoplowing dominates when the angle of impact is high (60° to 90°) and the initial kinetic energy of abrasive grain is low (100-500 eV). Nanoplowing mechanism involved plastic deformation and amorphous phase transformation, but does not have chip formation. Higher initial kinetic energies (600-900 eV) results in material removal through nanocracking mechanism due to the formation of nanoscale radial cracks in the bulk of the substrate.

- A two-dimensional MD simulation model has been implemented using LAMMPS and MD simulations were carried out to study the tool wear mechanism in the VANILA process. It is seen that at the number of tool atoms removed steadily increases with respect to increase in the impact velocity of the abrasive grain and abrasive grain size. Further, the variation in

number of atoms removed from the tool with respect to effective tip radius reveals four distinct wear zones suggesting that the wear process could happen through distinctive mechanism such as atom-by-atom loss, ductile mode and brittle modes.

- Tool wear rates are estimated to be of the order of 10^3 nm^3/s during the machining process for tool tips made of silicon. In order to validate the model, experiments are performed with different tools for varying machining durations. Reasonably good quantitative correlations (within 10%) are obtained between the model predictions and the corresponding experimental observations.

List of Publications and Presentations

Journal Papers

1. James, Sagil. and Sundaram, M.M., "*A feasibility study of Vibration Assisted Nano Impact-machining by Loose Abrasives using Atomic Force Microscope*", Journal of Manufacturing Science and Engineering, December 2012 - Volume 134, Issue 6, Pages 061014 (1-11)

2. James, Sagil. and Sundaram, M.M., "*A Molecular Dynamics Study of the Effect of Impact Velocity, Particle Size and Angle of Impact of Abrasive Grain in the Vibration Assisted Nano Impact- machining by Loose Abrasives*", Wear, 2013, Volume 303, Issue 1, Pages 510-518

3. James, Sagil., Blake L. and Sundaram, M.M., "*Modeling and Experimental Verification of Nano Positioning System for Nanomanufacturing*" International Journal of Manufacturing, Materials and Mechanical Engineering (IJMMME), 2013, Volume 3, Issue 4, Pages 1-13

4. James, Sagil. and Sundaram, M.M., "*A Study on the Vibration Induced Transport of Nano Abrasives in Liquid Medium*", Powder technology, 268 (2014) 150-157

5. James, Sagil. and Sundaram, M.M., "*Modeling of Material Removal Rate in Vibration Assisted Nano Impact-machining by Loose Abrasives*", Journal of Manufacturing Science and Engineering, International Journal of Manufacturing Engineering, 137 (2015) 021008, doi:10.1115/1.4028199

6. James, Sagil. and Sundaram, M.M., "*Molecular Dynamics Simulation Study of Tool Wear in Vibration Assisted Nano Impact-machining by Loose Abrasives*", Journal of Micro and Nano-Manufacturing, 3 (2015) 011001

7. James, Sagil. and Sundaram, M.M., "*Modeling of Tool Wear in Vibration Assisted Nano Impact-machining by Loose Abrasives*", International Journal of Manufacturing Engineering, vol. 2014, Article ID 291564, 8 pages, 2014, doi:10.1155/2014/291564

8. James, Sagil. and Sundaram, M.M., " *Effects of water molecules on material removal behavior in Vibration Assisted Nano Impact-machining by Loose Abrasives - A molecular dynamics simulation study*" , (Under Preparation)

9. James, Sagil. and Sundaram, M.M., "*Review of Impact based Abrasive Machining Processes*" , (Under Preparation)

10. James, Sagil. and Sundaram, M.M., "*A Molecular Dynamics Simulation Study of Material Removal Mechanisms in Vibration Assisted Nano Impact-machining by Loose Abrasives*" , (To be submitted)

Conference/ Presentations/Posters

1. Sundaram, M. M., James, Sagil. and Rajurkar, K.P , "Exploratory Study of Nano Ultrasonic Machining Process" Poster, Workshop on Nano and Micro Manufacturing on May 23, 2013, Dearborn, Michigan

2. James, Sagil. and Sundaram, M. M., "Study of Vibration Assisted Nano Impact-Machining by Loose Abrasives (VANILA) Process" 2013 Graduate Poster Forum at University of Cincinnati, Best poster award

3. Blake, L., James, Sagil., and Sundaram, M. M., "Design of a Nano-Positioning System for Nano-manufacturing" 8th Annual Dayton Engineering Sciences Symposium (DESS) on October 29, 2012 at Wright State University Student Union, Dayton, OH

4. Sundaram, M. M., James, Sagil. and Rajurkar, K.P., 2012, "Vibration Assisted Nano Machining By Loose Abrasives", Presented at the CIRP-2012 Collaborative Working Group meeting on Hybrid Processes held at Paris on Wednesday 25th January 2012

5. Sundaram, M.M. and James, Sagil. "Vibration Assisted Nano Abrasive Machining", 7th International Conference on Precision, Meso, Micro, and Nano Engineering (COPEN), December 10-11, 2011, College of Engineering Pune, pp.20-25

Bibliography

[1] Komanduri, R., Lucca, D. A., and Tani, Y., 1997, "Technological advances in fine abrasive processes," Annals of the CIRP, 46(2), pp. 545-596.

[2] Inasaki, I., Tönshoff, H., and Howes, T., 1993, "Abrasive machining in the future," CIRP Annals-Manufacturing Technology, 42(2), pp. 723-732.

[3] Loveless, T., Williams, R., and Rajurkar, K., 1994, "A study of the effects of abrasive-flow finishing on various machined surfaces," Journal of Materials Processing Technology, 47(1), pp. 133-151.

[4] Kordonski, W. I., and Jacobs, S., 1996, "Magnetorheological finishing," International Journal of Modern Physics B, 10(23n24), pp. 2837-2848.

[5] Jiang, M., and Komanduri, R., 1997, "Application of Taguchi method for optimization of finishing conditions in magnetic float polishing (MFP)," Wear, 213(1), pp. 59-71.

[6] Kordonski, W., and Golini, D., 1999, "Progress update in magnetorheological finishing," International Journal of Modern Physics B, 13(14n16), pp. 2205-2212.

[7] Mori, Y., Yamauchi, K., and Endo, K., 1987, "Elastic emission machining," Precision Engineering, 9(3), pp. 123-128.

[8] Jain, V., 2008, "Abrasive-based nano-finishing techniques: an overview," Machining Science and Technology, 12(3), pp. 257-294.

[9] Chung, C., Korach, C. S., and Kao, I., 2011, "Experimental study and modeling of lapping using abrasive grits with mixed sizes," Journal of Manufacturing Science and Engineering, 133(3), p. 031006.

[10] Gatzen, H. H., and Siekmann, H., "Investigations on the Tool Plate Preparation for Nanogrinding," Proc. Proceedings of the ASPE 15th Annual Meeting, Scottsdale, AZ (2000), pp. 90-93.

[11] Tian, C., Yang, J., Fan, J., and Zhou, H., "Micro topography of different material surface by solid abrasive lapped at high speed," Proc. 3rd International Symposium on Advanced Optical Manufacturing and Testing Technologies: Advanced Optical Manufacturing Technologies, International Society for Optics and Photonics, pp. 67223D-67223D-67224.

[12] Rajurkar, K. P., Wang, Z. Y., and Kuppattan, A., 1999, "Micro removal of ceramic material (Al_2O_3) in the precision ultrasonic machining," Precision Engineering, 23(2), pp. 73-78.

[13] Thoe, T., Aspinwall, D., and Wise, M., 1998, "Review on ultrasonic machining," International Journal of Machine Tools and Manufacture, 38(4), pp. 239-255.

[14] Wang, Z. Y., and Rajurkar, K. P., 1996, "Dynamic analysis of the ultrasonic machining process," Journal of Manufacturing Science and Engineering, Transactions of the ASME, 118(3), pp. 376-381.

[15] Sundaram, M. M., Cherku, S., and Rajurkar, K. P., "Micro ultrasonic machining using oil based abrasive slurry," Proc. ASME International Manufacturing Science and Engineering Conference, MSEC2008, October 7, 2008 - October 10, 2008, ASME Foundation, pp. 221-226.

[16] Tseng, A. A., 2004, "Recent developments in micromilling using focused ion beam technology," Journal of micromechanics and microengineering, 14, p. R15.

[17] Kikuchi, N., Hashimoto, T., Okamoto, S., Shen, Z., and Kitakami, O., 2011, "Uniform Magnetic Dot Fabrication by Nanoindentation Lithography," Japanese Journal of Applied Physics, 50(4), p. 6505.

[18] Chang, C.-W., Liao, J.-D., Chang, H.-C., Lin, L.-K., Lin, Y.-Y., and Weng, C.-C., 2011, "Fabrication of nano-indented cavities on Au for the detection of chemically-adsorbed DTNB molecular probes through SERS effect," Journal of Colloid and Interface Science, 358(2), pp. 384-391.

[19] Tsui, T., Pharr, G., Oliver, W., Bhatia, C., White, R., Anders, S., Anders, A., and Brown, I., 1995, "Nanoindentation and nanoscratching of hard carbon coatings for magnetic disks," Oak Ridge National Lab., TN (United States); Oak Ridge Associated Universities, Inc., TN (United States); Lawrence Berkeley Lab., CA (United States).

[20] Charitidis, C., Logothetidis, S., and Douka, P., 1999, "Nanoindentation and nanoscratching studies of amorphous carbon films," Diamond and related materials, 8(2), pp. 558-562.

[21] Gouldstone, A., Van Vliet, K. J., and Suresh, S., 2001, "Simulation of defect nucleation in a crystal," Nature, 411(6838), p. 656.

[22] Diegoli, S., Hamlett, C. A. E., Leigh, S., Mendes, P., and Preece, J., 2007, "Engineering nanostructures at surfaces using nanolithography," Proceedings of the Institution of Mechanical Engineers, Part G: Journal of Aerospace Engineering, 221(4), pp. 589-629.

[23] Buijs, M., and Houten, K. K.-v., 1993, "Three-body abrasion of brittle materials as studied by lapping," Wear, 166(2), pp. 237-245.

[24] Komanduri, R., Lucca, D., and Tani, Y., 1997, "Technological advances in fine abrasive processes," CIRP Annals-Manufacturing Technology, 46(2), pp. 545-596.

[25] Gatzen, H. H., and Chris Maetzig, J., 1997, "Nanogrinding," Precision engineering, 21(2-3), pp. 134-139.

[26] Yang, J. D., Tian, C. L., and Wang, C. X., 2007, "Nanometer lapping technology at high speed," Science in China Series E: Technological Sciences, 50(1), pp. 27-38.

[27] Li, X., Nardi, P., Baek, C. W., Kim, J. M., and Kim, Y. K., 2004, "Direct nanomechanical machining of gold nanowires using a nanoindenter and an atomic force microscope," Journal of micromechanics and microengineering, 15(3), p. 551.

[28] Briscoe, B., Fiori, L., and Pelillo, E., 1999, "Nano-indentation of polymeric surfaces," Journal of Physics D: Applied Physics, 31(19), p. 2395.

[29] Schuh, C., and Nieh, T., 2003, "A nanoindentation study of serrated flow in bulk metallic glasses," Acta materialia, 51(1), pp. 87-99.

[30] Fang, T. H., Chang, W. J., and Weng, C. I., 2006, "Nanoindentation and nanomachining characteristics of gold and platinum thin films," Materials Science and Engineering: A, 430(1), pp. 332-340.

[31] Dasari, A., Yu, Z. Z., and Mai, Y. W., 2007, "Nanoscratching of nylon 66-based ternary nanocomposites," Acta materialia, 55(2), pp. 635-646.

[32] Huang, L., Zhang, Z., Zhao, Y., Yao, W., Mukherjee, A. K., and Schoenung, J. M., 2010, "Scratch-induced deformation in fine-and ultrafine-grained bulk alumina," Scripta Materialia, 63(5), pp. 528-531.

[33] Yin, L., Vancoille, E. Y. J., Ramesh, K., Huang, H., Pickering, J., and Spowage, A., 2004, "Ultraprecision grinding of tungsten carbide for spherical mirrors," Proceedings of the Institution of Mechanical Engineers, Part B: Journal of Engineering Manufacture, 218(4), pp. 419-429.

[34] Jiao, F., Zhao, B., Liu, C. S., and Zhu, X. S., 2008, "Influences of Ultrasonic Assistance in High Speed Lapping of Nano ZTA Engineering Ceramic on the Surface Machining Quality," Key Engineering Materials, 359, pp. 355-359.

[35] Evans, C., Paul, E., Dornfeld, D., Lucca, D., Byrne, G., Tricard, M., Klocke, F., Dambon, O., and Mullany, B., 2003, "Material removal mechanisms in lapping and polishing," CIRP Annals-Manufacturing Technology, 52(2), pp. 611-633.

[36] Lee, J. W., Huang, J. C., Li, C. L., and Liao, Y. C., 2011, "Nano-scratching and nano-machining in different environments on Cr2N/Cu multilayer thin films," Thin Solid Films.

[37] Gao, W., Hocken, R. J., Patten, J. A., and Lovingood, J., 2000, "Experiments using a nano-machining instrument for nano-cutting brittle materials," CIRP Annals-Manufacturing Technology, 49(1), pp. 439-442.

[38] Fang, H., Guo, P., and Yu, J., 2006, "Surface roughness and material removal in fluid jet polishing," Applied optics, 45(17), pp. 4012-4019.

[39] Zhang, J., and Zhang, C., 2008, "Material removal model for non-contact chemical mechanical polishing," Chinese Science Bulletin, 53(23), pp. 3746-3752.

[40] Xu, X., Luo, J., Lu, X., Zhang, C., and Guo, D., 2008, "Effect of nanoparticle impact on material removal," Tribology transactions, 51(6), pp. 718-722.

[41] Zhang, F. H., Zhang, Y., and Song, X. Z., 2008, "Study on removal mechanism of nanoparticle colloid jet machining," Advanced Materials Research, 53, pp. 363-368.

[42] Dasari, A., Yu, Z.-Z., and Mai, Y.-W., 2009, "Fundamental aspects and recent progress on wear/scratch damage in polymer nanocomposites," Materials Science and Engineering: R: Reports, 63(2), pp. 31-80.

[43] Oluwajobi, J. A., and Chen, X., 2008, "Modelling abrasive machining techniques using molecular dynamics."

[44] Kim, Y.-S., Kim, C.-I., Park, J.-Y., and Na, K.-H., 2005, "Molecular dynamic study for nanopatterning using atomic force microscopy," Metallurgical and Materials Transactions A, 36(1), pp. 169-176.

[45] Kim, Y. S., Na, K. H., Choi, S. O., and Yang, S. H., 2004, "Atomic force microscopy-based nano-lithography for nano-patterning: a molecular dynamic study," Journal of Materials Processing Technology, 155-156(0), pp. 1847-1854.

[46] Oluwajobi, A. O., and Chen, X., 2010, "On Minimum Depth of Cut in nanomachining."

[47] Promyoo, R., El-Mounayri, H., and Martini, A., 2010, "AFM-Based Nanomachining for Nano-Fabrication Processes: MD Simulation and AFM Experimental Verification," ASME Conference Proceedings, 2010(49477), pp. 405-414.

[48] Yu, H., Adams, J. B., and Hector Jr, L. G., 2002, "Molecular dynamics simulation of high-speed nanoindentation," Modelling and Simulation in Materials Science and Engineering, 10(3), p. 319.

[49] Noreyan, A., and Amar, J., 2008, "Molecular dynamics simulations of nanoscratching of 3C SiC," Wear, 265(7), pp. 956-962.

[50] Komanduri, N. C. L. M. R., 2001, "Molecular dynamics simulation of the nanometric cutting of silicon," Plant Ecology and Diversity, 81(12), pp. 1989-2019.

[51] Kelchner, C. L., Plimpton, S. J., and Hamilton, J. C., 1998, "Dislocation nucleation and defect structure during surface indentation," Physical Review B, 58(17), p. 11085.

[52] Inamura, T., Shishikura, Y., and Takezawa, N., 2010, "Mechanism of ring crack initiation in Hertz indentation of monocrystalline silicon analyzed by controlled molecular dynamics," CIRP Annals - Manufacturing Technology, 59(1), pp. 559-562.

[53] Khan, H. M., and Sung-Gaun, K., "Atomistic modeling of scratching process based on Atomic Force Microscope: Effects of temperature," Proc. Nanoelectronics Conference (INEC), 2010 3rd International, pp. 134-135.

[54] Shimizu, J., 2006, "Molecular dynamics simulation of vibration-assisted cutting: influences of vibration, acceleration and velocity," International journal of nanomanufacturing, 1(1), p. 105.

[55] Huang, Z. G., Guo, Z. N., Chen, X., Yue, T. M., To, S., and Lee, W. B., 2006, "Molecular Dynamics Simulation for Ultrafine Machining," Materials and Manufacturing Processes, 21(4), pp. 393-397.

[56] Jun Shimizu, L. Z., Hiroshi Eda 2006, "Molecular dynamics simulation of vibration-assisted cutting: influences of vibration parameters," International journal of manufacturing technology and management, 9(1).

[57] Shimizu, J., 2004, "Molecular dynamics analysis of ultra high-acceleration and vibration cutting," Key Engineering Materials, 257, p. 21.

[58] Yamaguchi, Y., and Gspann, J., 2002, "Large-scale molecular dynamics simulations of cluster impact and erosion processes on a diamond surface," Physical Review B, 66(15), p. 155408.

[59] Makeev, M. A., and Srivastava, D., 2008, "Hypersonic velocity impact on a-SiC target: A diagram of damage characteristics via molecular dynamics simulations," Applied Physics Letters, 92, p. 151909.

[60] Popok, V., and Campbell, E. E. B., 2006, "Beams of atomic clusters: effects on impact with solids," Rev. Adv. Mater. Sci, 11, pp. 19-45.

[61] Chagarov, E., and Adams, J. B., 2003, "Molecular dynamics simulations of mechanical deformation of amorphous silicon dioxide during chemical–mechanical polishing," Journal of Applied Physics, 94(6), pp. 3853-3861.

[62] Valentini, P., and Dumitrică, T., 2007, "Microscopic theory for nanoparticle-surface collisions in crystalline silicon," Physical Review B, 75(22), p. 224106.

[63] Jiaxuan Chen, Y. L., Qingshun Bai, Yulan Tang and Mingjun Chen, 2008, "Mechanism of Material Removal and the Generation of Defects by MD Analysis in Three-Dimensional Simulation in Abrasive Processes," Key Engineering Materials, 359-360, pp. 6-10.

[64] Vahid Hosseini, S., Vahdati, M., and Shokuhfar, A., 2011, "Effect of Tool Nose Radius on Nano-Machining Process by Molecular Dynamics Simulation," Defect and Diffusion Forum, 312-315, pp. 977-982.

[65] D.D. Cui, K. M., Liang Chi Zhang, 2011, "Nano-Grooving on Copper by Nano-Milling and Nano-Cutting," Advanced Materials Research 325, pp. 576-581.

[66] Promyoo, R., El-Mounayri, H., and Yang, X., 2010, "Molecular dynamics simulation of nanometric cutting," Machining Science and Technology, 14(4), pp. 423-439.

[67] Oluwajobi, A. O. a. C., Xun, "On Minimum Depth of Cut in nanomachining," Proc. Proceedings of the 8th International Conference on Manufacturing Research ICMR 2010, pp. 174-179.

[68] Shi, J., Shi, Y., and Liu, C., 2011, "Evaluation of a three-dimensional single-point turning at atomistic level by a molecular dynamic simulation," The International Journal of Advanced Manufacturing Technology, 54(1), pp. 161-171.

[69] Zhu, P.-z., Hu, Y.-z., Ma, T.-b., and Wang, H., 2010, "Study of AFM-based nanometric cutting process using molecular dynamics," Applied Surface Science, 256(23), pp. 7160-7165.

[70] Noreyan, A., and Amar, J. G., 2008, "Molecular dynamics simulations of nanoscratching of 3C SiC," Wear, 265(7-8), pp. 956-962.

[71] Luo, J., Hu, Y., and Wen, S., 2008, Physics and Chemistry of Micro-nanotribology, ASTM International.

[72] Chen, R., Luo, J., Guo, D., and Lu, X., 2009, "Energy transfer under impact load studied by molecular dynamics simulation," Journal of Nanoparticle Research, 11(3), pp. 589-600.

[73] Fangli, D., Jianbin, L., Shizhu, W., and Jiaxu, W., 2005, "Atomistic structural change of silicon surface under a nanoparticle collision," Chinese Science Bulletin, 50(15), pp. 1661-1665.

[74] Hockey, B., Wiederhorn, S., and Johnson, H., 1977, "Erosion of Brittle Materials by Solid Particle Impact," DTIC Document.

[75] Evans, A., and Wilshaw, T. R., 1976, "Quasi-static solid particle damage in brittle solids--I. Observations analysis and implications," Acta Metallurgica, 24(10), pp. 939-956.

[76] Evans, A., Gulden, M., and Rosenblatt, M., 1978, "Impact damage in brittle materials in the elastic-plastic response regime," Proceedings of the Royal Society of London. A. Mathematical and Physical Sciences, 361(1706), pp. 343-365.

[77] Ruff, A. W., and Wiederhorn, S., 1979, "Erosion by solid particle impact," DTIC Document.

[78] Wakuda, M., Yamauchi, Y., and Kanzaki, S., 2002, "Effect of workpiece properties on machinability in abrasive jet machining of ceramic materials," Precision engineering, 26(2), pp. 193-198.

[79] Ichida, Y., Sato, R., Morimoto, Y., and Kobayashi, K., 2005, "Material removal mechanisms in non-contact ultrasonic abrasive machining," Wear, 258(1), pp. 107-114.

[80] Bridgman, P., and Simon, I., 1953, "Effects of very high pressures on glass," Journal of Applied Physics, 24(4), pp. 405-413.

[81] James, S., and Sundaram, M. M., 2013, "A Molecular Dynamics Study of the Effect of Impact Velocity, Particle Size and Angle of Impact of Abrasive Grain in the Vibration Assisted Nano Impact-machining by Loose Abrasives," Wear.

[82] Lawn, B. R., and Marshall, D., 1978, "Indentation fracture and strength degradation in ceramics," Fracture mechanics of ceramics, pp. 205-229.

[83] Marshall, D., Lawn, B., and Evans, A., 1982, "Elastic/plastic indentation damage in ceramics: the lateral crack system," Journal of the American Ceramic Society, 65(11), pp. 561-566.

[84] Finnie, I., 1960, "Erosion of surfaces by solid particles," Wear, 3(2), pp. 87-103.

[85] Jennings, W. H., Head, W. J., and Manning, C., 1976, "A mechanistic model for the prediction of ductile erosion," Wear, 40(1), pp. 93-112.

[86] Bitter, J., 1963, "A study of erosion phenomena part I," Wear, 6(1), pp. 5-21.

[87] Naim, M., and Bahadur, S., 1984, "Work hardening in erosion due to single-particle impacts," Wear, 98, pp. 15-26.

[88] Bitter, J., 1963, "A study of erosion phenomena: Part II," Wear, 6(3), pp. 169-190.

[89] Aquaro, D., and Fontani, E., 2001, "Erosion of ductile and brittle materials," Meccanica, 36(6), pp. 651-661.

[90] Wiederhorn, S., and Hockey, B., 1983, "Effect of material parameters on the erosion resistance of brittle materials," Journal of Materials Science, 18(3), pp. 766-780.

[91] Ahmed, Y., Cong, W., Stanco, M. R., Xu, Z., Pei, Z., Treadwell, C., Zhu, Y., and Li, Z., 2012, "Rotary Ultrasonic Machining of Alumina Dental Ceramics: A Preliminary Experimental

Study on Surface and Subsurface Damages," Journal of Manufacturing Science and Engineering, 134(6), p. 064501.

[92] Srinivasu, D., and Axinte, D., 2014, "Mask-Less Pocket Milling of Composites by Abrasive Waterjets: An Experimental Investigation," Journal of Manufacturing Science and Engineering, 136(4), p. 041005.

[93] Kushendarsyah, S., and Sathyan, S., 2013, "Orthogonal Microcutting of Thin Workpieces," Journal of Manufacturing Science and Engineering, 135(3), p. 031004.

[94] Li, K.-M., Hu, Y.-M., Yang, Z.-Y., and Chen, M.-Y., 2012, "Experimental Study on Vibration-Assisted Grinding," Journal of Manufacturing Science and Engineering, 134(4), p. 041009.

[95] Virkar, S. R., and Patten, J. A., 2013, "Combined effects of stress and temperature during ductile mode microlaser assisted machining process," Journal of Manufacturing Science and Engineering, 135(4), p. 041003.

[96] Mulik, R. S., and Pandey, P. M., 2012, "Experimental investigations and modeling of finishing force and torque in ultrasonic assisted magnetic abrasive finishing," Journal of Manufacturing Science and Engineering, 134(5), p. 051008.

[97] Cai, M., Li, X., and Rahman, M., 2007, "Characteristics of "dynamic hard particles" in nanoscale ductile mode cutting of monocrystalline silicon with diamond tools in relation to tool groove wear," Wear, 263(7), pp. 1459-1466.

[98] Liu, J., Notbohm, J. K., Carpick, R. W., and Turner, K. T., 2010, "Method for characterizing nanoscale wear of atomic force microscope tips," ACS nano, 4(7), pp. 3763-3772.

[99] Bhaskaran, H., Gotsmann, B., Sebastian, A., Drechsler, U., Lantz, M. A., Despont, M., Jaroenapibal, P., Carpick, R. W., Chen, Y., and Sridharan, K., 2010, "Ultralow nanoscale wear

through atom-by-atom attrition in silicon-containing diamond-like carbon," Nature nanotechnology, 5(3), pp. 181-185.

[100] Kim, H. J., Yoo, S. S., and Kim, D. E., 2012, "Nano-scale wear: A review," International Journal of Precision Engineering and Manufacturing, 13(9), pp. 1709-1718.

[101] Bassani, R., and D'Acunto, M., 2000, "Nanotribology: tip–sample wear under adhesive contact," Tribology international, 33(7), pp. 443-452.

[102] Colaço, R., 2009, "An AFM study of single-contact abrasive wear: The Rabinowicz wear equation revisited," Wear, 267(11), pp. 1772-1776.

[103] d'Acunto, M., 2004, "Theoretical approach for the quantification of wear mechanisms on the nanoscale," Nanotechnology, 15(7), p. 795.

[104] Cleveland, J., Anczykowski, B., Schmid, A., and Elings, V., 1998, "Energy dissipation in tapping-mode atomic force microscopy," Applied Physics Letters, 72, p. 2613.

[105] Agrawal, R., Moldovan, N., and Espinosa, H., 2009, "An energy-based model to predict wear in nanocrystalline diamond atomic force microscopy tips," Journal of Applied Physics, 106(6), pp. 064311-064311-064316.

[106] Chung, K. H., Lee, Y. H., and Kim, D. E., 2005, "Characteristics of fracture during the approach process and wear mechanism of a silicon AFM tip," Ultramicroscopy, 102(2), pp. 161-171.

[107] Bloo, M., Haitjema, H., and Pril, W., 1999, "Deformation and wear of pyramidal, silicon-nitride AFM tips scanning micrometre-size features in contact mode," Measurement, 25(3), pp. 203-211.

[108] Bhushan, B., and Kwak, K. J., 2007, "Platinum-coated probes sliding at up to 100 mm s− 1 against coated silicon wafers for AFM probe-based recording technology," Nanotechnology, 18(34), p. 345504.

[109] Khurshudov, A., and Kato, K., 1995, "Wear of the atomic force microscope tip under light load, studied by atomic force microscopy," Ultramicroscopy, 60(1), pp. 11-16.

[110] Chung, K. H., and Kim, D. E., 2007, "Wear characteristics of diamond-coated atomic force microscope probe," Ultramicroscopy, 108(1), pp. 1-10.

[111] Skårman, B., Wallenberg, L. R., Jacobsen, S. N., Helmersson, U., and Thelander, C., 2000, "Evaluation of intermittent contact mode AFM probes by HREM and using atomically sharp CeO2 ridges as tip characterizer," Langmuir, 16(15), pp. 6267-6277.

[112] Wong, T., Kim, W., and Kwon, P., 2004, "Experimental support for a model-based prediction of tool wear," Wear, 257(7), pp. 790-798.

[113] Cheng, K., Luo, X., Ward, R., and Holt, R., 2003, "Modeling and simulation of the tool wear in nanometric cutting," Wear, 255(7-12), pp. 1427-1432.

[114] Maekawa, K., and Itoh, A., 1995, "Friction and tool wear in nano-scale machining—a molecular dynamics approach," Wear, 188(1), pp. 115-122.

[115] Lu, C., Gao, Y., Michal, G., Huynh, N., Zhu, H., and Tieu, A., 2009, "Atomistic simulation of nanoindentation of iron with different indenter shapes," Proceedings of the Institution of Mechanical Engineers, Part J: Journal of Engineering Tribology, 223(7), pp. 977-984.

[116] Komvopoulos, K., and Yan, W., 1997, "Molecular dynamics simulation of single and repeated indentation," Journal of Applied Physics, 82(10), pp. 4823-4830.

[117] Zhu, P., Hu, Y., Wang, H., and Ma, T., 2011, "Study of effect of indenter shape in nanometric scratching process using molecular dynamics," Materials Science and Engineering: A, 528(13), pp. 4522-4527.

[118] Mylvaganam, K., and Zhang, L. C., 2009, "Scale Effect of Nano-indentation of Silicon–A Molecular Dynamics Investigation," Key Engineering Materials, 389, pp. 521-526.

[119] Gotsmann, B., and Lantz, M. A., 2008, "Atomistic wear in a single asperity sliding contact," Physical review letters, 101(12), p. 125501.

[120] Goel, S., Luo, X., and Reuben, R. L., 2012, "Molecular dynamics simulation model for the quantitative assessment of tool wear during single point diamond turning of cubic silicon carbide," Computational Materials Science, 51(1), pp. 402-408.

[121] Cheong, W. C. D., and Zhang, L., 2000, "Effect of repeated nano-indentations on the deformation in monocrystalline silicon," Journal of materials science letters, 19(5), pp. 439-442.

[122] Kang, K., and Cai, W., 2007, "Brittle and ductile fracture of semiconductor nanowires– molecular dynamics simulations," Philosophical Magazine, 87(14-15), pp. 2169-2189.

[123] Tersoff, J., 1989, "Modeling solid-state chemistry: Interatomic potentials for multicomponent systems," Physical Review B, 39(8), pp. 5566-5568.

[124] Cai, M., Li, X., Rahman, M., and Tay, A., 2007, "Crack initiation in relation to the tool edge radius and cutting conditions in nanoscale cutting of silicon," International Journal of Machine Tools and Manufacture, 47(3), pp. 562-569.

[125] Luo, X., Goel, S., and Reuben, R. L., 2012, "A quantitative assessment of nanometric machinability of major polytypes of single crystal silicon carbide," Journal of the European Ceramic Society, 32(12), pp. 3423-3434.

[126] Tanaka, H., Shimada, S., and Anthony, L., 2007, "Requirements for ductile-mode machining based on deformation analysis of mono-crystalline silicon by molecular dynamics simulation," CIRP Annals-Manufacturing Technology, 56(1), pp. 53-56.

[127] Inamura, T., Takezawa, N., and Shimada, S., 2002, "Importance of micro/macro interaction in the mechanism of brittle mode cutting," CIRP Annals-Manufacturing Technology, 51(1), pp. 487-490.

[128] Cheong, W., and Zhang, L., 2000, "Molecular dynamics simulation of phase transformations in silicon monocrystals due to nano-indentation," Nanotechnology, 11(3), p. 173.

[129] Mattoni, A., Ippolito, M., and Colombo, L., 2007, "Atomistic modeling of brittleness in covalent materials," Physical Review B, 76(22), p. 224103.

[130] Buehler, M. J., 2008, Atomistic modeling of materials failure, Springer.

[131] Holland, D. J. M., and Marder, M., 1999, Cracks and atoms, University of Texas at Austin.

[132] Sundaram, M. M., and James, S., 2011, "Vibration Assisted Nano Abrasive Machining," An International Conference on Precision, Meso, Micro, and Nano Engineering,College of Engineering, Pune, India.

[133] James, S., and Sundaram, M. M., 2012, "A Feasibility Study of Vibration-Assisted Nano-Impact Machining by Loose Abrasives Using Atomic Force Microscope," Journal of Manufacturing Science and Engineering, 134, p. 061014.

[134] James, S., and Sundaram, M. M., 2014, "A study on the vibration induced transport of nanoabrasives in liquid medium," Powder Technology, 268, pp. 150-157.

[135] Lawn, B. R., and Fuller, E., 1975, "Equilibrium penny-like cracks in indentation fracture," Journal of Materials Science, 10(12), pp. 2016-2024.

[136] Evans, A., 1973, "Strength degradation by projectile impacts," Journal of the American Ceramic Society, 56(8), pp. 405-409.

[137] Gilardi, G., and Sharf, I., 2002, "Literature survey of contact dynamics modelling," Mechanism and machine theory, 37(10), pp. 1213-1239.

[138] Sahin, O., Quate, C. F., Solgaard, O., and Atalar, A., 2004, "Resonant harmonic response in tapping-mode atomic force microscopy," Physical Review B, 69(16), p. 165416.

[139] Su, C., Huang, L., Kjoller, K., and Babcock, K., 2003, "Studies of tip wear processes in tapping mode™ atomic force microscopy," Ultramicroscopy, 97(1), pp. 135-144.

[140] Hibbeler, R., 2003, Engeineering mechanics dynamics,(international edition) Macmillan Publishing Company, New York.

[141] Ritter, J., 1992, "Spherical particle impact damage," Key Engineering Materials, 71, pp. 107-120.

[142] Ball, A., and Mckenzie, H., 1994, "On the low velocity impact behaviour of glass plates."

[143] Sulchek, T., Hsieh, R., Adams, J., Yaralioglu, G., Minne, S., Quate, C., Cleveland, J., Atalar, A., and Adderton, D., 2000, "High-speed tapping mode imaging with active Q control for atomic force microscopy," Applied Physics Letters, 76, p. 1473.

[144] Lawn, B., and Wilshaw, R., 1975, "Indentation fracture: principles and applications," Journal of Materials Science, 10(6), pp. 1049-1081.

[145] Langitan, F., and Lawn, B., 1969, "Hertzian fracture experiments on abraded glass surfaces as definitive evidence for an energy balance explanation of Auerbach's law," Journal of Applied Physics, 40(10), pp. 4009-4017.

[146] Wiederhorn, S., and Lawn, B., 1977, "Strength degradation of glass resulting from impact with spheres," Journal of the American Ceramic Society, 60(9-10), pp. 451-458.

[147] Frank, F., and Lawn, B., 1967, "On the theory of Hertzian fracture," Proceedings of the Royal Society of London. Series A. Mathematical and Physical Sciences, 299(1458), pp. 291-306.

[148] Revenko, I., and Proksch, R., 2000, "Magnetic and acoustic tapping mode microscopy of liquid phase phospholipid bilayers and DNA molecules," Journal of Applied Physics, 87(1), pp. 526-533.

[149] Rogers, B., York, D., Whisman, N., Jones, M., Murray, K., Adams, J., Sulchek, T., and Minne, S., 2002, "Tapping mode atomic force microscopy in liquid with an insulated piezoelectric microactuator," Review of Scientific Instruments, 73(9), pp. 3242-3244.

[150] Qi, Q., and Brereton, G. J., 1995, "Mechanisms of removal of micron-sized particles by high-frequency ultrasonic waves," Ultrasonics, Ferroelectrics and Frequency Control, IEEE Transactions on, 42(4), pp. 619-629.

[151] Savithiri, S., Pattamatta, A., and Das, S. K., 2011, "Scaling analysis for the investigation of slip mechanisms in nanofluids," Nanoscale research letters, 6(1), pp. 1-15.

[152] Tan, M. K., Friend, J. R., and Yeo, L. Y., 2007, "Direct visualization of surface acoustic waves along substrates using smoke particles," Applied Physics Letters, 91(22), pp. 224101-224101-224103.

[153] VandenBurg, D. M., 2011, "The Sonochemical Remediation of Phthalate Esters: An investigation into products and kinetics," University of Bath.

[154] Guz, A., and Zhuk, A., 2004, "Motion of solid particles in a liquid under the action of an acoustic field: The mechanism of radiation pressure," International Applied Mechanics, 40(3), pp. 246-265.

[155] King, L. V., 1934, "On the acoustic radiation pressure on spheres," Proceedings of the Royal Society of London. Series A-Mathematical and Physical Sciences, 147(861), pp. 212-240.

[156] Lighthill, S. J., 1978, "Acoustic streaming," Journal of Sound and Vibration, 61(3), pp. 391-418.

[157] KrishnaáJuluri, B., and JunáHuang, T., 2009, "A millisecond micromixer via single-bubble-based acoustic streaming," Lab on a Chip, 9(18), pp. 2738-2741.

[158] Abramov, O., 1987, "Action of high intensity ultrasound on solidifying metal," Ultrasonics, 25(2), pp. 73-82.

[159] Lan, J., Yang, Y., and Li, X., 2004, "Microstructure and microhardness of SiC nanoparticles reinforced magnesium composites fabricated by ultrasonic method," Materials Science and Engineering: A, 386(1), pp. 284-290.

[160] Zhang, Z., Li, T., Yue, H., Zhang, J., and Li, J., 2009, "Study on the preparation of Al–Si functionally graded materials using power ultrasonic field," Materials & Design, 30(3), pp. 851-856.

[161] Kim, S., Kihm, K. D., and Thundat, T., 2010, "Fluidic applications for atomic force microscopy (AFM) with microcantilever sensors," Experiments in fluids, 48(5), pp. 721-736.

[162] Gupta, S., and Feke, D. L., 1998, "Filtration of particulate suspensions in acoustically driven porous media," AIChE journal, 44(5), pp. 1005-1014.

[163] Zhou, D., 2004, "Heat transfer enhancement of copper nanofluid with acoustic cavitation," International Journal of Heat and Mass Transfer, 47(14), pp. 3109-3117.

[164] Horsch, C., Schulze, V., and Löhe, D., 2006, "Deburring and surface conditioning of micro milled structures by micro peening and ultrasonic wet peening," Microsystem technologies, 12(7), pp. 691-696.

[165] Heath, D., Širok, B., Hocevar, M., and Pečnik, B., 2013, "The Use of the Cavitation Effect in the Mitigation of CaCO3 Deposits," Strojniški vestnik-Journal of Mechanical Engineering, 59(4), pp. 203-215.

[166] Prozorov, T., Prozorov, R., and Suslick, K. S., 2004, "High velocity interparticle collisions driven by ultrasound," Journal of the American Chemical Society, 126(43), pp. 13890-13891.

[167] Wang, J., 2007, "Predictive depth of jet penetration models for abrasive waterjet cutting of alumina ceramics," International Journal of Mechanical Sciences, 49(3), pp. 306-316.

[168] Kuppa, R., and Moholkar, V. S., 2010, "Physical features of ultrasound-enhanced heterogeneous permanganate oxidation," Ultrasonics sonochemistry, 17(1), pp. 123-131.

[169] Song, Y., and Bhushan, B., 2006, "Simulation of dynamic modes of atomic force microscopy using a 3D finite element model," Ultramicroscopy, 106(8), pp. 847-873.

[170] Buongiorno, J., 2006, "Convective transport in nanofluids," Journal of Heat Transfer, 128, p. 240.

[171] Jang, S. P., and Choi, S. U., 2006, "Cooling performance of a microchannel heat sink with nanofluids," Applied Thermal Engineering, 26(17), pp. 2457-2463.

[172] Raeymaekers, B., Pantea, C., and Sinha, D. N., 2011, "Manipulation of diamond nanoparticles using bulk acoustic waves," Journal of Applied Physics, 109(1), pp. 014317-014317-014318.

[173] Chen, G., 1996, "Nonlocal and nonequilibrium heat conduction in the vicinity of nanoparticles," Journal of Heat Transfer, 118(3), pp. 539-545.

[174] Lanin, V., Dezhkunov, N., and Kotukhov, A., 2010, "Application of ultrasonic effects in liquid media for fabrication of nanomaterials," Surface Engineering and Applied Electrochemistry, 46(3), pp. 223-229.

[175] Michaelides, E. E., 2013, "Transport properties of nanofluids. A critical review," Journal of Non-Equilibrium Thermodynamics, 38(1), pp. 1-79.

[176] Plimpton, S., 1995, "Fast parallel algorithms for short-range molecular dynamics," Journal of Computational Physics, 117(1), pp. 1-19.

[177] Kumar, M., Chang, C.-J., Melkote, S. N., and Joseph, V. R., 2013, "Modeling and Analysis of Forces in Laser Assisted Micro Milling," Journal of Manufacturing Science and Engineering, 135(4), p. 041018.

[178] Arif, M., Rahman, M., and San, W. Y., 2012, "A Model to Determine the Effect of Tool Diameter on the Critical Feed Rate for Ductile-Brittle Transition in Milling Process of Brittle Material," Journal of Manufacturing Science and Engineering, 134(5), p. 051012.

[179] James, S., and Sundaram, M., 2014, "Modeling of Material Removal Rate in Vibration Assisted Nano Impact-machining by Loose Abrasives," Journal of Manufacturing Science and Engineering.

[180] Zarepour, H., and Yeo, S., 2012, "Predictive modeling of material removal modes in micro ultrasonic machining," International Journal of Machine Tools and Manufacture.

[181] Wu, J., Zhou, S., and Li, X., 2013, "Acoustic Emission Monitoring for Ultrasonic Cavitation Based Dispersion Process," Journal of Manufacturing Science and Engineering, 135(3), p. 031015.

[182] Booij, S. M., 2003, Fluid Jet Polishing: Possibilities and limitations of a new fabrication technique.

[183] Sooraj, V., and Radhakrishnan, V., 2013, "Elastic impact of abrasives for controlled erosion in fine finishing of surfaces," Journal of Manufacturing Science and Engineering, 135(5), p. 051019.

[184] Zhao, Y., Maietta, D. M., and Chang, L., 2000, "An asperity microcontact model incorporating the transition from elastic deformation to fully plastic flow," Journal of Tribology, 122(1), pp. 86-93.

[185] Ganguly, V., Schmitz, T., Graziano, A., and Yamaguchi, H., 2013, "Force Measurement and Analysis for Magnetic Field–Assisted Finishing," Journal of Manufacturing Science and Engineering, 135(4), p. 041016.

[186] Shipway, P., and Hutchings, I., 1994, "A method for optimizing the particle flux in erosion testing with a gas-blast apparatus," Wear, 174(1), pp. 169-175.

[187] Basak, A., Fan, J., Wang, J., and Mathew, P., 2010, "Material removal mechanisms of monocrystalline silicon under the impact of high velocity micro-particles," Wear, 269(3), pp. 269-277.

[188] Robinson, G. M., Jackson, M. J., and Whitfield, M. D., 2007, "A review of machining theory and tool wear with a view to developing micro and nano machining processes," Journal of Materials Science, 42(6), pp. 2002-2015.

[189] Lane, B. M., 2012, "Material Effects and Tool Wear in Vibration Assisted Machining," Doctor of Philosophy Dissetation, North Carolina State University, Dissetation.

[190] Abdel-Al, H. A., and Smith, S. T., "Thermal modeling of silicon machining–issues and challenges," Proc. Proceedings of the ASPE Spring Topical Meeting: Silicon Machining, Carmel-by-the Sea, California, pp. 27-31.

[191] Rhee, Y. W., Kim, H. W., Deng, Y., and Lawn, B. R., 2001, "Brittle fracture versus quasi plasticity in ceramics: a simple predictive index," Journal of the American Ceramic Society, 84(3), pp. 561-565.

[192] Johnson, K. L., 1987, Contact mechanics, Cambridge university press.

[193] James, S., and Sundaram, M. M., 2015, "Molecular Dynamics Simulation Study of Tool Wear in Vibration Assisted Nano-Impact-Machining by Loose Abrasives," Journal of Micro and Nano-Manufacturing, 3(1), p. 011001.

[194] Maugis, D., 1992, "Adhesion of spheres: the JKR-DMT transition using a Dugdale model," Journal of Colloid and Interface Science, 150(1), pp. 243-269.

[195] Laidler, K. J., 1984, "The development of the Arrhenius equation," Journal of Chemical Education, 61(6), p. 494.

[196] D'Acunto, M., 2010, "Controlling Wear on Nanoscale," Scanning Probe Microscopy in Nanoscience and Nanotechnology, Springer, pp. 647-686.

[197] Bertoni, C., Bortolani, V., Calandra, C., and Tosatti, E., 1972, "Dielectric Matrix and Phonon Frequencies in Silicon," Physical review letters, 28(24), pp. 1578-1581.

[198] Tsukruk, V. V., and Bliznyuk, V. N., 1998, "Adhesive and friction forces between chemically modified silicon and silicon nitride surfaces," Langmuir, 14(2), pp. 446-455.